The design of an FM-CW proximity radar

By **Robert Kellerman**

Thesis in partial fulfillment of the requirements for the degree Master of Science in Engineering at the University of Stellenbosch

Supervisor:
Prof JB de Swardt

March 2004

Declaration

I, the undersigned, hereby declare that the work contained in this thesis is my own original work and that I have not previously in its entirety or in part submitted it at any university for a degree.

Signed by RA Kellerman Date

Abstract

The development of a small, cost effective short range FM-CW radar as well as the design and optimization of a double helix antenna is discussed. The FM-CW radar operates at S-band (2450 – 2550 MHz) and is limited at a maximum transmitted power of 5 dBm. The system is required to detect reflections from objects up to a 30 m range. This was made possible largely by the effective high gain antenna design and improved system isolation between the transmitted and received signals.

The complete design process from fundamental requirements, through various simulations and system analysis to the final electronic circuit is discussed. The design was also built and measured in the laboratory and initial field measurements were taken. The following aspects were considered:

- Relation between the beat frequency and various FM-CW radar system parameters based on the theory, preliminary measurements and simulations.
- Radar component assessment and design.
- Design of a low cost Lange coupler that isolates the system's transmit and receive signals, which operates as a 90° hybrid and is used to feed a dual-fed circularly polarized patch antenna.
- A circularly polarized patch antenna and double helix antenna were designed, built and measured in an anechoic chamber. The antennas were implemented in the final radar system and compared on the basis of their contribution to the system's performance.
- Integrating the final radar system on a circular 60 mm diameter PCB with a double helix antenna mounted on top.

The final radar system is able to measure range up to 40 m and meets all the design requirements. The signal processing of the measured beat frequency, however, can be taken further.

Opsomming

Die ontwikkeling van 'n klein, koste effektiewe kort-afstand FM-CW radar, sowel as die onwerp en optimalisering van 'n dubbele heliks-antenna word bespreek. Die FM-CW radar werk by S-band (2450 – 2550 MHz) en is beperk tot 'n maksimum uitsaaidrywing van 5 dBm. Van die stelsel word vereis om weerkaatsings van voorwerpe tot op 'n afstand van 30 m waar te neem. Dit is grootliks moontlik gemaak deur die hoë aanwins antenna-ontwerp en verbeterde isolasie tussen die stelsel se uitsaai- en ontvangseine.

Die volledige ontwerpsproses van die fundamentele vereistes af tot die finale elektroniese stroombaan word bespreek. Verskeie simulasies and stelselanalises is gebruik om die finale FM-CW radar te realiseer. Die ontwerp is vervolgens in die laboratorium gebou en gemeet en aanvangsveldmetings is geneem. Die volgende aspekte is in nagevors:

- Verband tussen die puls-frekwensie en verskeie FM-CW radar stelsel-parameters gebaseer op die teorie, inleidende metings en simulasies.
- Ontleding van verskeie radarkomponente en -stelselontwerp.
- Ontwerp van 'n lae koste Lange-koppelaar met die doel om die stelsel se uitsaai- en ontvangseine te isoleer. Die Lange-koppelaar dien as 'n 90° hibriede wat gebruik word om 'n dubbele-voer sirkulêr gepolariseerde mikrostrook-antenna aan te dryf.
- Verder is 'n sirkulêr gepolariseerde mikrostrook-antenna en 'n dubbele heliks-antenna ontwerp en opgemeet in 'n anargoïese kamer. Beide antennas is geïmplimenteer in die finale radarstelsel en is vergelyk op grond van hulle rol in die stelsel se funksionering.
- Die finale stelsel is geïntegreer en gebou op 'n ronde 60 mm deursnit PCB met 'n dubbele helix-antenna bo-op gemonteer.

Die finale radarstelsel kan afstand tot op 40 meter bepaal en voldoen aan al die gestelde vereistes. Seinverwerking van die gemete puls-frekwensie kan nog verder ontwikkel word.

Acknowledgements

I would like to thank the following persons who helped me in various ways during the completion of my thesis,

My Lord and Saviour, my best friend, Jesus Christ. You indeed levelled the mountains and filled up the valleys for me to have come thus far. Thank you God! Without Your supernatural help, this M wouldn't have been possible.

My fiancé, Valpré: You have inspired me and have helped me more that I could have imagined. It is impossible for me to repay you for all your sacrifice and support. I love you so much.

Professor J.B. de Swardt: You are the best study leader in the world. Thank you for your patience, knowledge and understanding. There were times when I thought beat frequency signals do not exist.

Professor K.D. Palmer and J.H. Cloete: Thank you for your knowledgeable inputs. I admire your expertise in the field of antennas and radar systems.

Janine Kullenkampff: Thank you for proof reading my final thesis. I know you were very busy and I really appreciate that you sacrificed your time to help me.

My parents: Thank you for believing in me and for all your support. I know you have and are still praying for me. May God bless you in abundance.

Linda and Pieter Oosthuizen. Thank you for all your love and support. How will I ever forget every home cooked lab meal that you have blessed me with so often.

Cobus, Dan, Pottie and Anton: Thank you for all your support. You define true friendship. I can not wait for our next Indo surf trip.

Drommedaris 3 cell: Thank you for your prayers and support.

All the guys and girl in E212: It has been a pleasure to work with you. From playing games, drinking coffee, watching birds, refurnishing the lab and reading all Quintin's funny emails.

Wessel Croukamp and Ulrich Buttner: I admire your technical ability and your patience with my last minute alterations. The excellence in your work has never stopped amazing me.

M.J. Siebers: Thank you for helping me with my antenna measurements and for organizing the fifth floor lab.

Ashley: Thank you for making my final radar PCB in one afternoon. I still owe you another BP-pie and coke.

Table of contents

List of figures

List of tables

List of abbreviations

RADAR	radio detection and ranging
LO	Local oscillator
RF	Radio frequency
IF	Intermediate frequency
FFT	Fast Fourier transform
FM-CW	Frequency modulated continuous wave
WWII	World War II
US	United States
m	Meter
mm	Millimetre
km	kilometre
v_d	Difference-frequency signal
v_r	Received signal
v_t	Transmitted signal
f_b	Beat frequency
f_0	Center frequency
f_r	Beat frequency due to difference in range
f_t	Transmitter signal
f_m	Modulation frequency
Δf	Deviation frequency
LPF	Low pass filter
R	Absolute distance between radar and target or the distance between two antennas under test
dB	Decibel
dBm	Decibel with reference to 1 mW
PCB	Printed circuit board
G_t	Transmitting antenna's gain
G_r	Receiving antenna's gain
G	Antenna gain
P_t	Total transmitted power
P_r	Minimum received power
λ	Wavelength of signal
λ_d	Wavelength of signal in a dielectric medium
σ	Radar cross section
Hz	Hertz

kHz	Kilo Hertz
MHz	Mega Hertz
GHz	Giga Hertz
ω_d	Doppler angular frequency
ε_r	Dielectric constant
T	Substrate thickness
S	Line-spacing
W	Line-width
C	Coupling factor
Z_0	Characteristic impedance
Z_{0o}	Odd mode characteristic impedance
Z_{0e}	Even mode characteristic impedance
α	Pitch angle
AUT	Antenna under test
RHC	Right-hand circularly polarized
LHC	Left-hand circularly polarized
VCO	Voltage controlled oscillator

1. Introduction

1.1 Background

The advent of radio technology at the end of the 19th century led to the development of various kinds of wireless systems. This dramatic advancement is considered to be one of the most exciting scientific achievements of the 20th century. In 1904 a patent was filed for a unit detecting reflected radio waves from objects. Practical applications, however, required further technological advancement and it was not until the early thirties that prototypes with various functions appeared in US, British and German navies, under acronyms such as RADAR (**ra**dio **d**etection **a**nd **r**anging). The period during World War II (WWII) was the golden age of radar development, with the appearance of numerous new systems, some of which had a decisive impact on the development of the war. The radar, having much longer wavelengths than light waves, had the great advantage of being able to penetrate even the densest fog and rain and, of course, operate in darkness. During these early development stages, all radar equipment required bulky and expensive units requiring lethal voltages of several kV [1] [4 p1527].

The oldest and best-known radar system (since WWII) is the pulse radar. This system uses short pulses which distributes the power over a certain bandwidth in the frequency spectrum. With modern components, 1 ns low-power pulses can be obtained at low cost which is sufficient for a resolution of a few tenths of a metre. This attribute has been utilized in a number of radar level gauging systems. Some pulse radar systems use a DC-pulse of 1 ns, where the more advanced systems have a pulse formed by a carrier at, for instance, 5.8 GHz. Low-power pulsed systems can have very low power consumption but, as a result, they usually have low sensitivity and inadequate accuracy in a practical environment. Sensitivity is the most important system parameter in many applications as it determines whether measurements are possible in non-ideal conditions. The system used most frequently for radar level gauging is the Frequency Modulated Continuous Wave (FM-CW) radar. It spreads the frequency by means of a linear sweep of a signal of constant amplitude. Custody-transfer approved FM-CW systems have been used since the late eighties. The FM-CW method can provide supreme performance of both accuracy and sensitivity, though there is a great deal of different design combinations [1] [2 p86].

The modern FM-CW radar has found various applications in

- Radio Altimeters

- Level-Measuring Radar
- Navigational Radar
- Vehicle Collision Warning Systems
- Precision Range Meter for Fixed Targets
- Measurement of Very Small Motions [3 p5-8]

1.2 Problem statement

The aim of this project was to design and build an FM-CW radar for short range measurements. One of the aims was to design the radar to be used for a specific military application. A the present time, a need exists for a device that can be used to measure the altitude of a parashoot jumper just before landing when doing night jumps. The device has to be light weight, cost efficient and has to measure the jumper's altitude up to 30 m. An FM-CW radar has to be designed, however, to be used in general short range measurement applications with the following design specifications:

- Maximum detectable range: 30 meter
- Resolution: 1 meter
- Maximum transmitted power: 10 dBm
- Maximum continuous current: 200 mA
- Maximum total cost: R 500 (five hundred South African Rands).
- Size restriction: 200 mm cylinder with 60 mm diameter
- Total weight: less than 150 g
- Easy to manufacture

An important design specification of the radar system that was considered is the isolation between the transmitted and received signals. The isolation protects the mixer from being saturated by the transmitter power, coupling to the mixer RF-port. There are, however, various methods of obtaining good isolation. Some of the methods that were considered are:

1. *The use of two separate transmit and receive antennas*. This achieves good isolation but requires too much physical space since the air between the antennas functions as the main insulator.
2. *The use of a single transmit and receive antenna with a circulator*. This method requires less space than when using two separate antennas. Circulators are, however, very expensive which makes the system less cost efficient.
3. *The use of a circularly polarized transmit and receive patch antenna with a Lange coupler*. The Lange coupler is a micro-strip component which is cost efficient and replaces the need for a circulator when a circularly polarized antenna is used. The disadvantage of circular polarization is that 3 dB of the transmitted power is wasted

when aiming at a target which lies only in the horizontal or vertical plane. However, it has the advantage of detecting any of these targets and is not limited to a target's physical alignment.

4. *The use of a double helix antenna to transmit and receive, with a Lange coupler.* The double helix antenna consists of two helices, each with different polarization, wound inside each other. They operate as a single antenna to transmit and receive respectively. The main advantage of this antenna is that it can be designed with good isolation between the two helices, improving the isolation between the transmitted and received signals in the radar system. A helix antenna generally has higher gain than a patch antenna and is more directional but some of the gain has to be sacrificed to achieve better isolation. The disadvantage of the double helix is that it takes up more physical space and is rather complex to design and manufacture.

The above methods were implemented and compared and the final radar system design was based on no. 4 of the above mentioned. The design process and simulations of the double helix antenna design are well documented in chapter 5 and may be found helpful by future antenna designers.

Another area of design that required extra attention was the choice of the different system frequencies that would best meet the design requirements. Since there is very little literature available explaining the relationship between the modulation frequency and beat frequency, or the effect of higher or lower frequency deviation, a simulation program was written to demonstrate these relationships before choosing the optimal final values.

A software program called *RadarOpt* was written to analyze the radar system design. It indicates the maximum range, minimum detectable signal and total cost from the user's defined component parameters. It also gives a good indication of the system performance prior to the physical design stages.

1.3 Thesis outline

This document consists of eight chapters. A short introductory summary is given at the beginning of each chapter.

The design approach and theory of an FM-CW radar and simulations of the different radar signals are discussed in **chapter 2**. The design parameters that were chosen after considering the results obtained from the simulations are summarized at the end of this chapter. **Chapter 3** follows with a discussion of the radar software analyses program, *RadarOpt* which was written to analyze the radar's performance. This is done by using the specifications of each component specified by the radar architect.

Chapter 4 describes the possible radar components that were considered for the design. Comparisons were made between similar components' theory, simulations and measurements. The coupled line and Lange coupler that were designed and constructed from their fundamental theory are discussed in detail. The measured S parameters of these components are considered in the light of the final radar design performance.

Chapter 5 focuses on the antenna design. This chapter describes the design of two antennas, namely, the circularly polarized patch antenna and the double helix antenna. The gain, reflection parameters, radiation patterns and axial ratio of each antenna were measured and compared. More emphasis was placed on the helix antenna design since there exists little literature regarding this rather unique topology, explaining the effect of each design parameter on the antenna gain, isolation and reflection parameters. An iterative optimization method was developed to obtain an adequate design that would best meet the system requirements. The design process and relationship of each design parameter on the antenna performance are summarized in flow diagrams and tables.

The measurements of the preliminary FM-CW radar system are covered in **chapter 6**. This system uses cables to duplicate the delay between the transmitted and received signals without the use of an antenna and a circulator or Lange coupler. The measurement setup has the advantage of eliminating unwanted noise and interfering signals and enables the designer to determine whether the basic system functions as expected. The difference-frequency signal at the mixer IF-port was measured in the time and frequency domains and the results were compared with the simulations done in chapter 2 and 4. **Chapter 7** contains the final radar system measurements. In the first radar system, the cable that was used in the preliminary system was replaced with two separate horn antennas to transmit and receive separately. Thereafter it was reduced to a single antenna system using a circulator. In the second radar system the horn antenna and circulator were replaced with the patch antenna and Lange coupler that were designed and built as explained in chapters 4 and 5. The final radar system made use of the double helix in stead of the patch antenna.

The initial radar system measurements were done on a flat surface with an upright steel plate reflector that served as the target. Each radar's minimum and maximum range was measured on a spectrum analyzer by moving the vertical plate nearer and further from the radar.

The final radar system was rebuilt on a 60 mm diameter printed circuit board (PCB) with the antenna mounted on top. Final measurements were done with an upright reflector to measure the range up to 40 m. Initial field measurements were taken outside to measure the range of two non-ideal reflective objects.

Chapter 8 concludes with the performance of the final design that is compared to the initial design requirements and specifications. Recommendations and possible improvements on the final system are considered.

2. System design

The first step in the design process was to do some research on the fundamentals of FM-CW radar. There are different possible ways to approach the design. One of the initial design considerations, was to decide on the type of modulation frequency that would give the best beat frequency measurement. A challenging aspect was to find the relationship between the different signal parameters in the beat frequency equation and the influence that they will have on later measurements, because this could not be found in any literature.

This chapter consists of three sections. Section 2.1 focuses on the FM-CW radar from a system point of view, discussing the basic operation. Section 2.2 explains the theory of FM-CW radar using triangular modulation where section 2.3 explains how the software package, *Matlab* [31], was used to simulate the operation of the FM-CW radar. The transmitted and received signals were created in the time domain and the difference-frequency signals were inspected in both the time- and frequency- domains. One of the questions that was answered by these simulations was, 'Is it possible to use a modulation frequency that is higher than the beat frequency?'. The chapter concludes with a summary of the simulations, thus allowing the selection of the best design parameters for the radar design.

2.1 Design Approach

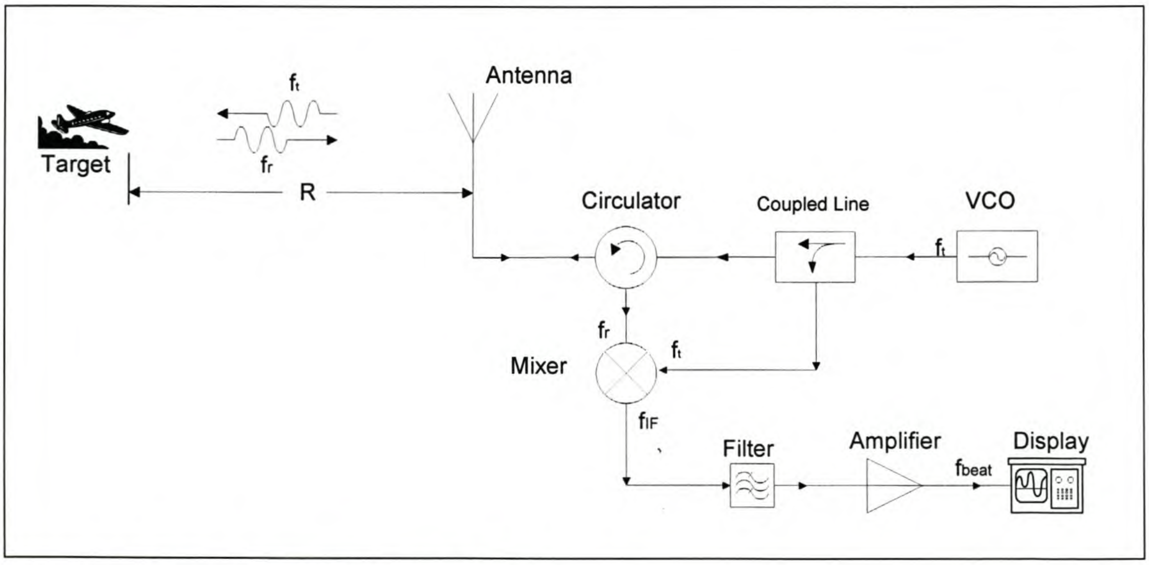

Figure 2-1. Block diagram of the FM-CW radar system.

The block diagram of a basic single antenna FM-CW radar system shown in Figure 2-1 will be used to give a short description of the operation of this type of radar. Each system component will later be discussed in comprehensive detail in chapter 4 and 5.

A voltage controlled oscillator (VCO) is used to generate the transmitter signal f_t, of which the frequency is changed against time in a known manner. A coupler then couples a fraction of the transmitter signal which is amplified to drive the LO- port (local oscillator port) of the mixer. The rest of the transmitter signal goes through a circulator and is then transmitted by the antenna. The function of the circulator is to isolate the received signal from the transmitted signal. The target reflects the signal which is received from the radar after a specific time delay due to the distance, R travelled. The returned signal f_r is sent via the circulator to the RF- port of the mixer. The time delay causes a small difference in frequency between the transmitted and received signals, known as the beat frequency. The difference-frequency signal is detected by the mixer (later explained in section 4.4) and the mixer signal at the IF-port is filtered and amplified and can be measured using a frequency counter. The range, as a direct function of the beat frequency, can then easily be determined [2].

2.2 Basic FM–CW radar theory

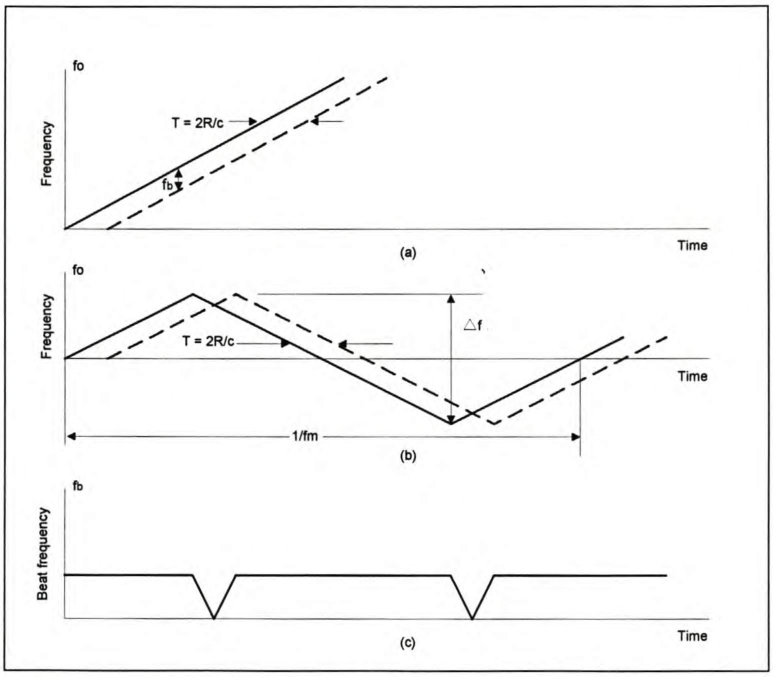

Figure 2-2: Frequency-time relationships in FM-CW radar.

As already stated in section 2.1, in an FM-CW radar, the transmitter frequency is changed as a function of time in a known manner. For the best accuracy this function, called the modulation frequency, should be linear as shown by the solid line in Figure 2-2a. A sinusoid or any known time function can be used but the non-linearity causes the beat frequency to be less accurate and as the average frequency is taken to determine the range. If there is a target at distance R from the radar, an echo signal will return after a time

$$T = 2R / c \tag{2.1}$$

where c is the velocity of propagation = 3 x 10^8. The echo signal is represented in Figure 2-2 by the dashed line. If the echo signal is heterodyned with a portion of the transmitter signal by a non-linear element such as a mixer, a beat note, f_b will be produced. If the target and radar is stationary, i.e. there is no doppler frequency shift, the difference-frequency signal is a measure of the target's range and $f_b = f_r$, where f_r is the beat frequency only due to the target's range [2] [26].

Since the transmitter frequency cannot be continually changed in one direction, periodicity is introduced, and the result is typically a triangular frequency-modulated waveform as shown in Figure 2-2b. This produces the most constant beat note as shown in Figure 2-2c. The beat note stays constant except at the turn-around region. If the transmitter frequency is modulated at a rate f_m over a deviation in frequency Δf, the beat frequency becomes

$$f_r = \frac{2R}{c} 2f_m \Delta f = \frac{4Rf_m \Delta f}{c} \tag{2.2}$$

thus the measurement of the beat frequency determines the range, R [2].

If it cannot be assumed that both the target and radar are stationary, the effect of the doppler frequency shift has to be taken into account. The total number of wavelengths (λ) in the two-way path between the radar and target is 2R/λ. Since one wavelength corresponds to an angular excursion of 2π radians, the total angular exertion (φ) made by the electromagnetic wave during its transit to and from the target is 4πR/λ radians. With a moving target, the range R and the phase φ are continuously changing. The doppler angular frequency ω_d due to the change in φ with respect to time is given by [2][25]

$$\omega_d = 2\pi f_d = \frac{d\varphi}{dt} = \frac{4\pi}{\lambda}\frac{dR}{dt} = \frac{4\pi v_r}{\lambda} \tag{2.3}$$

where f_d = doppler frequency shift [Hz] and
v_r = relative velocity of target with respect to radar [m/s].

The doppler frequency shift is

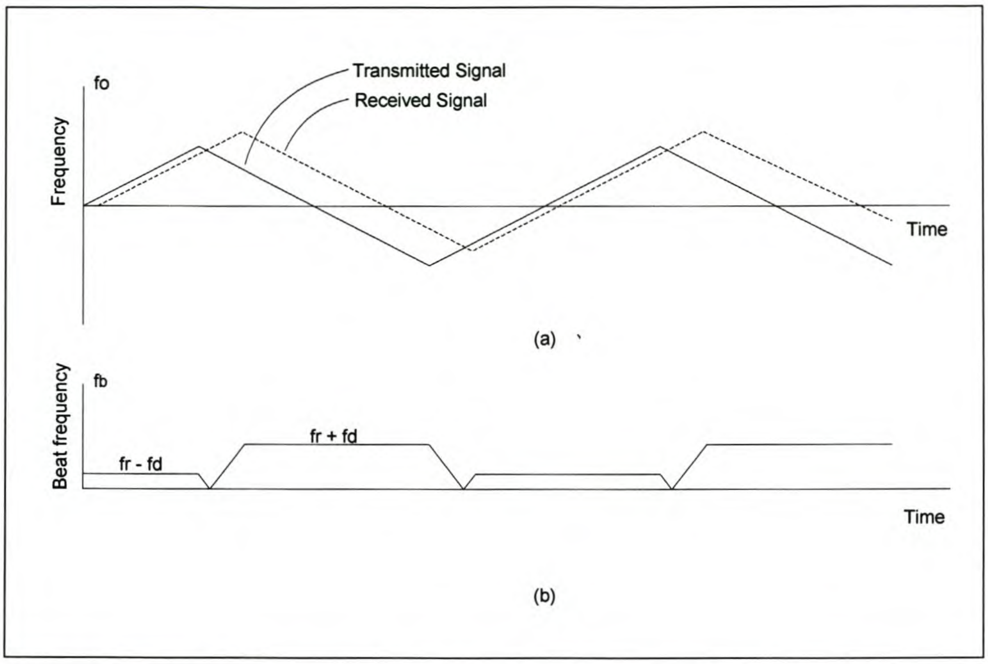

Figure 2-3: Frequency-time relationships in FM-CW radar when the received signal is shifted in frequency by the doppler effect. (a) Transmitted (solid curve) and echo (dashed curve) frequencies; (b) beat frequency.

$$f_d = \frac{2v_r}{\lambda} = \frac{2v_r f_0}{c} \tag{2.4}$$

where f_0 is the center frequency of the modulated transmitted frequency.

This doppler frequency shift will be superimposed on the FM range beat frequency and an incorrect range measurement results. The new echo signal can be seen in Figure 2-3a. In this case, the target is approaching the radar and the beat frequency f_b (up) produced during the increasing portion of the FM cycle is the difference between the beat frequency due to range, f_r and the doppler frequency shift f_d (2.5). Similarly during the decreasing portion, the beat frequency f_b (down) is the sum of the two (2.6).

$$f_b(up) = f_r - f_d \tag{2.5}$$

$$f_b(down) = f_r + f_d \tag{2.6}$$

This result is shown in Figure 2-3b. The range frequency f_r may be extracted by measuring the average beat frequency that is $f_r = ½[f_b(up) + f_b(down)]$. The center frequency does not influence the beat frequency in (2.2) but is directly proportional to the doppler frequency in (2.4). The center frequency for the conceptual design was chosen as 2.5 GHz with 100 MHz bandwidth. A future aim is to change the center frequency to 10 GHz after the final FM-CW radar has been developed and tested.

If the transmitted signal is assumed to be linearly modulated, the voltage waveform can be written in the time domain

$$v_t = V_t \sin\left(2\pi f_0 t + 2\pi t\left(2 f_m \Delta f\, t - \frac{\Delta f}{2}\right)\right) \tag{2.7}$$

The voltage received from a slow moving target delayed by a time T = 2R/c may be written

$$v_r = V_r \sin\left(2\pi f_0 t + 2\pi t\left(2 f_m \Delta f\, (t+T) - \frac{\Delta f}{2}\right)\right) \tag{2.8}$$

The received signal v_r and the transmitted signal v_t are heterodyned in a mixer to give a difference-frequency signal v_b. In the next section, *Matlab* [31] is used to simulate these signals in the time and frequency domain and to determine the best signal parameters to meet the design specifications [2].

2.3 Simulations

The software package, *Matlab [31]*, was used to write a program to simulate all the transmitted and received FM-CW radar signals in both the time and frequency domain. Different values for the parameters in (2.7) and (2.8) were chosen to determine the effect of each parameter on the radar system and enable the selection of the best design values for f_m, f_0 and Δf.

2.3.1 Ideal linear modulation

The ideal modulation frequency signal was chosen for the first few simulations where f_m is triangular, but the effect of the turn around region is not included. The first simulation was done by choosing f_0 = 2.5 GHz, R = 15 m, Δf = 100 MHz (or 4 % bandwidth) and f_m = 1 kHz. The simulated difference-frequency signal v_b, is shown in Figure 2-4 and Figure 2-5 for the time and frequency domain respectively. The envelope in the time domain graph represents the beat frequency signal. The high carrier frequency is equal to Δf and can be filtered out by a low pass filter (LPF). An FFT (Fast Fourier Transform) was performed on the time domain signal to view the frequency response shown in Figure 2-5, and Zero padding was used to improve the frequency spectrum. The vertical axis is normalized and represents only the difference in decibel (dB) between each peak value. It is interesting to see that all the side lobes are multiples of the modulation frequency. The next simulation was done by changing only the modulation frequency to f_m = 10 Hz as shown in Figure 2-6 and Figure 2-7. The only significant difference that resulted is that the beat frequency is 100 times smaller, f_b = 200 Hz, while the form remained largely unchanged. This is expected because, from the beat frequency equation (2.2), f_b and f_m are directly proportional.

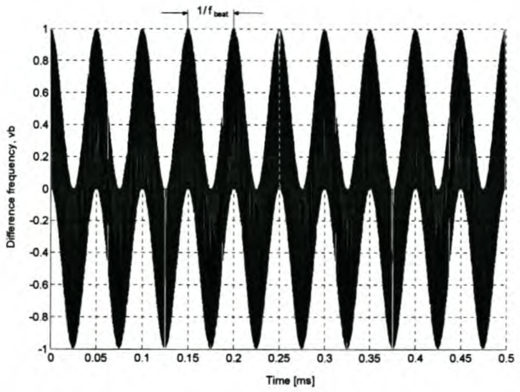

Figure 2-4 **Difference-frequency signal v_b – Time domain. f_m = 1 kHz.**

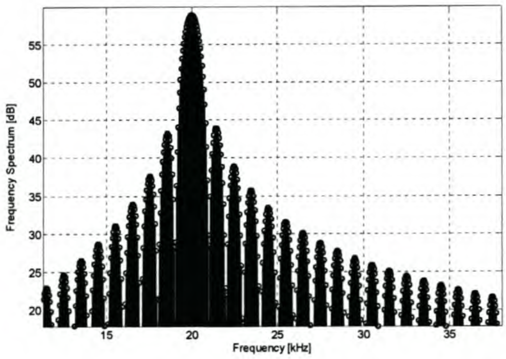

Figure 2-5 **Difference-frequency signal v_b – Frequency domain. f_m = 1 kHz, f_b = 20 kHz.**

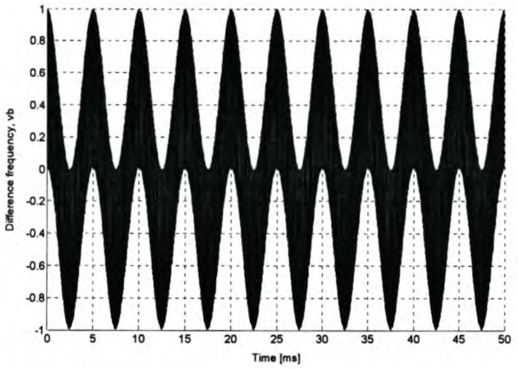

Figure 2-6 **Difference-frequency signal v_b – Time domain. f_m = 10 Hz.**

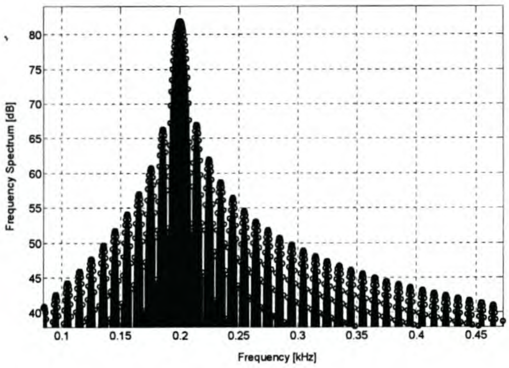

Figure 2-7 **Difference-frequency signal v_b – Frequency domain. f_m = 1 kHz, f_b = 200 Hz.**

The next three simulations were done with f_0 = 2.5 GHz, R = 15 m, f_m = 1 kHz and different values for Δf. The time-and frequency domain results are shown through Figure 2-8 to Figure 2-13. F_b is proportional to Δf as from equation (2.2) and thus changes correspondingly while f_m stays constant. The closer f_b is to f_m, the more difficult it becomes to distinguish it in the frequency domain until $f_b < f_m$ and f_b cannot be distinguished from the rest of the frequency spectrum (see Figure 2-13).

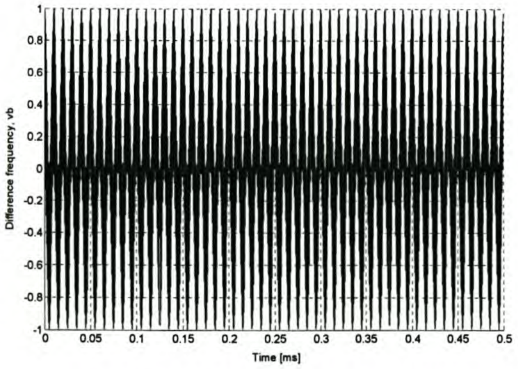

Figure 2-8 **Difference-frequency signal v_b – Time domain. Δf = 500 MHz.**

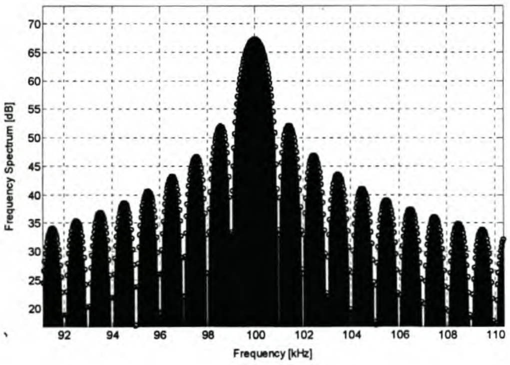

Figure 2-9 **Difference-frequency signal v_b – Frequency domain. Δf = 500 MHz, f_b = 100 kHz.**

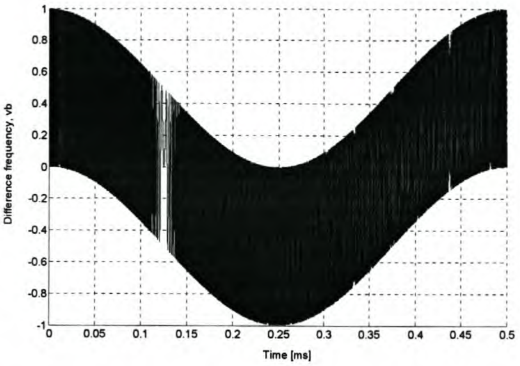

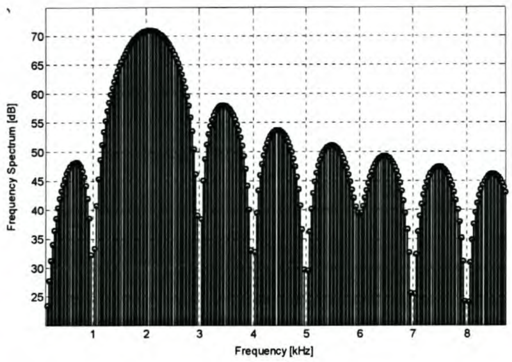

Figure 2-10 Difference-frequency signal v_b – Time domain. Δf = 10 MHz.

Figure 2-11 Difference-frequency signal v_b – Frequency domain. Δf = 10 MHz, f_b = 2 kHz.

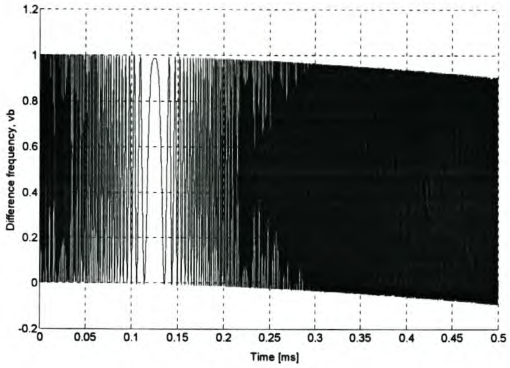

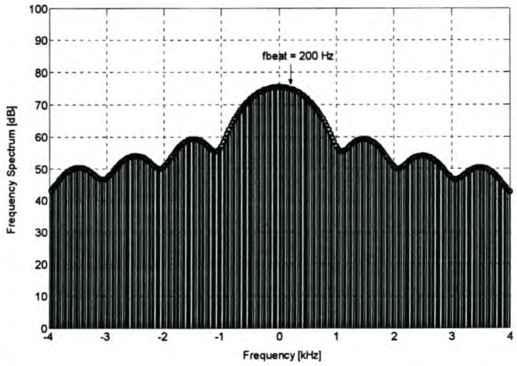

Figure 2-12 Difference-frequency signal v_b – Time domain. Δf = 1 MHz.

Figure 2-13 Difference-frequency signal v_b – Frequency domain. Δf = 1 MHz, f_b = 200 Hz < f_m.

The next four simulations were done with f_0 = 2.5 GHz, Δf = 100 MHz, f_m = 1 kHz and R = 1 m, 10 m, 25 m and 50 m respectively. The greater the target's range, the easier it is to distinguish the beat frequency from all the frequency lobes.

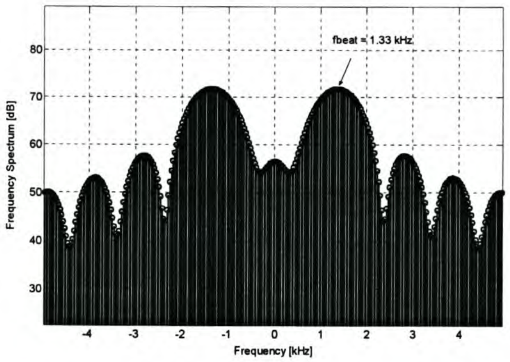

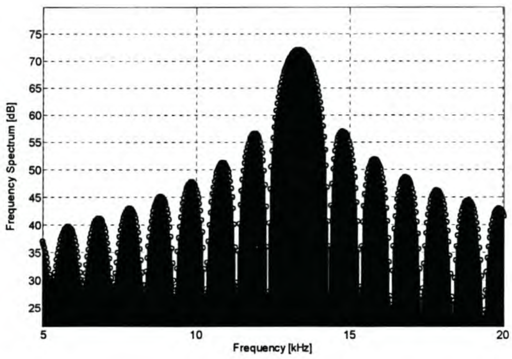

Figure 2-14 Difference-frequency signal v_b – Frequency domain. R = 1 m and f_b = 1.33 kHz.

Figure 2-15 Difference-frequency signal v_b – Frequency domain. R = 10 m and f_b = 13.33kHz.

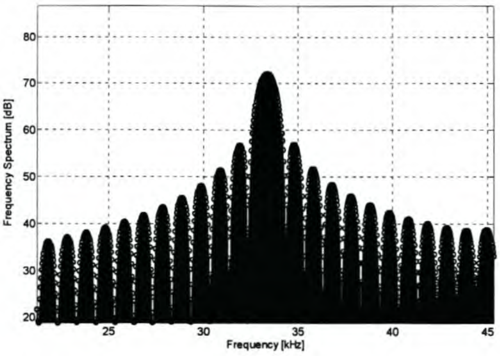

Figure 2-16 Difference-frequency signal v_b – Frequency domain. R = 25 and f_b = 33.3 kHz.

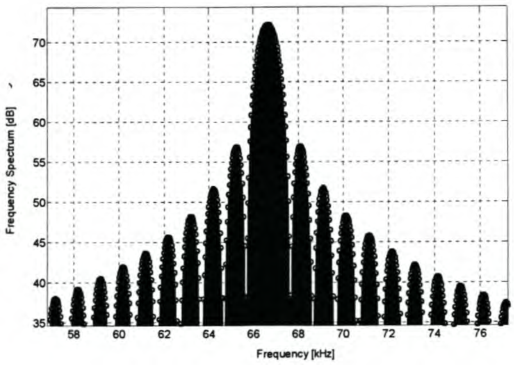

Figure 2-17 Difference-frequency signal v_b – Frequency domain. R = 50 m and f_b = 66.67 kHz.

2.3.2 Effect of the turn-around region

The previous simulations were done for linear modulation, ignoring the effect of the turn-around region of the beat note as discussed earlier in this section. The next simulation was done to simulate the effect of the turn-around region as shown through Figure 2-18 to Figure 2-21. The effect could not be seen for low modulation frequencies, but the separation between the transmitted and received VCO-frequencies as shown in Figure 2-18 increases with the modulation frequency or target range also increasing the turn-around region. The effect of the turn around region on the simulated beat frequency can also be seen in Figure 2-19. For this instance f_m = 100 kHz, R = 100 m and Δf = 10 MHz. The effect of the beat note on the time domain difference-frequency signal is shown in Figure 2-20 with the added normalized VCO frequencies. At every turn around region of the modulation frequency, the time domain signal is totally scrambled. The peak signal in the frequency domain (Figure 2-21) is not affected by the beat note, but there are some unwanted frequencies that appears to be close to the main peak and might become a problem during later measurements.

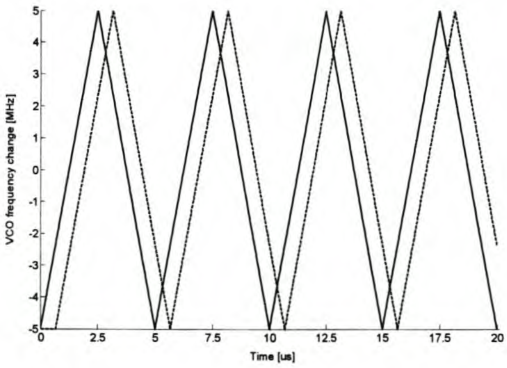

Figure 2-18 Simulation of the transmitted and received signal frequency change with triangular modulation f_m = 100 kHz

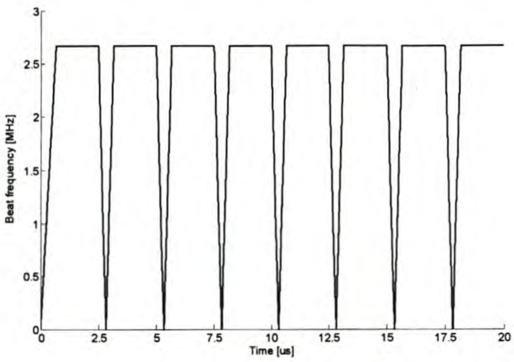

Figure 2-19 Simulated difference-frequency f_b and beat note Frequency vs time. f_b = 2.67 MHz.

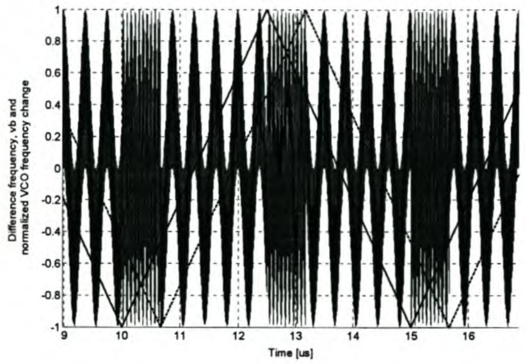

Figure 2-20 Effect of the beat note on the difference-frequency with triangular modulation f_m = 100 kHz – Time domain

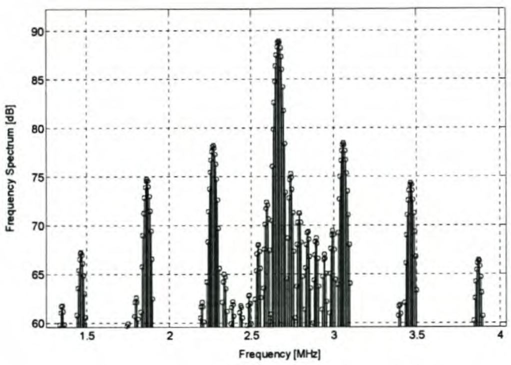

Figure 2-21 Effect of the beat note on the difference-frequency with triangular modulation f_m = 100 kHz – Frequency domain

In some radar systems where triangular modulation is used, the maximum range is limited by the modulation frequency. When the separation between the transmitted and the received frequencies increases to the point where the delay time is equal to half the modulation period the difference-frequency becomes zero. For further separation, f_b will increase from zero again, giving incorrect measurements. By using smaller modulation frequencies, the beat frequency decreases and due to the increase of the modulation period, it allows for a higher maximum range.

A few simulations were done by changing the carrier frequency f_c, but it had no influence on the difference-frequency.

2.3.3 Sinusoidal modulation

The transmitted signal can also be modulated sinusoidally as shown in Figure 2-22a. From basic trigonometry it is known that the difference between two sinusoidal waveforms with the same frequency delayed in time is a sinusoid, thus, the beat frequency will have the form of a sinusoidal signal with an absolute amplitude, since only the positive frequency spectrum is visible. The range R can be determined by taking the average or mean value of the beat frequency as shown in Figure 2-22b [2] [26].

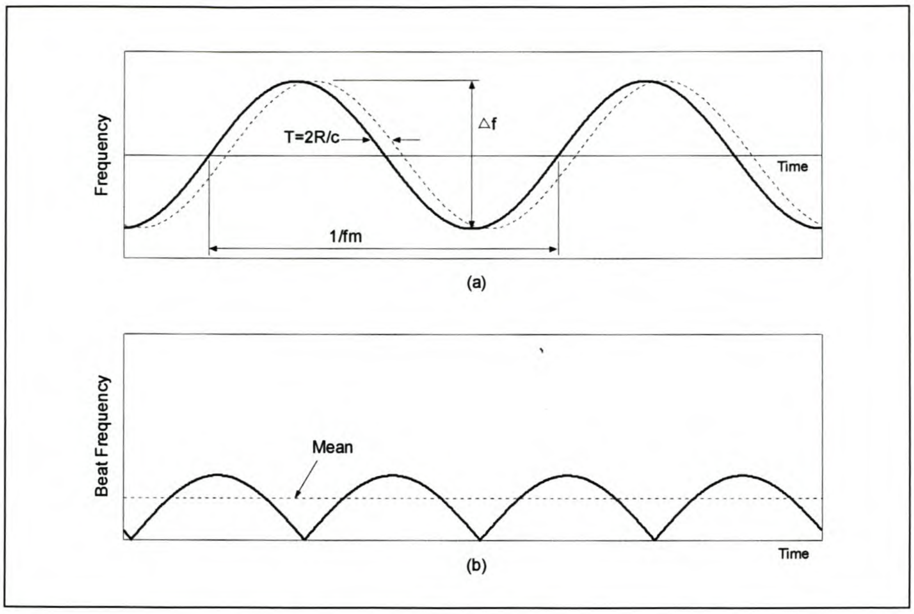

Figure 2-22: Frequency-time relationships with sinusoidal modulation in FM-CW radar.

The voltage waveform of the transmitted signal in Figure 2-22a. becomes

$$v_t=V_t\sin\left(2\pi f_0 t+\frac{\Delta f}{2f_m}\sin 2\pi f_m t\right) \quad (2.9)$$

The voltage received from a slow moving target is delayed by a time T = 2R/c and may be written as

$$v_r=V_r\sin\left(2\pi f_0(t-T)+\frac{\Delta f}{2f_m}\sin 2\pi f_m(t-T)\right) \quad (2.10)$$

The difference-frequency signal obtained after heterodyning v_t and v_r was also simulated in *Matlab* [31]. The following two figures show the simulated difference-frequency signal v_b in the time and frequency domain respectively with f_0 = 2.5 GHz, f_m = 1 kHz, Δf = 100 MHz and R = 15 m. The frequency of difference-frequency signal in Figure 2-23 changes with time as expected. The calculated mean value gives the beat frequency f_b = 6.67 kHz. Due to the non-linearity effect, there is no definite peak representing the beat frequency in the frequency spectrum. The disadvantage of sinusoidal modulation is that it requires more signal processing to determine the range and is not as accurate as linear modulation.

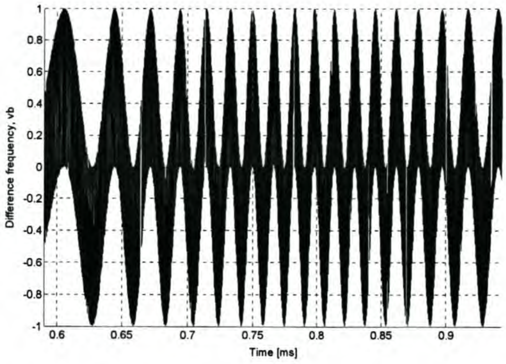

Figure 2-23 Simulation of the difference-frequency signal with sinusoidal modulation f_m = 1 kHz – Time domain.

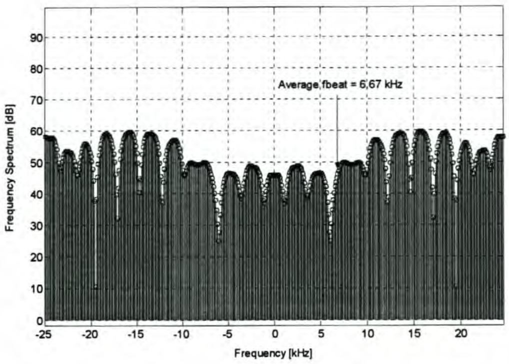

Figure 2-24 Simulation of the difference-frequency signal with sinusoidal modulation f_m = 1 kHz – Frequency domain.

2.4 Conclusion

A few conclusions could be made from the simulations. The ideal simulations showed that f_b must be greater than f_m, seeing that the smaller f_b becomes, the more difficult it is to measure in the frequency domain until it becomes impossible when $f_b < f_m$. A good ratio between the modulation-and beat frequency was chosen as 1:10 or $f_b > 10 \times f_m$. The only two parameters that influence this relationship are R and Δf. The first design parameter that needs to be specified is the minimum detectible range to determine the minimum deviation frequency Δf_{min}. The minimum range was not specified, but is chosen as R_{min} = 10 m and from (2.2) it gives Δf_{min} = 75 MHz. Choosing a higher Δf is better for measuring the beat frequency although Δf is limited by the available bandwidth and by the bandwidth of the antenna. The modulation frequency should be chosen according to the minimum and maximum beat frequency to simplify the filtering and signal processing needed to calculate the measured range. Given the specified range: 10 m < R < 30 m and Δf chosen as 100 MHz, the beat frequency can be expressed in terms of f_m: $13.3 f_m < f_b < 40 f_m$ and choosing f_{bMax} = 40 kHz, f_m becomes 1 kHz. Fortunately this modulation frequency is so low that the turn-around region has no visible effect on the difference-frequency signal as discussed in section 2.3.2. The maximum range limited by the modulation period is determined by setting the delay time in (2.1) equal to $0.5/f_m$ giving $R_{max} = T_m c/4$ = 75 km, which is much greater than the specified maximum range of 30 m.

The sinusoidal simulations illustrated that it will be the best to use linear modulation in this design, seeing that it is more accurate and does not need extra signal processing to determine the average beat frequency. The effect of the non-linearity of the VCO also plays an important role in measuring the beat frequency and will be discussed in detail in section 4.1.

3. System analysis

It is important to begin with an analysis of the whole radar system before deciding which specific components to use in the design. The analysis has to show the effect of each component on the different system parameters like loss, gain, cost, maximum transmitted and received power, and detectable range. An analysis program was written in the software package, *Delphi 6* [32] , which can be used to analyse, optimize and design an FM-CW radar system. This program is called *RadarOpt* and can be used by anyone with very basic radar knowledge (See the Appendix CD attached at the back of this document).

This chapter explains the design and working of this software analysis program in five sub-divisions. Section 3.1 introduces the user to the basic structure of the program while explaining the user interface. Section 3.2 explains how to run an analysis and includes the design logic used to attain specific results. Extra functions were added in the software and are explained in section 3.3. The error and warning messages and data recall is discussed in section 3.4, ending the chapter with a short conclusion in section 3.5.

3.1 User interface

RadarOpt is written with a graphic user interface, with every component linked together in block-diagram form representing the whole radar system. Each component has different design parameters that can be changed by clicking on the component box. A window appears with the parameters that can be changed as is shown in Figure 3-1 for the VCO.

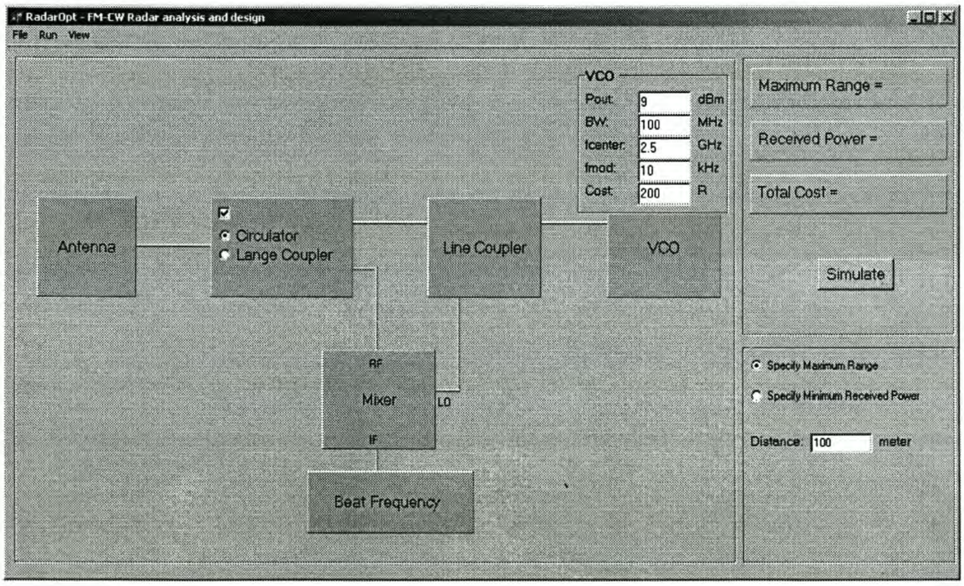

VCO
Pout: 9 dBm
BW: 100 MHz
fcenter: 2.5 GHz
fmod: 10 kHz
Cost: 200 R

☑
● Circulator
○ Lange Coupler

● Specify Maximum Range
○ Specify Minimum Received Power
Distance: 100 meter

Figure 3-1: *RadarOpt* user interface.

All the component windows can be opened and changed simultaneously as shown in Figure 3-2 and can be closed by again clicking on each component. The small box between the *Line Coupler* and *Mixer* is an *RF-amplifier* that was added to raise the LO power level to 10 dBm for normal mixer operation. The amplifier properties are shown in a window just below the VCO which behaves in the same manner as the other component property windows. More amplifiers can be inserted between all the component boxes except between the *Antenna* and *Circulator/Lange coupler* as it is a two-way line. This is done by simply clicking on the connecting line where the amplifier is desired and can be removed by clicking next to it on the same line. In Figure 3-3, all the property windows are closed, *Amp-4* is removed and two extra amplifiers are added showing *Amplifier 3*'s properties.

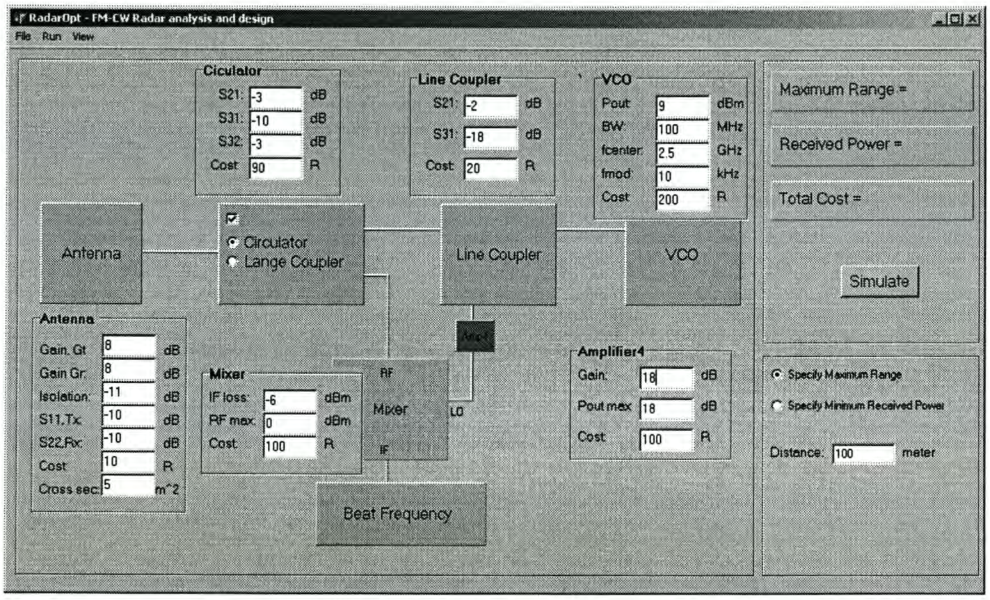

Ciculator
S21: -3 dB
S31: -10 dB
S32: -3 dB
Cost 90 R

Line Coupler
S21: -2 dB
S31: -18 dB
Cost 20 R

VCO
Pout 9 dBm
BW 100 MHz
fcenter 2.5 GHz
fmod 10 kHz
Cost 200 R

Maximum Range =
Received Power =
Total Cost =

☑
● Circulator
○ Lange Coupler

Antenna
Gain, Gt 8 dB
Gain Gr 8 dB
Isolation -11 dB
S11,Tx -10 dB
S22,Rx -10 dB
Cost 10 R
Cross sec 5 m^2

Mixer
IF loss -6 dBm
RF max 0 dBm
Cost 100 R

Amplifier4
Gain 18 dB
Pout max 18 dB
Cost 100 R

● Specify Maximum Range
○ Specify Minimum Received Power
Distance: 100 meter

Figure 3-2: *RadarOpt* user interface showing all the component windows.

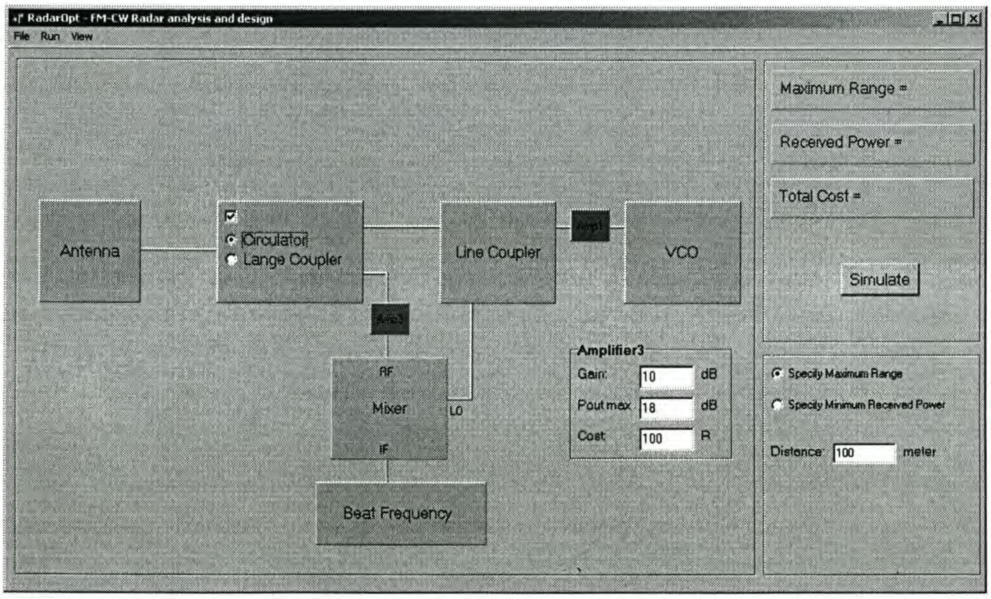

Maximum Range =
Received Power =
Total Cost =

☑
● Circulator
○ Lange Coupler

Amplifier3
Gain 10 dB
Pout max 18 dB
Cost 100 R

● Specify Maximum Range
○ Specify Minimum Received Power
Distance: 100 meter

Figure 3-3: *RadarOpt* – Amp4 removed and Amp1 and Amp3 added.

The radar can be designed either with two separate antennas or with a single antenna. To use two separate antennas the *Circulator/Lange* coupler box needs to be closed by clicking on the small tick box. The component moves to the background and two lines directly connect the *Antenna* box to the line coupler and mixer. The coupling-parameter $|S_{21}|$ and each antenna's gain and reflection have to be specified in the amplifier property window as shown in Figure 3-4. Otherwise, the second antenna will be assumed to have the same properties as the first one.

When using a single antenna, the user can choose between the Circulator or Lange coupler by selecting the appropriate bullet. These two components will be explained in more detail in chapter 4, but their basic function is to separate the transmitted and received signals. The Lange coupler has four ports of which two are connected to a circularly polarized antenna and the other two are connected to the *Line Coupler* and *Mixer* respectively. Thus an extra line is added between the *Antenna* and *Lange coupler* as shown in Figure 3-5

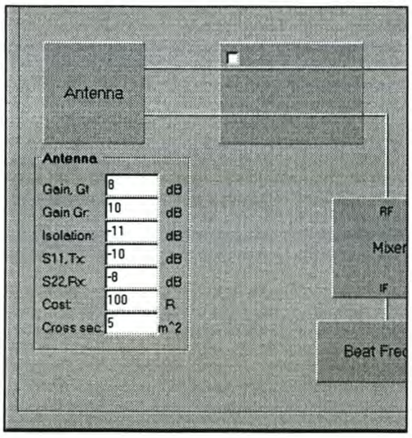

Antenna
Gain, Gt: 8 dB
Gain Gr: 10 dB
Isolation: -11 dB
S11,Tx: -10 dB
S22,Rx: -8 dB
Cost: 100 R
Cross sec: 5 m^2

Figure 3-4 Illustration of a two antenna system.

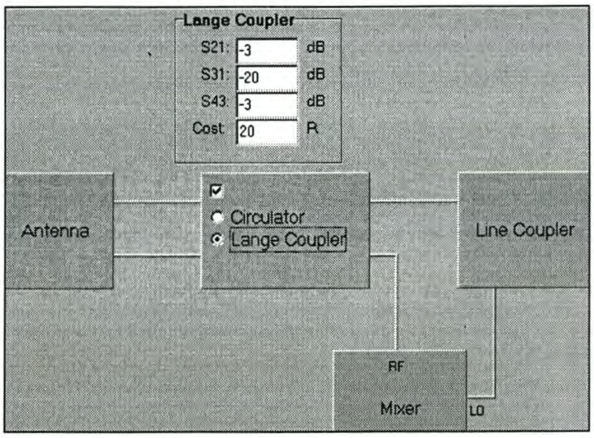

Lange Coupler
S21: -3 dB
S31: -20 dB
S43: -3 dB
Cost: 20 R

☑
○ Circulator
● Lange Coupler

Figure 3-5 Illustration of a single antenna system using a Lange coupler.

3.2 Analysis

RadarOpt can be used to simulate the total system cost, maximum detectible range and the minimum received power reflected from the target. The user can choose to simulate the maximum range by specifying the minimum received power or vice versa by choosing the appropriate bullet in the right hand corner and entering the desired value. The analysis begins by clicking the 'Simulate' button and the results are shown in the upper right hand corner of the screen, as illustrated in Figure 3-6 for the specified maximum range of 50 m.

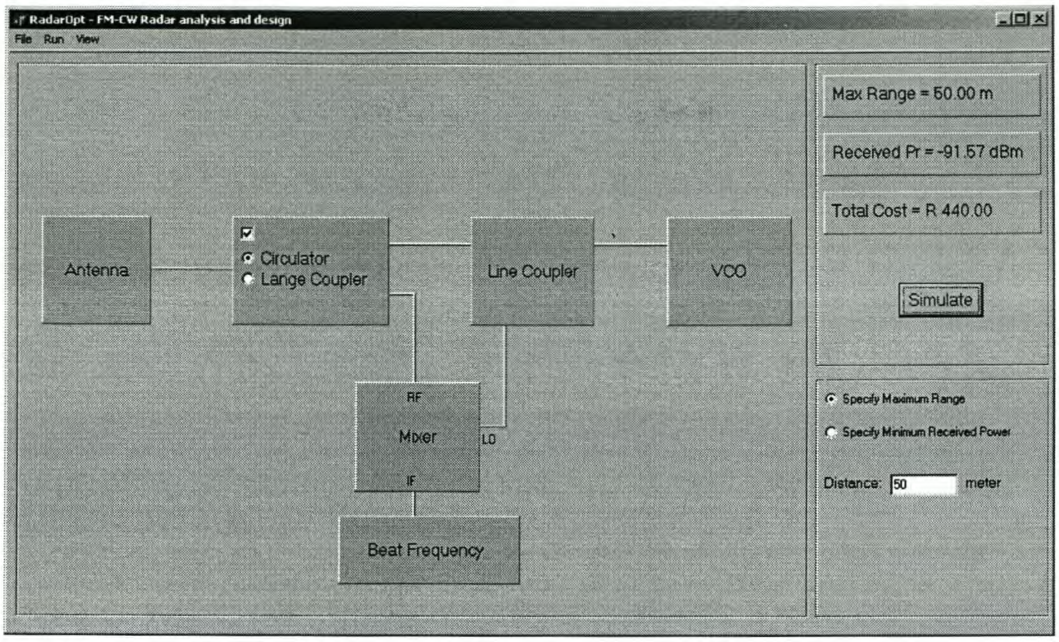

Max Range = 50.00 m

Received Pr = -91.57 dBm

Total Cost = R 440.00

● Specify Maximum Range

○ Specify Minimum Received Power

Distance: 50 meter

Figure 3-6: ***RadarOpt*** **analysis for minimum received power with a specified maximum range.**

The analysis is done by calculating the total transmitted power from the gain or loss specified for each component. The component parameters can be altered at any time if the desired results are not attained. The *radar equation,* [5 p673-674] [23]

$$P_r = \frac{P_t G^2 \lambda^2 \sigma}{(4\pi)^3 R^4}, \tag{3.1}$$

is used during each simulation to calculate the maximum range or minimum received power where P_t is the total transmitted power, G is the antenna gain, λ is the wavelength of the transmitted signal in free space, σ is the radar cross section of the target, R is the maximum range and P_r is the minimum received power. When two separate antennas are used, the G^2 factor in (3.1) is replaced by G_rG_t where G_r and G_t are the receiving and transmitting antenna gains respectively [5 p673-674].

3.3 Extra functions

RadarOpt has three special functions:

1) Beat frequency calculation
2) Antenna gain calculation and
3) Show power levels.

3.3.1 Beat frequency calculation

The radar beat frequency can be calculated by clicking on the 'Beat Freq Calculation' command under 'Run' in the top menu bar. A window will appear in the middle of the screen, shown in Figure 3-7. Equation (2.2) is used to calculate the beat frequency from the entered values, rendering the result in the answer box below as shown in Figure 3-8.

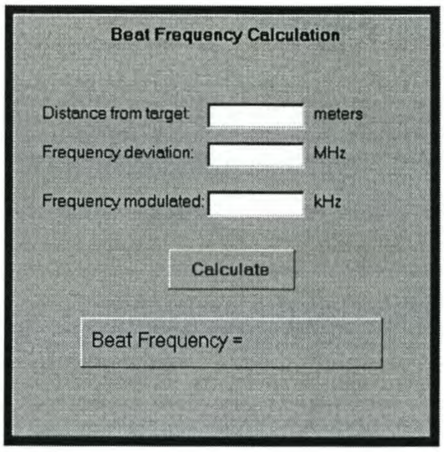

Beat Frequency Calculation

Distance from target: meters

Frequency deviation: MHz

Frequency modulated: kHz

Beat Frequency =

Figure 3-7 Beat Frequency Calculation window.

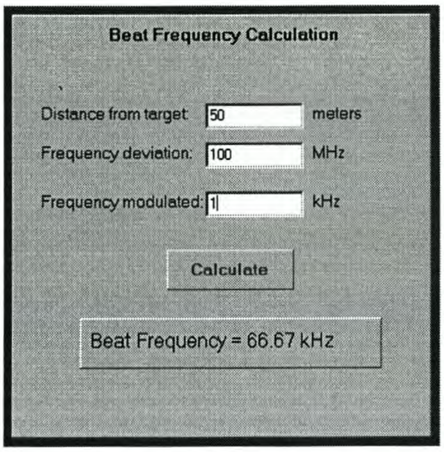

Beat Frequency Calculation

Distance from target: 50 meters

Frequency deviation: 100 MHz

Frequency modulated: 1 kHz

Beat Frequency = 66.67 kHz

Figure 3-8 Example of the Beat Frequency Calculation.

3.3.2 Antenna gain calculation

The antenna gain function was added to *RadarOpt* to calculate antenna gain from the two antenna measurements inside an anechoic chamber. The function is also found under 'Run' in the top menu bar. The window that appears on the screen is shown in Figure 3-9 and the requested parameter values are used in the *friis power transmission equation* [6 p79] [27 p 604]

$$P_r = P_t \frac{G_t G_r \lambda^2}{(4\pi R)^2} \tag{3.2}$$

to calculate the antenna gain. R is the distance between the two antennas under test and G_t and G_r are the two antennae gains respectively. If two identical antennas were tested, the gain will be equal and G_t needn't be specified. When an $|S_{21}|$ measurement is done, the values for the received and transmitted power, P_r and P_t should be left empty. The relationship between the antenna S parameters and the transmitted and received power is given [5 p608-609],

$$\frac{P_r}{P_t} = \frac{|S_{21}|^2}{(1-|S_{11}|^2)(1-|S_{22}|^2)} \tag{3.3}$$

Each antenna is assumed to be well matched thus, ignoring $|S_{11}|$ and $|S_{22}|$, in (3.3) and (3.2) becomes

$$|S_{21}|^2 = \frac{G_t G_r \lambda^2}{(4\pi R)^2} \tag{3.4}$$

RadarOpt was used to calculate the gain of a patch antenna at 2.5 GHz. The second antenna was a horn with a known gain of 10 dB and the distance was given R = 5 meters. The measured $|S_{21}|$ = -38 dB giving the patch antenna gain G_r = 6.4 dB (See Figure 3-10).

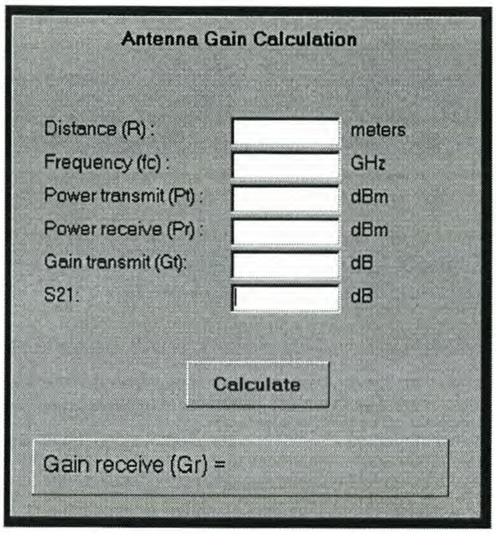
Antenna Gain Calculation

Distance (R): ☐ meters
Frequency (fc): ☐ GHz
Power transmit (Pt): ☐ dBm
Power receive (Pr): ☐ dBm
Gain transmit (Gt): ☐ dB
S21: ☐ dB

Gain receive (Gr) =

Figure 3-9 Antenna Gain Calculation window.

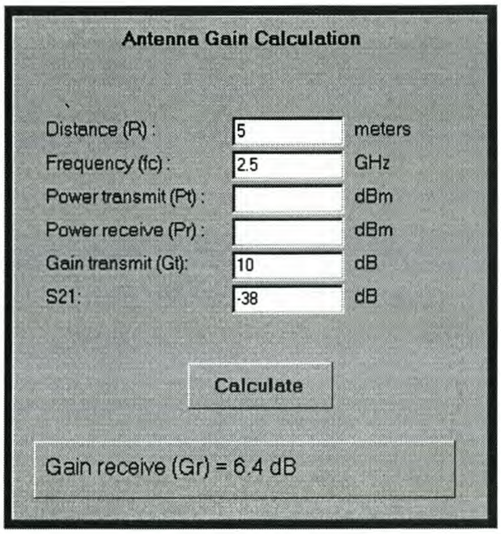
Antenna Gain Calculation

Distance (R): 5 meters
Frequency (fc): 2.5 GHz
Power transmit (Pt): ☐ dBm
Power receive (Pr): ☐ dBm
Gain transmit (Gt): 10 dB
S21: -38 dB

Gain receive (Gr) = 6.4 dB

Figure 3-10 Example of an Antenna Gain Calculation

3.3.3 Show Power Levels

This function, found under the main menu bar, 'View', was added for the user to view the power level of the signals at the input and output ports of the each component. The power level at each port is calculated and displayed as shown in Figure 3-11. The extra value above the mixer gives the total coupled power at the RF-port in green. When this value exceeds the mixer RF-port power limit, a red warning light goes on. The 'Hide power levels' command hides all the power levels.

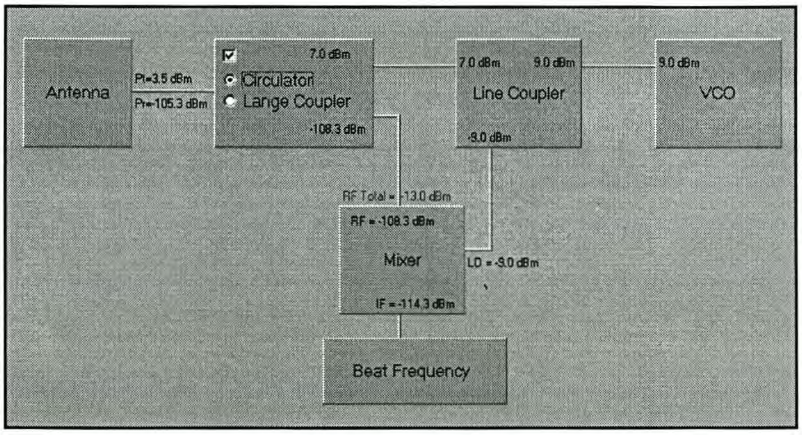

Figure 3-11. Demonstration of the 'Show power level' function.

3.4 Error messages and data recall

Before closing the program, the design can be saved using the ‘Save as’ command in the ‘File’ menu. The parameters of each component are saved in a text file and can later be recalled by the ‘Open’ command. *RadarOpt* gives very basic error messages if the wrong values or filenames are entered and is overall a very stable program. There are a few warning messages which indicate when a component is driven beyond saturation, i.e. if an amplifier clips, the used output power is limited to its maximum output power and the component colour changes to red. It changes back to normal when the input power is lowered.

3.5 Conclusion

RadarOpt gives a good idea of what should be expected from each component to achieve a reasonable design. It was used during the rest of the design process to analyze each component in the system. It was also used to calculate the expected power levels before each measurement.

4. Radar components

Prior to the design of a new radar system, individual component assessment is necessary as understanding each component's function and behaviour is crucial in eliminating unforeseen system errors. Some radar modules are designed and built from fundamental theory to reduce the cost of the final system. Similar components were compared on the basis of their contribution to the system's performance.

This chapter has five sections in which each radar system component will be discussed. Section 4.1 focuses on the *Voltage Controlled Oscillator (VCO)*, examining its stability and linearity. Frequency signal simulations were done to show the effect of the VCO's non-linear characteristics on the measured time and frequency response. Section 4.2 discusses the complete design process of the *Coupled Line*. Its theory and function in the system is examined and it is explained how a new coupled line was designed, built and measured. Section 4.3 deals with the essential radar system component that is designed to isolate the transmitted and received signals. The *Circulator* and *Lange coupler* were considered and are discussed separately. More attention is given to the Lange coupler as the way in which it is used in the system is unusual and relatively new. Some of the Lange coupler theory could not be found in literature, making it a bit more challenging. This component's operation is explained in detail in this section. The mixer is discussed in section 4.4 and section 4.5 gives a short conclusion of the chapter. The antenna is not mentioned in this chapter as a lot more attention was given to its simulation and design which is explained in the chapter 5.

4.1 Voltage Controlled Oscillator (VCO)

The operation of an FM-CW radar is based on, by knowing how the transmitted frequency is changed as a function of time, the beat frequency can accurately be determined. If the actual transmitted frequency signal is non-linear, the detected range will be inaccurate. The linearity of the VCO determines the accuracy of the radar system and is defined by [7]

$$L=\frac{\text{Slope}_{max}-\text{Slope}_{min}}{\text{Slope}_{min}} \tag{4.1}$$

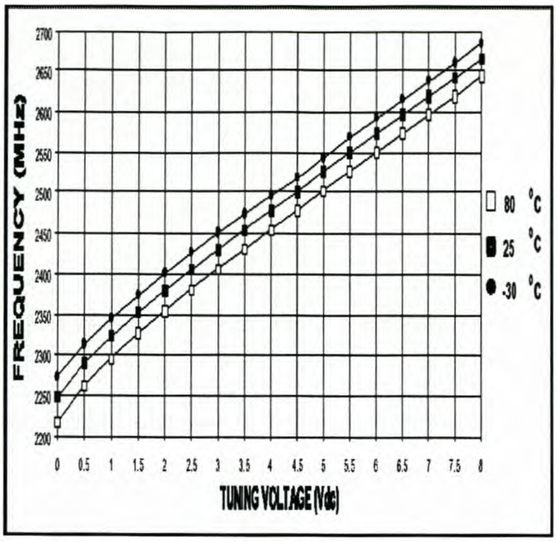

Figure 4-1 Z-Comm VCO - Frequency vs tuning voltage.

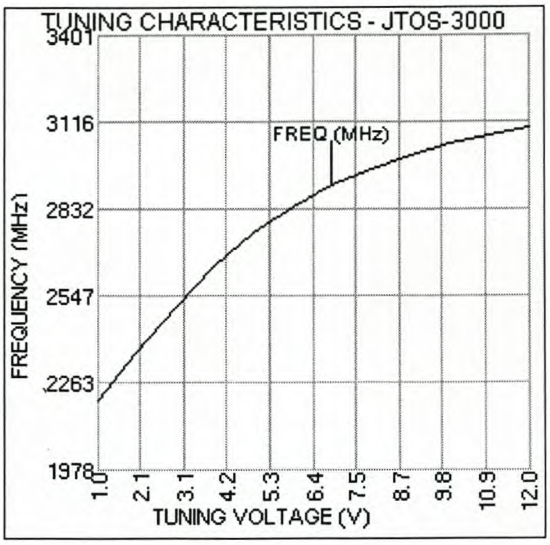

Figure 4-2 MCL VCO - Frequency vs tuning voltage.

where Slope_{max} and Slope_{min} are the maximum and minimum gradients of the measured non-linear VCO signal. This is determined by measuring the frequency against tuning-voltage. Two available fixed VCO models are compared, namely Z-Communications' (Z-COMM) V807ME01 and Mini-Circuits' (MCL) JTOS-J3000. The linearity curves of both models as found in their datasheets, are shown in Figure 4-1 and Figure 4-2 respectively, but are not easily comparable as the frequency axes differ in range.

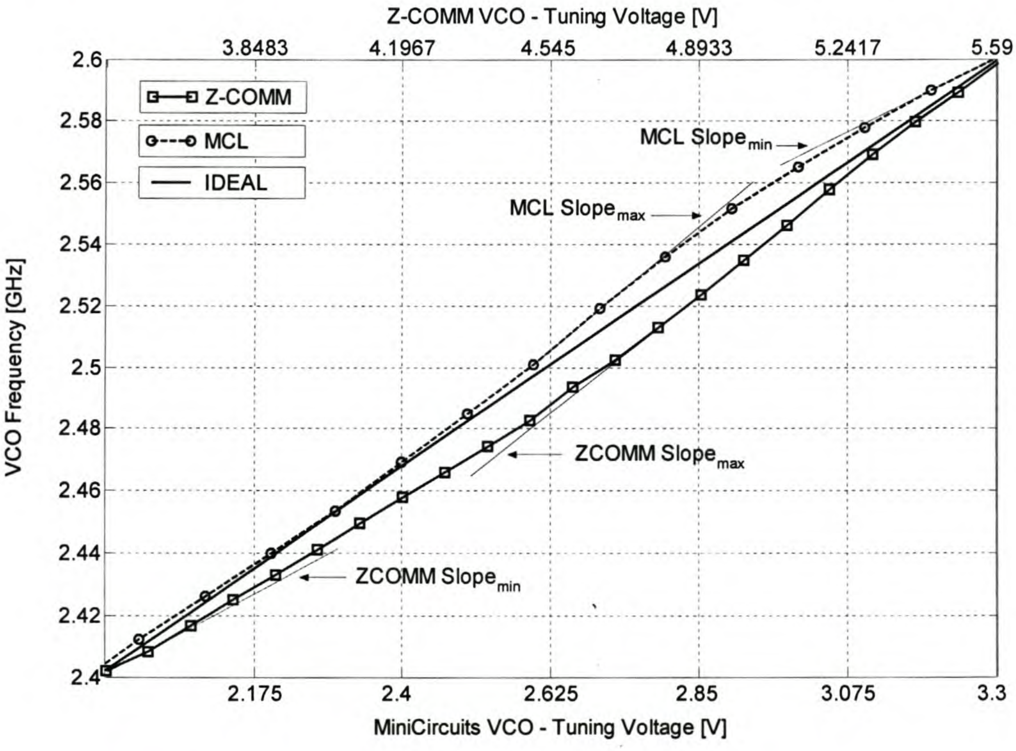

Figure 4-3: Measured linearity of the Z-COMM and MCL VCO 's.

To solve this problem, each VCO was measured over a narrower frequency band (2.4 – 2.6 GHz) to inspect how the non-linearity would influence the accuracy of the radar system. These measurements are displayed in Figure 4-3. The linearity curves are plotted on the same frequency axis using the top and bottom axes to distinguish between the tuning voltages, which were scaled to fit on the same grid. The solid line represents the ideal linear curve and the measured maximum and minimum gradients of each VCO are indicated on the graph. These gradients are used in (4.1) to determine the linearity of both VCO's giving $L_{Z\text{-}COMM} = 0.58$ % and $L_{MCL} = 0.68$ % with $L = 0$ for perfect linearity.

The effect of the VCO's non-linearity on the measured radar difference-frequency signal can be simulated by using the same method as explained in section 2.3 for a perfectly linear VCO signal. A new non-linear VCO signal using triangular modulation is formulated in *Matlab* [31] by using the measured values of the Z-COMM and MCL VCOs. The negative influence on the difference-frequency signal as a result of the non-linearity of the VCOs can clearly be seen when comparing the time and frequency domain simulations for the ideal case in Figure 2-4 and Figure 2-5 with the non-linear simulations of the Z-COMM and MCL VCOs shown in Figure 4-4 to Figure 4-9. The frequency spectrums of both VCOs give a vague indication of the beat frequency. The difference-frequency signal is spread forming a band of frequencies that masks the desired beat frequency. The broadened difference-frequency spectrums of both VCOs are shown in Figure 4-8 and Figure 4-9 giving a closer view of the non-linearity effect. The beat frequency can be distinguished by looking at the frequency spectrum. This measurement, however, will be more challenging and less accurate when using a frequency counter or oscilloscope to determine the beat frequency.

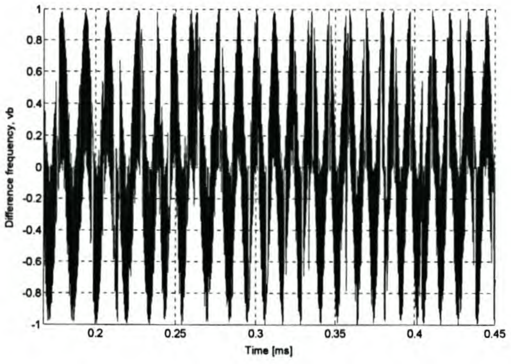

Figure 4-4 Non-linear effect of the Z-COMM VCO. Time domain difference-frequency signal simulation.

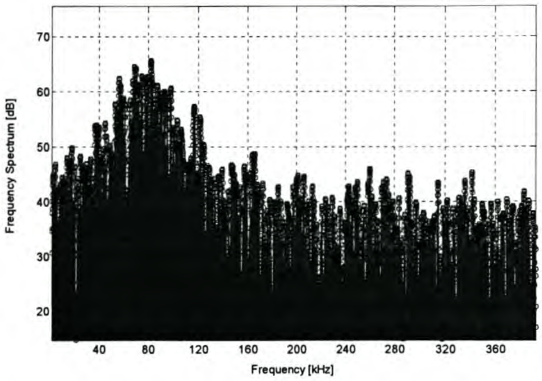

Figure 4-5 Non-linear effect of the Z-COMM VCO. Frequency spectrum of the difference-frequency signal.

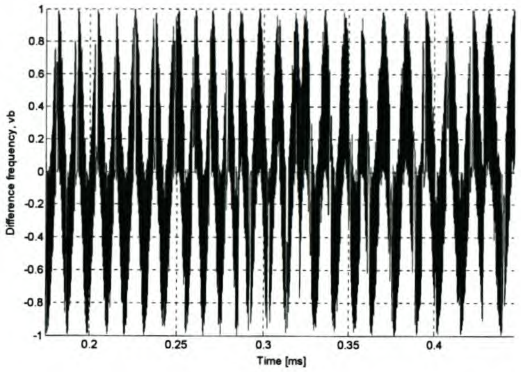

Figure 4-6 Non-linear effect of the MCL VCO. Time domain difference-frequency signal simulation.

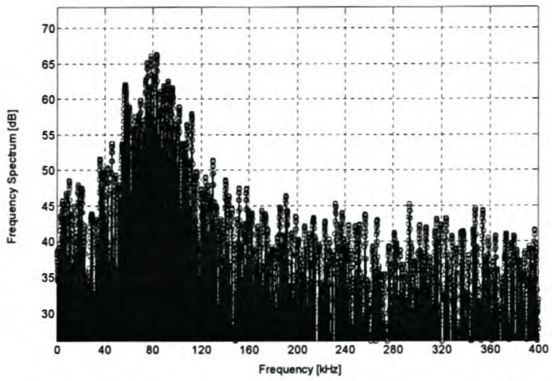

Figure 4-7 Non-linear effect of the MCL VCO. Frequency spectrum of the difference-frequency signal.

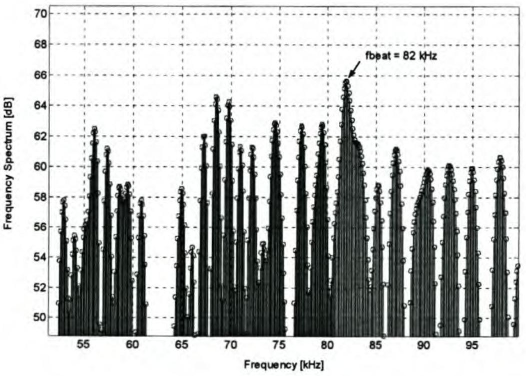

Figure 4-8 Enlarged Z-COMM frequency spectrum.

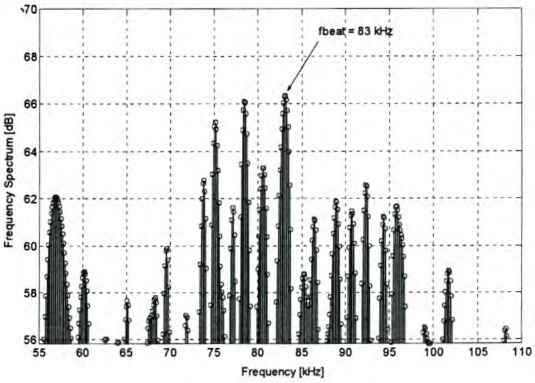

Figure 4-9 Enlarged MCL frequency spectrum.

To conclude:

- The VCO's non-linearity does lower the accuracy of the beat frequency measurement.
- To linearize the VCO a phase lock loop (PLL) must be implemented but is not feasible, as it overcomplicates the FM-CW radar system and makes it less cost efficient.
- Some of the radar system's accuracy has to be sacrificed for cost efficiency and simplicity. The degree of accuracy loss, however, can only be determined after the system measurements.
- The two measured VCO's have nearly the same non-linear effect on the system and hence the lower cost, the Z-COMM VCO, was chosen for the final design.

4.2 Coupled Line

The output signal of the VCO has to be divided between the mixer and the antenna. This is made possible by using a coupled line to couple a fraction of the VCO signal which will be amplified and used to drive the LO-port of the mixer. This simple cost efficient structure is shown in Figure 4-10 [5 p389-393].

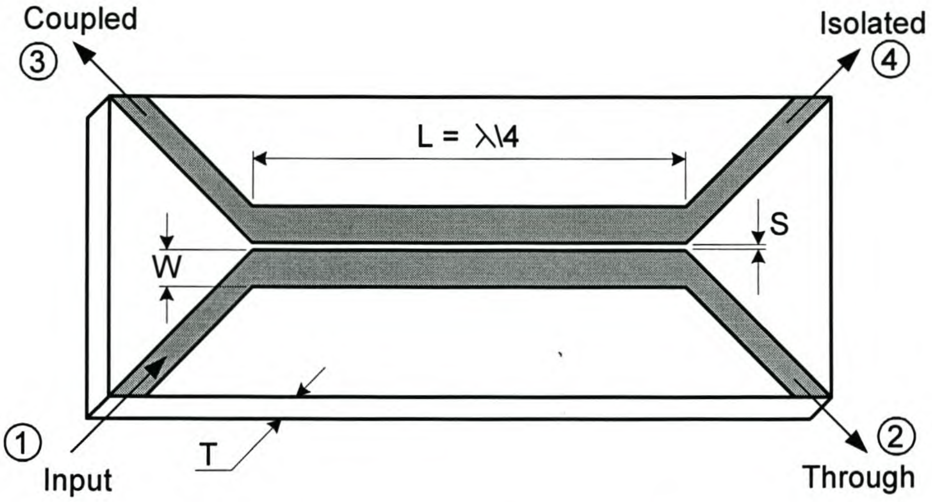

Figure 4-10: A single section coupled line – Geometry and port designations.

A coupled line with -10 dB coupling and center frequency of f_0 = 2.5 GHz was designed to be introduced in the existing system. First, the characteristic impedances were calculated from (4.2) and (4.3) [8]

$$Z_{0e} = Z_0\sqrt{\frac{1+C}{1-C}} \tag{4.2}$$

$$Z_{0o} = Z_0\sqrt{\frac{1-C}{1+C}} \tag{4.3}$$

with coupling factor, C = -10 dB = 0.316 and Z_0 = 50 Ω giving Z_{0e} = 69. 4 Ω and Z_{0o} = 36.1 Ω. The length of each line is one quarter wavelength of the center frequency in the substrate medium. Fabrication is difficult if a thin substrate with high dielectric constant ε_r is used because this will result in small line-width and spacing. The chosen substrate for this design is the *RT/duroid 5870*. This has a relatively low ε_r = 2.33 and low loss tangent tan δ = 0.0012, substrate thickness T = 0.787 mm and cost of 72 cent/ cm^2. The substrate used in the design is double the standard thickness of 2 x 0.787 mm = 1.574 mm [8] [5 p389-393].

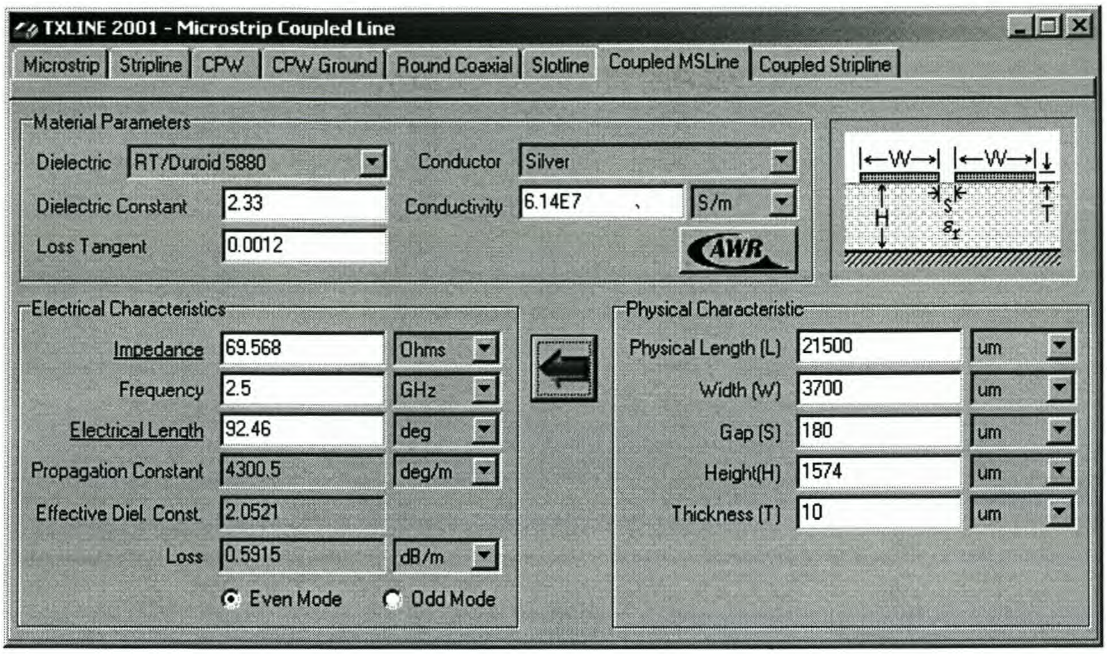

Dielectric: RT/Duroid 5880
Dielectric Constant: 2.33
Loss Tangent: 0.0012
Conductor: Silver
Conductivity: 6.14E7 S/m

Impedance: 69.568 Ohms
Frequency: 2.5 GHz
Electrical Length: 92.46 deg
Propagation Constant: 4300.5 deg/m
Effective Diel. Const.: 2.0521
Loss: 0.5915 dB/m
● Even Mode ○ Odd Mode

Physical Length (L): 21500 um
Width (W): 3700 um
Gap (S): 180 um
Height(H): 1574 um
Thickness (T): 10 um

Figure 4-11: *Txline* is used to compute the line-width and line-spacing for equivalent characteristic impedances.

An interactive transmission line calculator included in the *Microwave Office Suite* [22], *Txline* [9] (Figure 4-11) was used to find the equivalent line-width and line-spacing S to match the calculated characteristic impedances Z_{0e} and Z_{0o}. The effective ε_r = 2.05, was simulated by *Txline* and was used to calculate the quarter wavelength, $\lambda/4 = \frac{c}{4f\sqrt{\varepsilon r}} = 21.5\ \text{mm}$. The latter is equal to the line length L. The computed width and line-spacing for the design were W = 3.7 mm and S = 0.18 mm respectively.

The design was simulated in *Microwave Office* [22] and the coupling between the ports is shown in Figure 4-12. The coupled power at the *coupled* port is -10 dB, as expected, and insertion loss at the *through* port is -0.51 dB. The simulated reflection at all ports is below –30 dB.

The manufactured coupled line is shown in Figure 4-12 and the measured coupling and reflection S parameters are shown in Figure 4-14 and Figure 4-15 respectively. The impedance at the ports of the measured coupled line was well matched to 50 Ω over the required frequency band. Both the *input* and *through* ports had reflection coefficients below -27 dB. The *coupled* port was matched to an impedance of 50 Ω at a lower center frequency of 2.4 GHz, and had a reasonable reflection coefficient below -10 dB for the total measured frequency band and $|S_{33}|$ = -19 dB at the desired center frequency (2.5 GHz). This slight impedance mismatch at the desired center frequency is attributed to the difference between the real and the simulated substrate dielectric constant. The *Txline* [9] simulation indicated a remarkably low effective ε_r of 2.05 from which the line length was computed. The measured *coupled* port reflection indicates that a higher effective ε_r had to be used in the calculation. This would result in a shorter line length which would change the impedance of the *coupled* port to be matched to 50 Ω at a higher center frequency of 2.5 GHz.

The measured insertion loss between the *input* and *through* ports was -0.51 dB as expected and the coupling between the *input* and *coupled* ports was -11 dB. This 1 dB difference from the expected -10 dB coupling is attributed to the sensitivity of the coupling factor C to variation of the substrate thickness. Two *RT/duroid* substrates were glued together to achieve the correct thickness for the design and this might have slightly changed the characteristic impedances that would effect the coupling factor. This difference should not effect the system as the *coupled* port output signal will be amplified above the minimum power needed to drive the LO- port of the mixer.

To conclude, the measured coupled line should perform well in the radar system and the small difference between the measured and simulated S parameters should not influence the system.

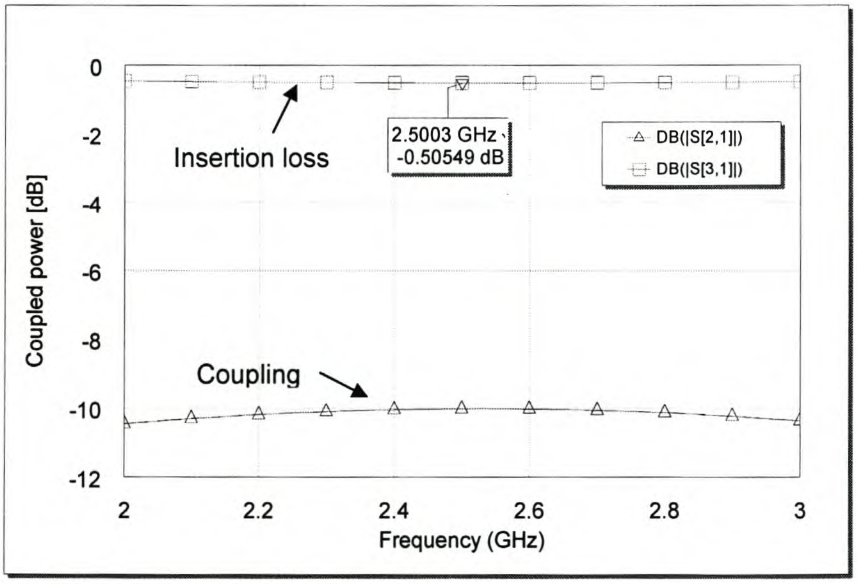

Figure 4-12: Simulated coupling and insertion loss between the ports of the coupled line.

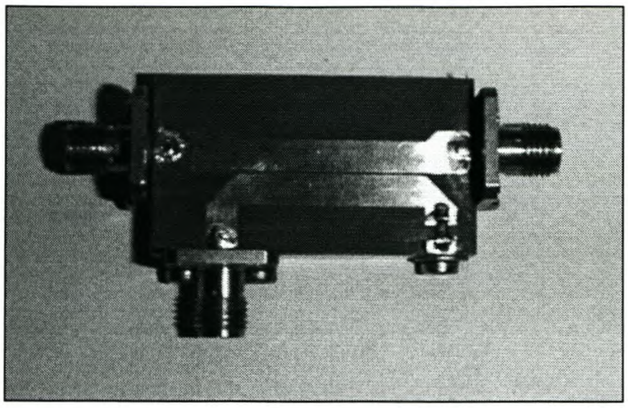

Figure 4-13: Photograph of the manufactured coupled line that will be used in the FM-CW radar.

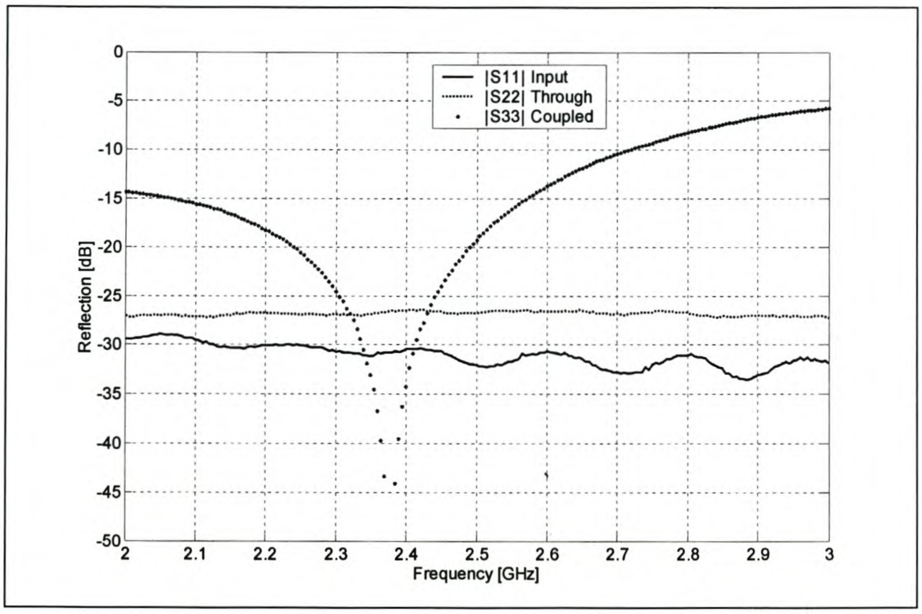

Figure 4-14: Measured reflection at the input, through and coupled ports of the coupled line.

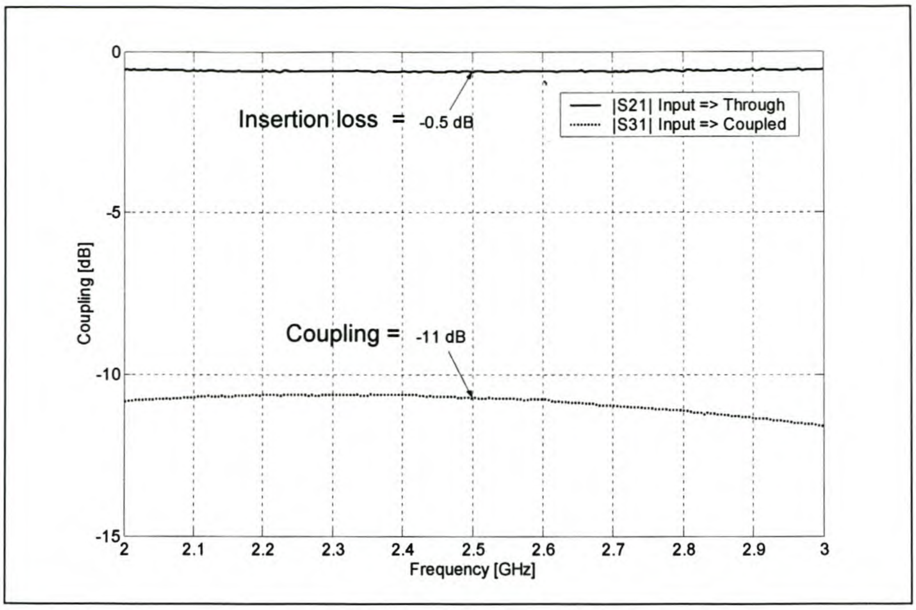

Figure 4-15: Measured coupling and insertion loss between the coupled line input and output ports.

4.3 Circulator and Lange Coupler

When using a single transmit and receive antenna in an FM-CW radar system it is important to isolate the transmitted and received signals to prevent the mixer from being saturated by the coupled transmitted power. This section discusses two methods that can be used to isolate transmitter and receiver signals by using a circulator or Lange coupler.

4.3.1 The Circulator

The circulator is a three-port device that can be practically lossless and matched at all ports. The scattering matrix of an ideal clockwise circulator has the following form: [5 535-537],

$$[S]=\begin{bmatrix} S_{11} & S_{12} & S_{13} \\ S_{21} & S_{22} & S_{23} \\ S_{31} & S_{32} & S_{33} \end{bmatrix} = \begin{bmatrix} 0 & 0 & 1 \\ 1 & 0 & 0 \\ 0 & 1 & 0 \end{bmatrix} \qquad (4.4)$$

which shows that power can flow from ports 1 to 2, 2 to 3 and 3 to 1, but not in reverse direction, since S_{12} , S_{23} and S_{32} are zero. Figure 4-16 demonstrates the function of the circulator in the FM-CW system. The transmitted power P_t flows from port 1 to 2 towards the antenna while being isolated from port 3. The power received from the antenna P_r flows from port 2 to port 3 into the mixer-RF port. The measured reflection, insertion loss and isolation of the *Nova 0245CAS* circulator is shown in Figure 4-17 and Figure 4-18.

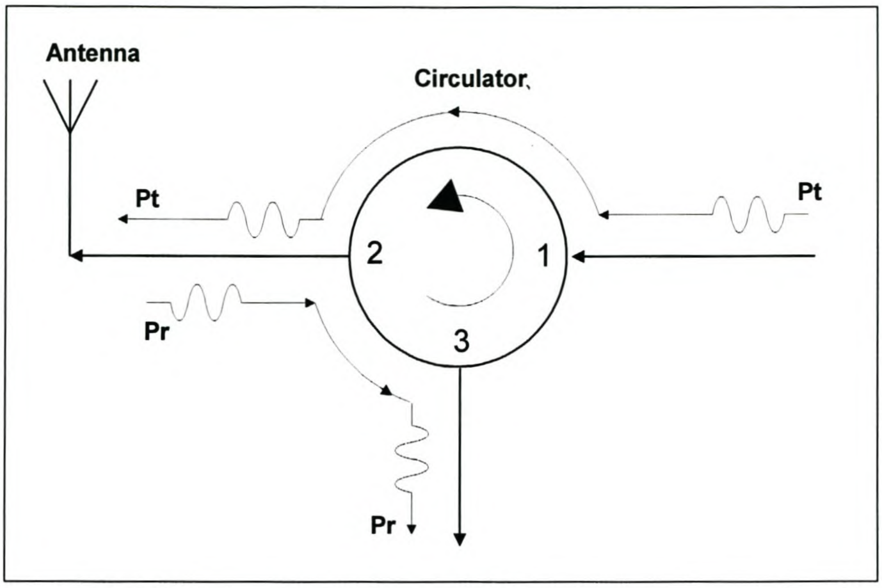

Figure 4-16: Basic operation of the Circulator in the FM-CW radar system.

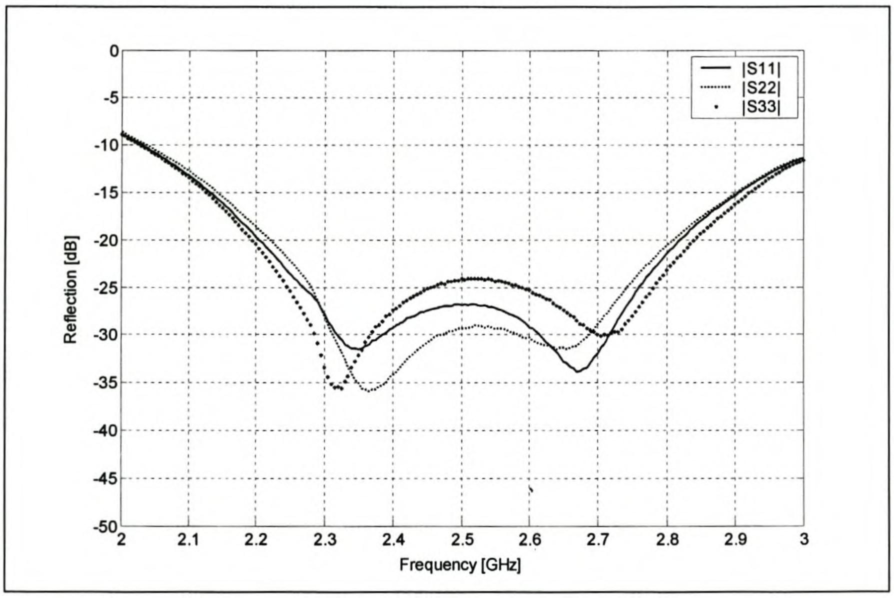

Figure 4-17: Measured reflection S parameters of the Nova circulator

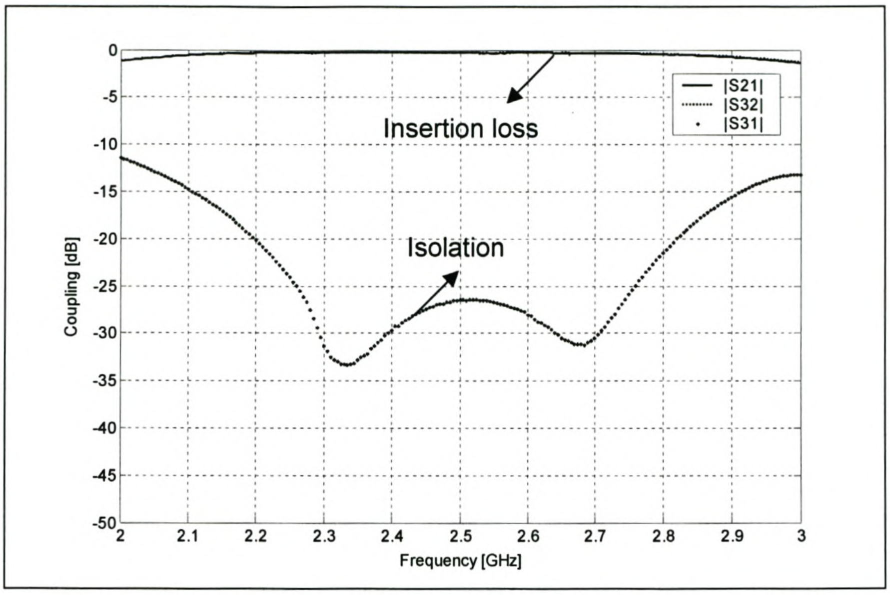

Figure 4-18: Measured coupling and insertion loss of the *Nova* circulator

This circulator was used in radar system measurements with a single horn antenna, but was not used in the final design due to cost restriction.

4.3.2 The Lange coupler

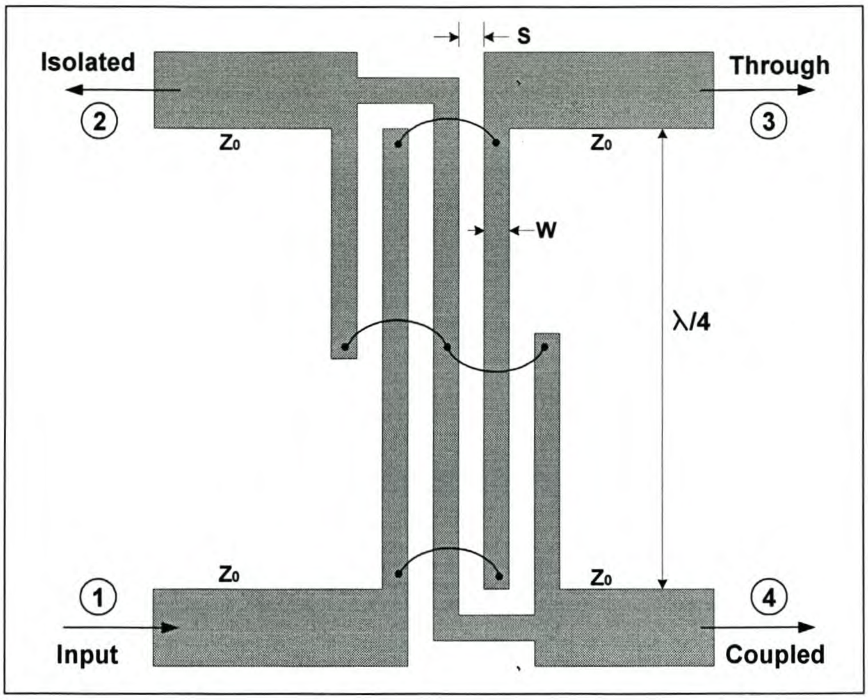

Figure 4-19: The Lange coupler.

The Lange coupler was originally designed to improve the coupling achieved by using single coupled lines. This was achieved by using several lines in parallel to each other so that the fringing fields at both edges of a line contribute to the coupling. Figure 4-19 shows the layout of the Lange coupler in microstrip form. When working with circularly polarized signals in the FM-CW radar system, the Lange coupler can also be used for isolation between the transmitted and received signals, fulfilling the same role as the circulator [5 398-401] [35].

The operation of the Lange coupler in the radar system can be explained with the help of Figure 4-20. The transmitted signal P_t is connected to the input, port 1 and can be represented in phazor form, as $P_t\angle 0^\circ$. There is a 90° phase difference between ports 1 and 3 and between ports 4 and 2. The transmitted power, divided evenly between ports 3 and 4, can be represented in phazor form as $\frac{1}{2}P_t\angle 90^\circ$ and $\frac{1}{2}P_t\angle 0^\circ$ respectively. Ports 3 and 4 are connected to a dual-fed antenna i.e. a circularly polarized patch or helix (explained in chapter 5) and the transmitted signal then becomes circularly polarized. When reflected off a flat surface i.e. a dam or wall, the polarization of the received signal P_r is reversed (undergoes a 180° phase difference). The received power at ports 3 and 4 can then be represented in phazor form as $\frac{1}{2}P_R\angle 270^\circ$ and $\frac{1}{2}P_R\angle 90^\circ$ respectively. The received signal at port 3 couples to port 1, undergoing a 90° phase shift, and adds to the received signal coupled from port 4 with zero phase shift. The signal at port 1 becomes $\frac{1}{2}P_R\angle 360° + \frac{1}{2}P_R\angle 180° = 0$. This results in zero power reflected at port 1. Similarly the received signal at port 4 couples to port 2, undergoing a 90° phase shift and adding to the received signal coupled from port 3 with zero phase shift. The signal at port 2 becomes $\frac{1}{2}P_R\angle 270° + \frac{1}{2}P_R\angle 270° = P_R\angle 270°$ and this results in maximum received power at port 2.

To conclude: Theoretically no received power is reflected at the *input* port 1 and all the received power is coupled to the *isolated* port 2. Secondly very little transmitted power will directly couple from port 1 to the *isolated* port.

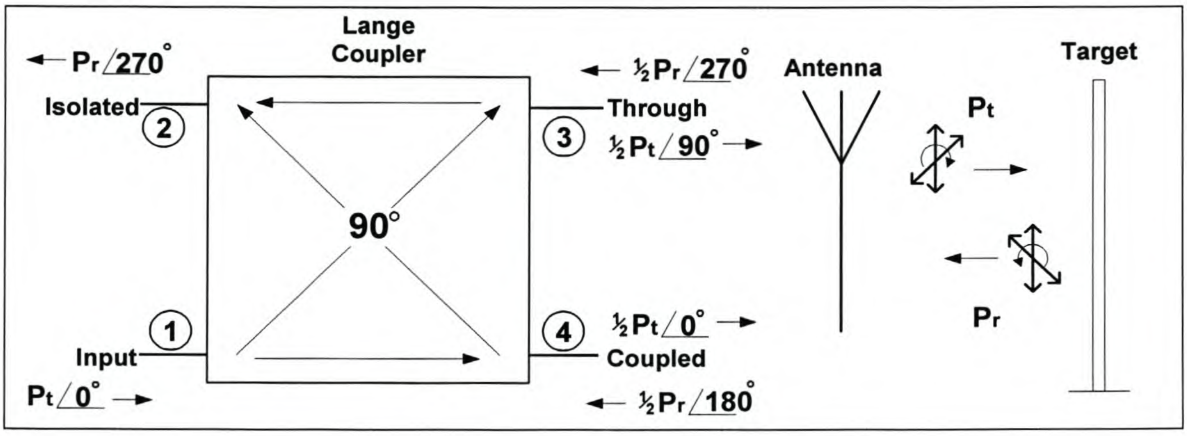

Figure 4-20: Using the Lange coupler in an FM-CW radar system.

The main disadvantage of the Lange coupler is its difficulty to fabricate since the lines are narrow and very closely spaced. Another restriction is the fact that the above topology can only be used in radar with circularly polarized antennas. The radiation pattern of a circularly polarized antenna is identical in the vertical and horizontal planes, thus the transmitted power is equally divided between these planes. This has the advantage of detecting targets that lie in the horizontal and vertical planes but has the disadvantage that 3 dB (or half) of the transmitted power will dissipate in the plane having no reflecting object.

The first step in designing the Lange coupler was to calculate the even- and odd mode characteristic impedances Z_{0e} and Z_{0o} by using (4.5) and (4.6) for a given coupling coefficient C and characteristic impedance Z_0 [5].

$$Z_{0e} = \frac{4C - 3 + \sqrt{9 - 8C^2}}{2C\sqrt{(1-C)/(1+C)}} Z_0 \tag{4.5}$$

$$Z_{0o} = \frac{4C + 3 - \sqrt{9 - 8C^2}}{2C\sqrt{(1+C)/(1-C)}} Z_0 \tag{4.6}$$

For an even power division between the input port 1 and output ports 3 and 4, the coupling coefficient had to be 3 dB giving $C = 10^{-3/20} = 0.708$. The characteristic impedances were calculated as Z_{0e} = 176. 5 Ω and Z_{0o} = 52.5 Ω for a 50 Ω system.

The line-spacing S and line-width W can be determined from the characteristic impedances for a given substrate by using *Txline* or available design tables [9]. The substrate thickness T and effective dielectric constant ε_r determines the overall size of the Lange coupler. To simplify the fabrication process it is better to use a slightly thicker substrate with a lower dielectric constant.

Txline was used to design a Lange coupler at 2.5 GHz. (See Figure 4-21.) The same substrate that was used for the coupled line designed in section 4.2 namely the *RT/duroid 5870* is chosen for the Lange coupler design as both components were used in the final design. The final physical dimensions of the Lange coupler are given as substrate thickness T = 1.574 mm, line-spacing, S = 0.11 mm, line-width, W = 0.69 mm and effective ε_r = 2.33. The wavelength is $\lambda = \frac{c}{f\sqrt{\varepsilon_r}} = 80\text{ mm}$ giving the physical line length of λ/4 = 20 mm [5 p398-401].

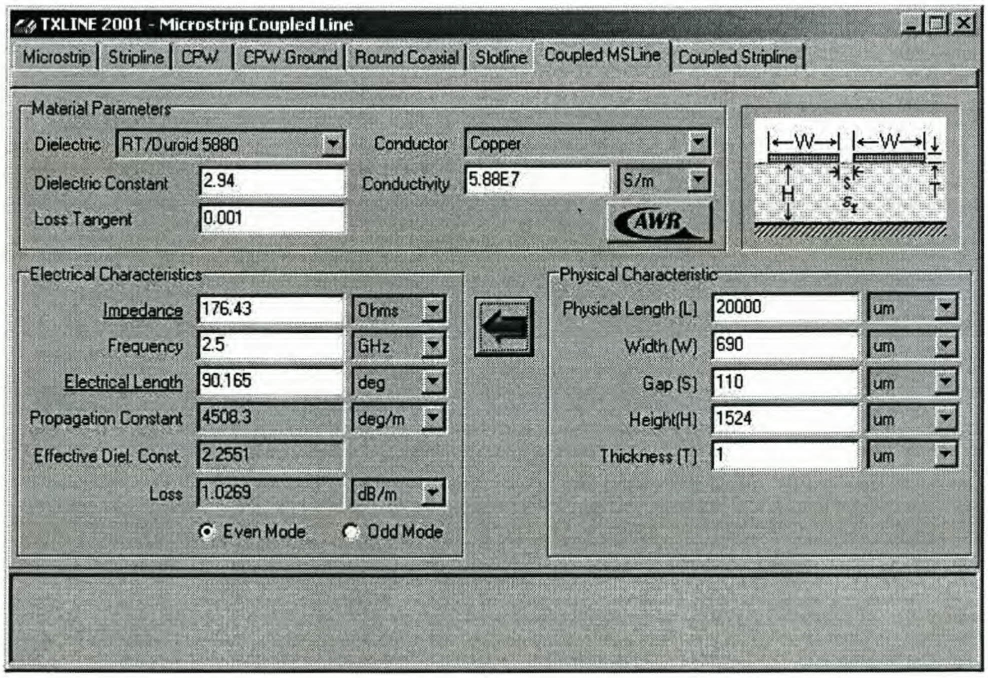

Dielectric: RT/Duroid 5880
Dielectric Constant: 2.94
Loss Tangent: 0.001
Conductor: Copper
Conductivity: 5.88E7 S/m

Impedance: 176.43 Ohms
Frequency: 2.5 GHz
Electrical Length: 90.165 deg
Propagation Constant: 4508.3 deg/m
Effective Diel. Const.: 2.2551
Loss: 1.0269 dB/m
● Even Mode ○ Odd Mode

Physical Length (L): 20000 um
Width (W): 690 um
Gap (S): 110 um
Height(H): 1524 um
Thickness (T): 1 um

Figure 4-21: *Txline* design of a Lange coupler with given characteristic impedances, substrate thickness and dielectric constant.

The design was simulated in *Microwave Office* and the magnitude and phase of the coupling between the ports are shown in Figure 4-22 and Figure 4-23. The phase difference between the *through* and *coupled* ports is exactly 90° and the -3 dB coupling indicates that the input power is equally divided. The coupling between the *input* and *isolated* ports is below -25 dB over the whole frequency band. The port reflections are not shown but all the ports had reflection below -25 dB between 2 and 3 GHz. The simulated results reflect a good Lange coupler design that was considered suitable to use in the final radar system.

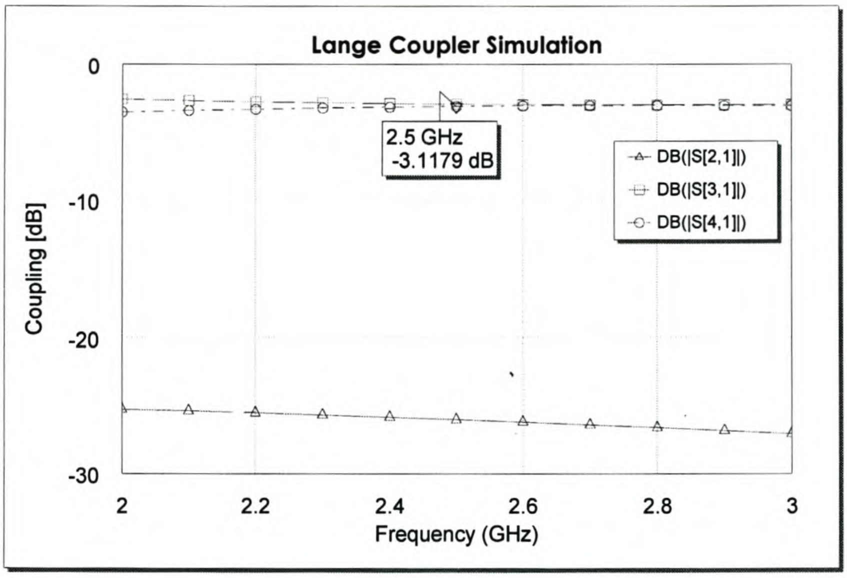

Figure 4-22: Simulation of the Lange coupler's coupling in *Microwave Office*.

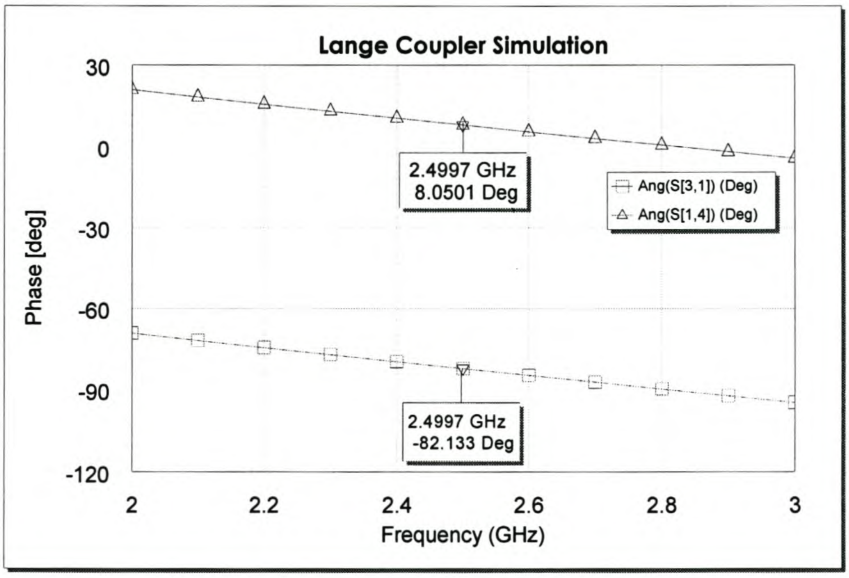

Figure 4-23: Simulation of the Lange coupler's phase response in *Microwave Office*.

The manufactured Lange coupler is shown in Figure 4-24 and the measured S parameters are shown in Figure 4-25 to Figure 4-27. From Figure 4-25, the reflection at all the ports is not as low as expected from the simulation, but is still below -15 dB across the whole frequency band which indicates a good impedance matched design. The magnitude of the measured coupling between the ports is shown in Figure 4-26. The measured $|S_{21}|$ and $|S_{41}|$ coupling S parameters are both nearly -3.1 dB, as expected, indicating very little insertion loss and equal power distribution between these ports. The measured $|S_{31}|$ is -18 dB, which is not as low as expected, indicating less isolation between the *input* and *isolated* ports. This might lower the radar's dynamic range as more of the transmitted power couples to the mixer's RF- port. The measured phase difference between the *input* and *through* ports is exactly 90° as shown in Figure 4-27. The phase difference between the *input* and *coupled* ports is -180° indicating a -90° phase difference between the *through* and *coupled* ports. The Lange coupler theory and simulation uses a positive 90° phase difference in the calculations but the results are the same for a -90° phase difference.

To conclude, the measured Lange coupler should perform well in the radar system seeing that the most important design parameter, namely, the phase difference between all the ports, was measured and meets the design expectation. The isolation between the *input* and *coupled* ports is not as low as expected and might lower the radar's dynamic range. The input and output impedance of the Lange coupler is well matched at all ports. The power at the *input* port is evenly distributed between the *through* and *coupled* ports with a -90° phase difference and low insertion loss.

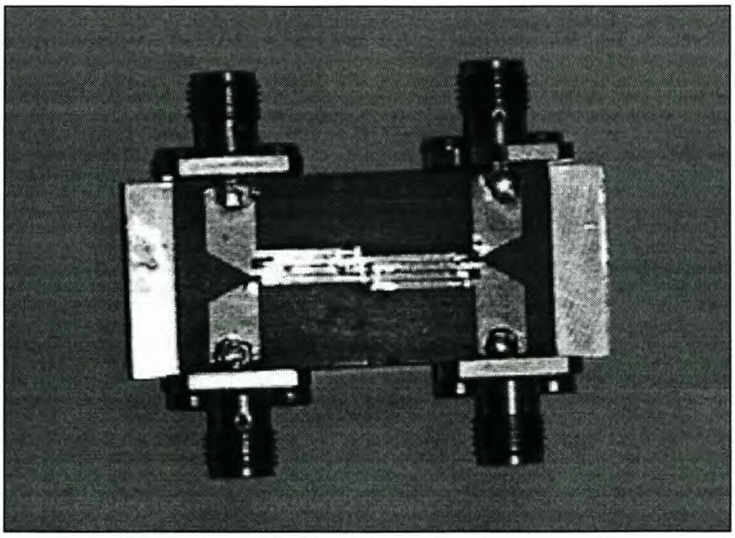

Figure 4-24: Photograph of the manufactured Lange coupler.

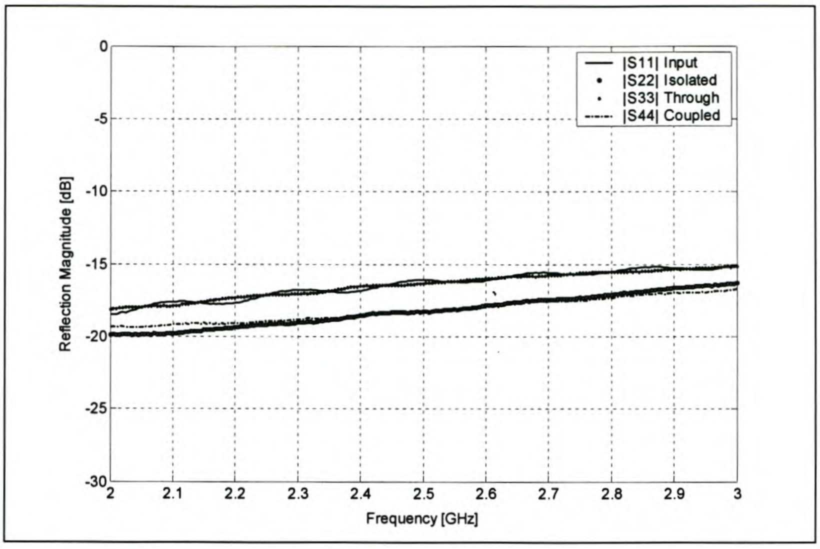

Figure 4-25: Lange coupler: Measured reflection at all ports.

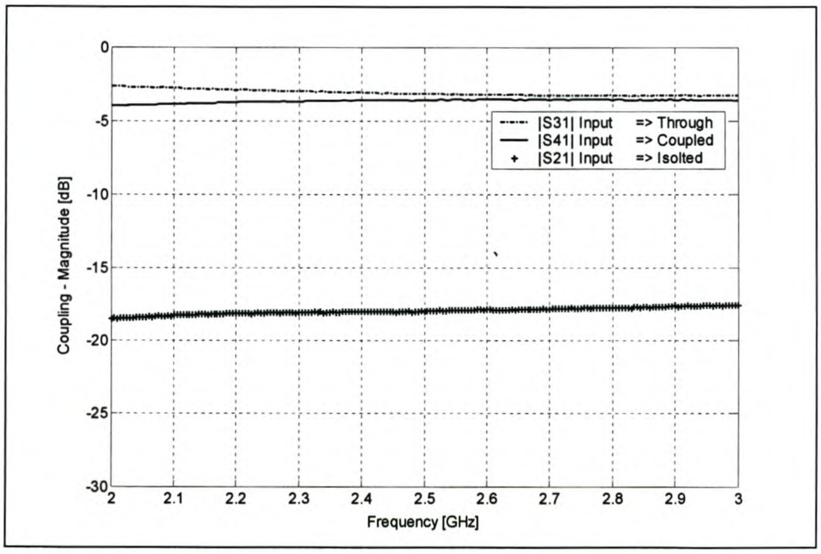

Figure 4-26: Lange coupler: Measured Coupling between all ports.

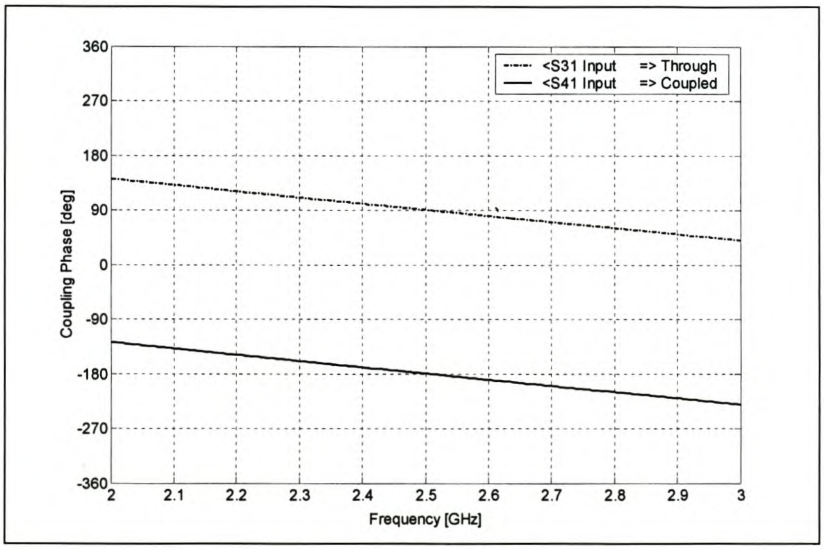

Figure 4-27: Lange coupler: Measured Phase at all ports.

4.4 Mixer

A mixer is a three-port device that uses a non-linear or time-varying element to achieve frequency conversion. An ideal mixer produces an output consisting of amongst other things, the sum and difference frequencies of its two input signals. Operation of mixers is typically based on the non-linearity provided by either a diode or transistor. Important mixer properties that will influence the radar system are *conversion loss, isolation, dynamic range* and *noise figure* [10-12] [34].

The mixer *conversion loss* is the amount of attenuation of the signal from the RF input to the IF output port of the mixer and can be expressed in dB [10],

$$L_c = 10\log\frac{\text{available RF input power}}{\text{available IF output power}} \geq 0\text{dB} \qquad (4.7)$$

Equation (4.7) is mostly used for passive mixers seeing that most active mixers have *conversion gain* up to a few dB. If the power of the received signal is small the difference-frequency signal might not be discernible from the noise, due to mixer conversion loss. By minimizing the conversion loss, the receiver noise figure is also minimized. Typical conversion losses for diode mixers are between 4 and 7 dB in the 1 – 10 GHz range [12].

The *isolation* between the mixer LO- and RF- ports is very important in the radar because LO power that couples through to the mixer RF port will be radiated by the antenna, causing undesired interference. For this design, it will not interfere with other services as the transmit and receive signals fall in the same frequency band. The unwanted radiated signal will, however, interfere with the radar received signal. The desired and interfering received signals will have different time delays causing an extra unwanted beat frequency signal. This may result in an inaccurate range measurement [10] [33].

The minimum detectable signal and maximum power that can be received at the RF port before compression determines the *dynamic range* of the receiver. In the radar system, the maximum measurable distance is determined by the minimum receivable power. Likewise, the minimum measurable distance is determined by the maximum power allowed at the RF port. As earlier mentioned, the isolation between the transmitted and received signals is of paramount importance as it will also determine the maximum power that will be received at the mixer RF port. The higher the coupled transmitted power, the lower the receiver's dynamic range [5] [10] [11] [33].

The *noise figure* of a mixer is the difference between the input- and output signal-to-noise ratio in dB. The double sideband (DSB) noise figure includes signal and noise powers at the

RF and image signals, where the single sideband (SSB) noise figure includes the noise power at the image signal. The SSB noise figure rejects the image signal power and is twice that of the DSB noise figure because half of the signal is discarded. Noise figures of practical mixers range from 1 dB to 5 dB, with diode mixers generally achieving lower noise figures than transistor mixers [10] [12].

There are two basic types of mixers, namely passive and active mixers. Passive mixers have the advantage that they perform well in nearly all the mixer characteristics and are less expensive and complicated than active mixers. They have generally better noise figures and are very reliable although they have the disadvantage of a higher LO input power requirement and have a smaller dynamic range [10-12].

Active mixers have the advantage of conversion gain, requiring less LO power, and perform very well in some of the mixer characteristics, but not for all. They are more expensive than passive mixers and typically have worse noise figures [11-12].

Mixers can also be divided into three basic categories, i.e single ended, singly balanced and double balanced mixers. Other mixer topologies, such as triple balanced and image reject mixers, are also available but will not be discussed in this section [10-12].

Single ended mixers translate frequency by using a single non-linear device such as a diode or transistor. Their advantages are high conversion efficiency and lower noise figures and they are inexpensive, although they have poor isolation properties and are not very well matched at the RF input [12].

Single balance mixers consist of two single device mixers that are typically combined with either a 90 degree or 180 degree hybrid junction. The use of the 180 degree hybrid junction results in nearly perfect RF-LO isolation over a wider (15 %) frequency range, while the use of a 90 degree hybrid leads to an almost perfect input match at the RF port. Both mixers reject certain even-ordered intermodulation products [12].

Double balanced mixers combine four single ended elements by using two hybrid junctions or transformers. They provide good isolation between all three ports as well as rejection of all even harmonics of the RF and LO signals but are not as well matched at the RF input port. The conversion loss is slightly higher than single balanced mixers because double the amount of diodes are used [12] [34].

Several different types of mixers were measured in the radar system, to determine their influence on the system's performance. The mixer that performed best in all the requirements is the ADE-3G from *Mini-Circuits*. This mixer is a double balanced mixer and was chosen for the final design. It has very good LO-RF isolation (36 dB), low noise figure, a high required LO power (7 dBm), a maximum RF input power of 1 dB and a low conversion loss (L_s = 5.6 dB) [13 p70].

4.5 Conclusion

Most of the RF- components that were chosen for the radar design have been discussed. A lot more attention, however, was given to the antenna design which will be discussed separately in chapter 5. The filtering and amplification of the mixer IF- output signal has to be designed for specific application of this radar and recommendations can only be made after the final IF measurements.

5. Antenna design

More emphasis was placed on the antenna design and simulation in the radar system and thus a separate chapter is devoted to its explanation. The Lange coupler, as previously stated, was chosen for the final design. This implies that a circularly polarized antenna will have to be used.

Two types of antennas were considered, namely the *Microstrip Patch antenna*, discussed in section 5.1, and the *Helix antenna* which is discussed in section 5.2. Each of these sections covers the basic theory, design, simulation, building and final measurements of the specific antenna. A double helix antenna with counter clockwise and clockwise polarization was designed. It is unusual to use this type of antenna in radar systems and there is little literature explaining the design method and influence of each design parameter on the gain, reflection and isolation. The aim was to design and build an antenna with sufficient gain that would improve the isolation between the transmitted and received signals. Section 5.2.2 summarizes the design method and influence of each design parameter and will be useful for future double helix designs. The chapter ends with a conclusion in which the advantages and disadvantages of each antenna in the radar system are summarized.

5.1 Patch antenna

5.1.1 Patch antenna theory

A microstrip patch antenna is one of the most effective radiators for exciting circular polarisation. There are two available feeding methods to achieve circular polarization: Singly-fed without a polarizer or dual-fed with an external polarizer such as a 3 dB hybrid or Lange coupler, as explained in section 4.3.2 [14 p220-221] [27].

When the dual-fed method is used, the two feeds are usually centred on adjacent edges of the patch and can be moved towards the middle. This variation of the feed position is a design parameter that can be changed to achieve a better impedance match and corresponding resonance frequency [15 p981].

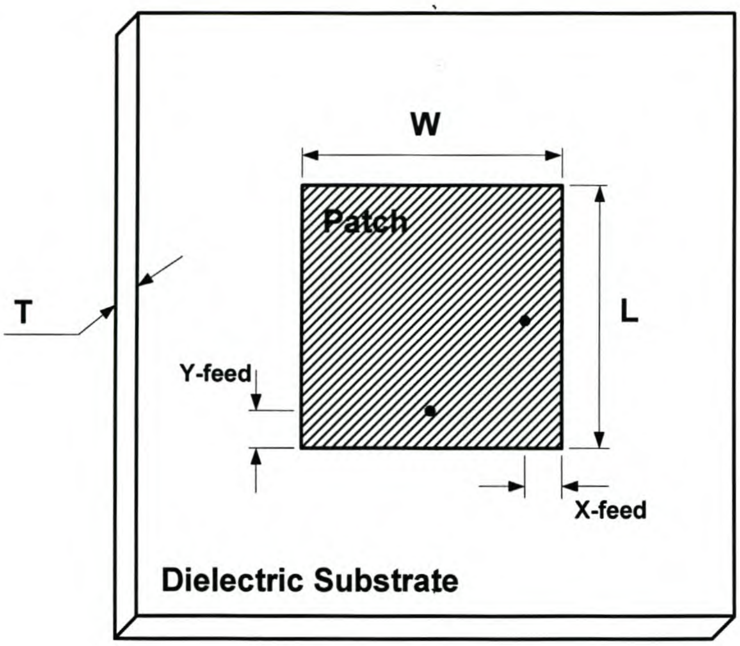

Figure 5-1: Dual-fed Circular Patch Antenna.

A typical circular polarized dual-fed patch antenna is shown in Figure 5-1. The length and width of the patch is equal but slightly less than a half-wavelength in the dielectric substrate material ($W = L < \lambda/2$). This is to achieve resonance. The amount of length reduction is dependent on the substrate dielectric constant ε_r and thickness T. Formulae are available to estimate resonant length but empirical adjustments are mostly necessary in practice. RE Munson authored a paper in 1974, giving a formula to approximate the length of a resonant half-wavelength patch as [16 p74-78]

$$L \approx 0.49\lambda_d = 0.49\frac{\lambda}{\sqrt{\varepsilon_r}} \quad (5.1)$$

where λ is the free-space wavelength, λ_d the wavelength in the dielectric medium, and ε_r the substrate dielectric constant. The bandwidth is approximately proportional to the substrate thickness and decreases with increasing substrate dielectric constant, thus a thick substrate with low dielectric constant has a wider bandwidth. Unfortunately, problems arise when using a thick substrate, namely, high feed pin reactance if fed coaxially and unwanted surface waves that flow inside the substrate, causing the antenna to radiate less energy. This will decrease the antenna gain and efficiency [17 p9]. Therefore, there is always a trade-off involved between the antenna bandwidth and gain and the radar specifications must be considered when choices are made.

If the antenna bandwidth is less than the maximum deviation of the VCO signal, the amplitudes of the transmitted and received signals will be a maximum at the center frequency and will decrease when the VCO frequency falls outside the antenna bandwidth. This will lower the accuracy of the radar beat frequency measurement. The bandwidth needed for this radar design was specified (chapter 2) as Δf = 100 MHz (4 % at 2.5 GHz center frequency).

As previously mentioned, the antenna that will be used in the radar system is required to transmit and receive right–and left hand circularly polarized (RHC and LHC) signals respectively. A big advantage of the dual-fed patch antenna is that it can be used for both RHC and LHC due to its diagonal symmetry. Thus, a single patch antenna can be used in the radar system to meet this requirement.

5.1.2 *Feko* design and simulation

The approximate length and estimated feed dimensions and substrate properties of the circular patch antenna were chosen using (5.1). *Feko* [18] was used to design and simulate the final circular patch antenna at a center frequency of 2.5 GHz.

The final dimensions were determined as:

- L = W = 37.4 mm
- X- and Y-feed distance = 12.9 mm
- Substrate: Taconic with ε_r = 2.48 and Thickness = 1.58 mm
- The ground plane is square with sides = 80 mm

The simulated reflection coefficients, gain and axial ratio of the final patch design are shown in Figure 5-2, Figure 5-3 and Figure 5-4 respectively.

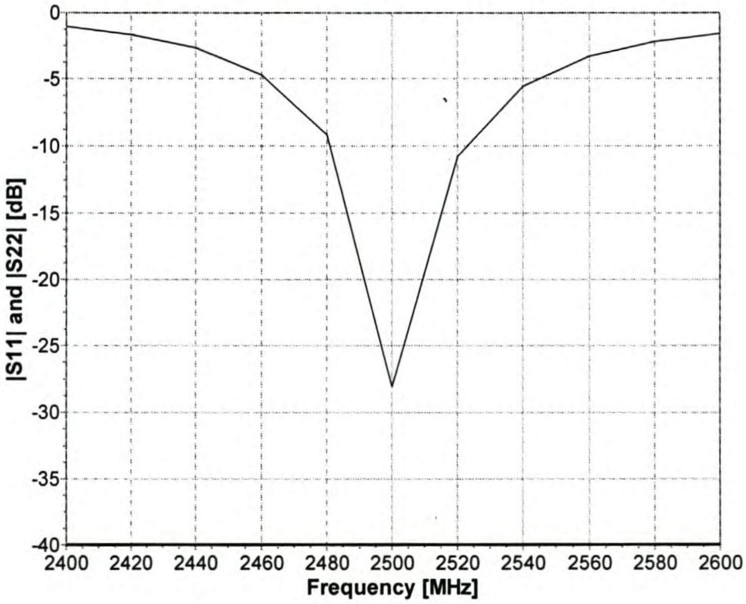

Figure 5-2: Simulated reflection coefficients at both feeds.

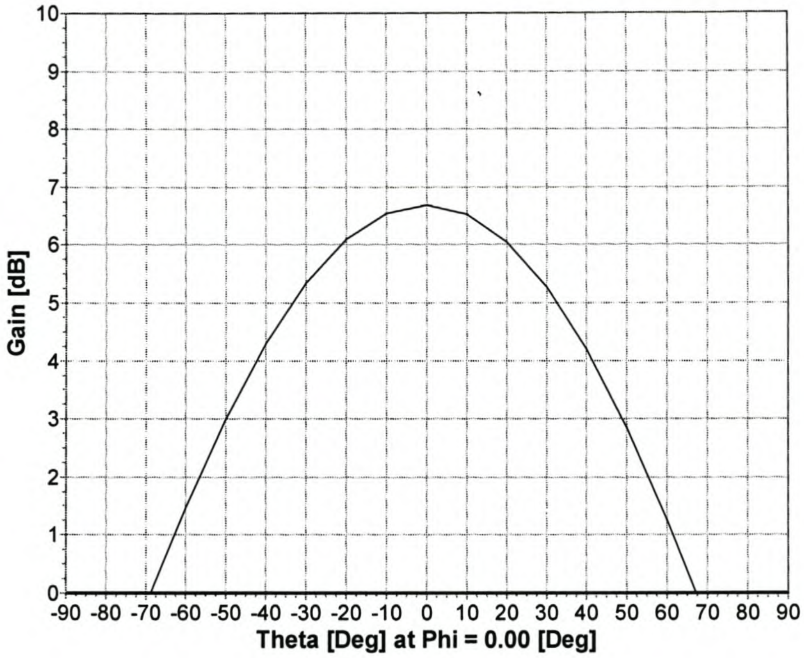

Figure 5-3: Simulated radiation pattern of the circular patch antenna.

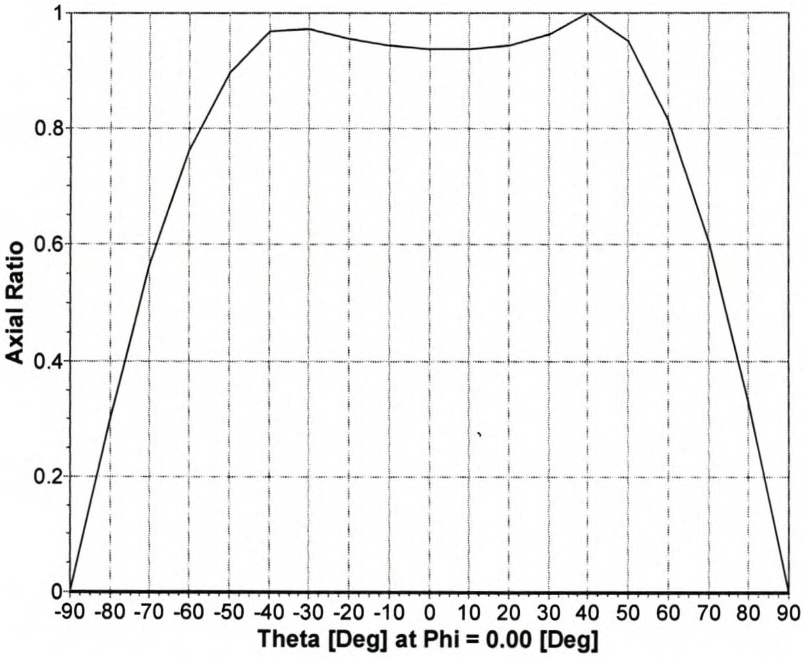

Figure 5-4: Simulated axial ratio pattern of the circular patch antenna.

5.1.3 Building and measuring of the patch antenna

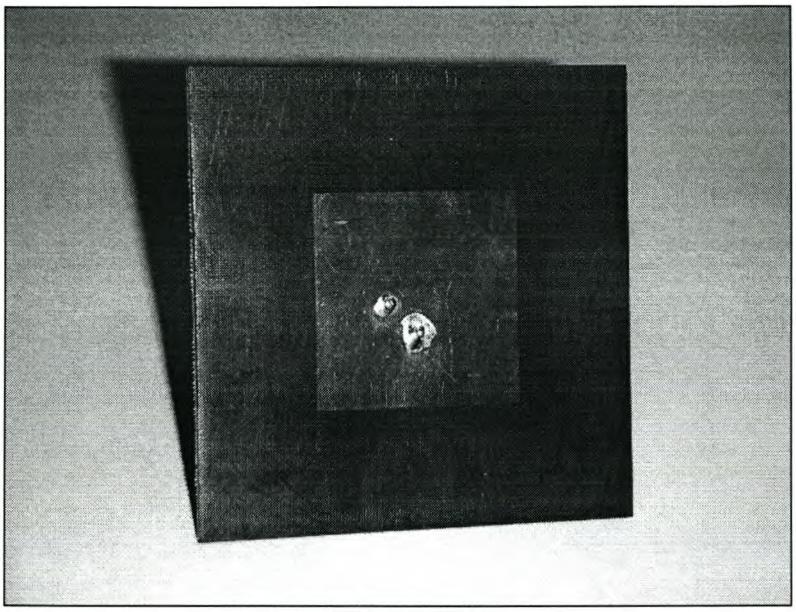

Figure 5-5. Photograph of the dual-fed circular patch antenna.

The manufactured dual-fed circular patch antenna, shown in Figure 5-5 was measured on the 8753-Network Analyzer. The $|S_{11}|$ and $|S_{22}|$ reflection coefficients are shown in Figure 5-6. This measurement correlates with the *Feko* simulation of Figure 5-2.

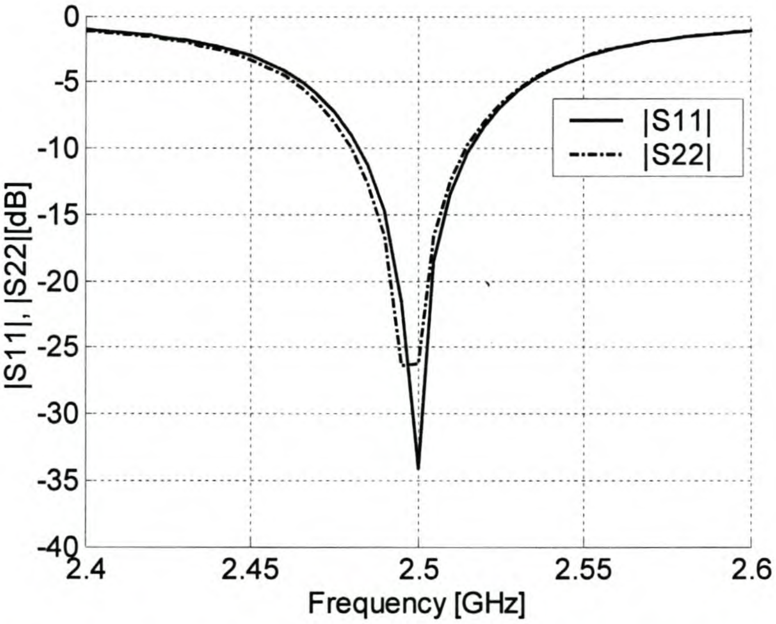

Figure 5-6: Measured reflection coefficients at both ports of the circular patch antenna.

To measure the gain of a circular polarized antenna, the source must be either rotatable linear, purely circular, rotatable circular or accurately calibrated across the band. The easiest is to obtain pure linear polarization, in which case three methods are available to determine the circular components:

1. Measure phase and amplitude of two linear components (e.g. vertical and horizontal)
2. Measure amplitude of three or four linear components (e.g. vertical, 45°, horizontal and 135°)
3. Rapidly rotate the source [19]

The first of the above methods were chosen to measure the circularly polarized patch antenna. Two identical linearly polarized horn antennas were used as two separate source antennas. The antenna under test's (AUT) vertical and horizontal components are given in terms of real and imaginary magnitudes [19],

$$H = x_r + jx_i \tag{5.2}$$

$$V = y_r + jy_i \tag{5.3}$$

The right-and left hand circularly polarized components are then determined from [19],

$$V_{RHC} = (x_r + y_i)/2 + j(x_i - y_r)/2 \tag{5.4}$$

$$V_{LHC} = (x_r - y_i)/2 + j(x_i + y_r)/2 \tag{5.5}$$

The above equations were used to determine the AUT's circularly polarized S_{21}-parameter components and the three antenna method was used to determine the AUT's gain.

Assuming the antennas to be well matched, the gain of each antenna can be calculated from equation (3.4) by simultaneously solving,

$$|S_{21}|^2 = \frac{G_1 G_2 \lambda^2}{(4\pi R)^2} \tag{5.6}$$

$$|S_{21}|^2 = \frac{G_1 G_{AUT} \lambda^2}{(4\pi R)^2} \tag{5.7}$$

$$|S_{21}|^2 = \frac{G_2 G_{AUT} \lambda^2}{(4\pi R)^2} \tag{5.8}$$

where G_1 and G_2 are the gains of each horn antenna respectively and G_{AUT} is the gain of the AUT (in this case the circular patch).

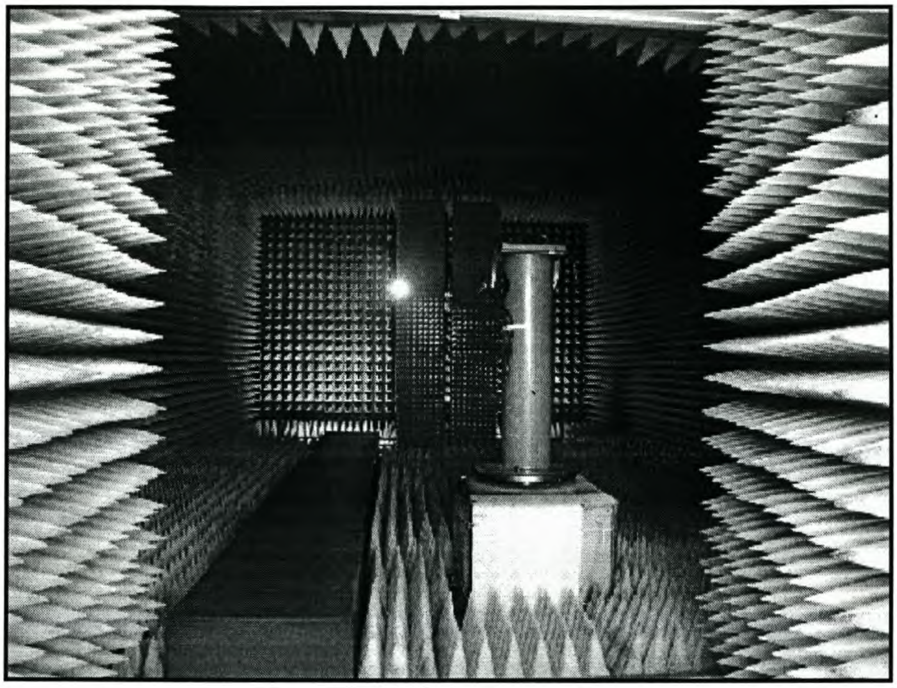

Figure 5-7: Anechoic antenna measurement room.

The antenna $|S_{21}|$ parameter measurements were done in an anechoic measurement room shown in Figure 5-7. The Lange coupler designed in section 4.3.2 was used as a 90° hybrid to polarize the antenna. *Matlab* [31] was used to first compute the RHC and LHC S_{21} – parameters for the patch antenna from (5.4) and (5.5). The measured and calculated S_{21} parameters are shown in Figure 5-8 to Figure 5-10. Equations (5.6) to (5.8) were simultaneously solved to find the gain of each antenna shown in Figure 5-11. Axial ratio is essentially the antenna property which defines the circularity of an antenna's radiation pattern. Strictly speaking this is the difference between the maximum and minimum on-axis gains as the antenna is rotated through all angles. The axial ratio was determined by measuring the vertical and horizontal S_{21} real and imaginary components of the AUT. The left and right hand circularly polarized field vectors, E_R and E_L are given by [37]

$$E_L = \frac{S_{21H} + jS_{21V}}{\sqrt{2}}$$

$$E_R = \frac{S_{21H} - jS_{21V}}{\sqrt{2}} \quad (5.9)$$

where S_{21V} and S_{21H} are the measured vertical and horizontal S_{21} parameters respectively. The axial ratio, AR is then determined by [37]

$$AR = \frac{E_{maj}}{E_{min}} = \left|\frac{|E_R| + |E_L|}{|E_R| - |E_L|}\right| \quad (5.10)$$

The measured axial ratio in Figure 5-12 is 0.5 dB at the center frequency which indicates that the patch antenna is nearly perfectly circularly polarized [8].

The $|S_{21}|$, gain and axial ratio patterns for the patch antenna are shown in Figure 5-13 to Figure 5-15. The measured antenna gain in Figure 5-14 is very similar to the simulation in Figure 5-3. Both graphs show a maximum gain of 6.5 dB at the center frequency and have comparable gain patterns.

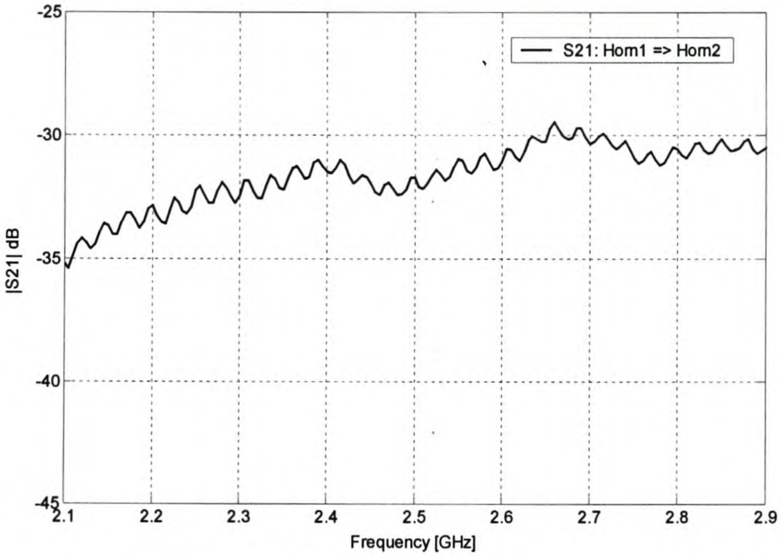

Figure 5-8: Measured $|S_{21}|$ between the two horn antennas.

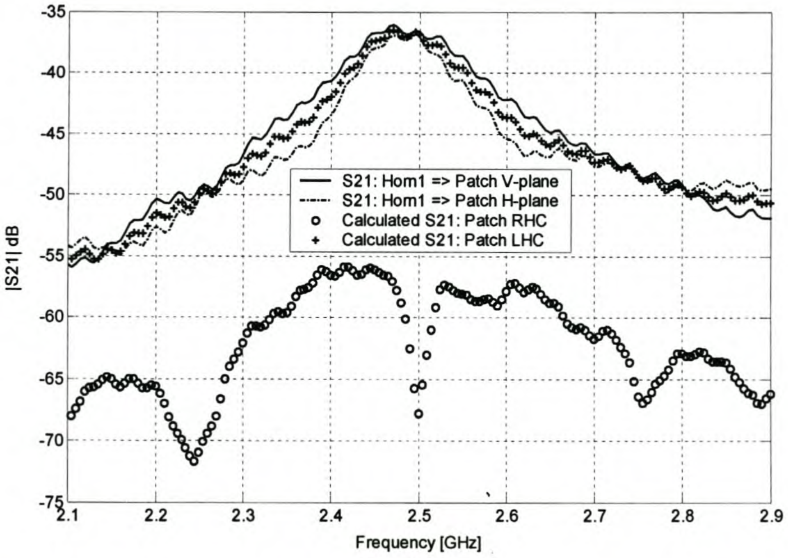

Figure 5-9: Measured $|S_{21}|$ between the patch and horn-1 in the vertical and horizontal planes and the calculated LHC and RHC $|S_{21}|$.

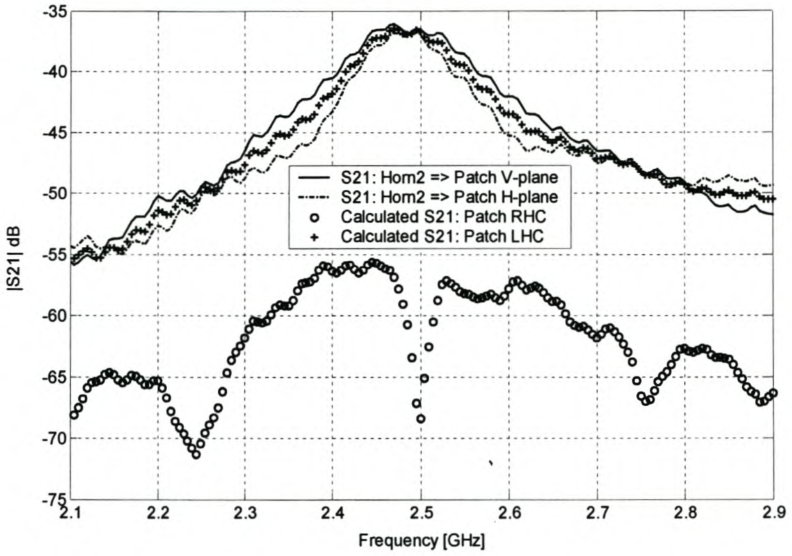

Figure 5-10: Measured $|S_{21}|$ between the patch and horn-2 in the vertical and horizontal planes and the calculated LHC and RHC $|S_{21}|$.

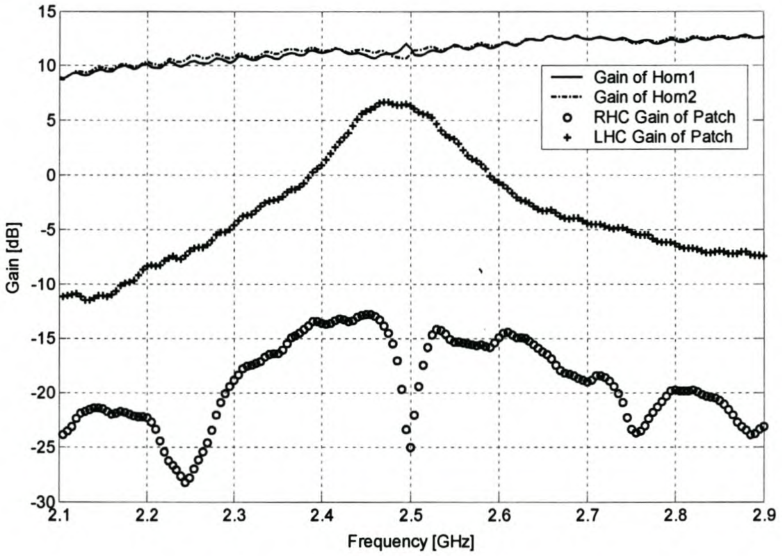

Figure 5-11: Measured gain of both horn antennas and LHC and RHC gain of the patch antenna.

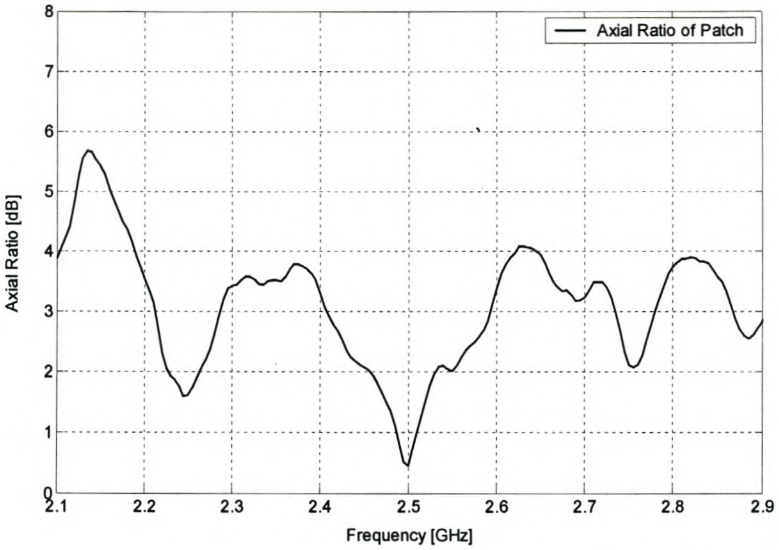

Figure 5-12: Measured axial ratio of the patch antenna.

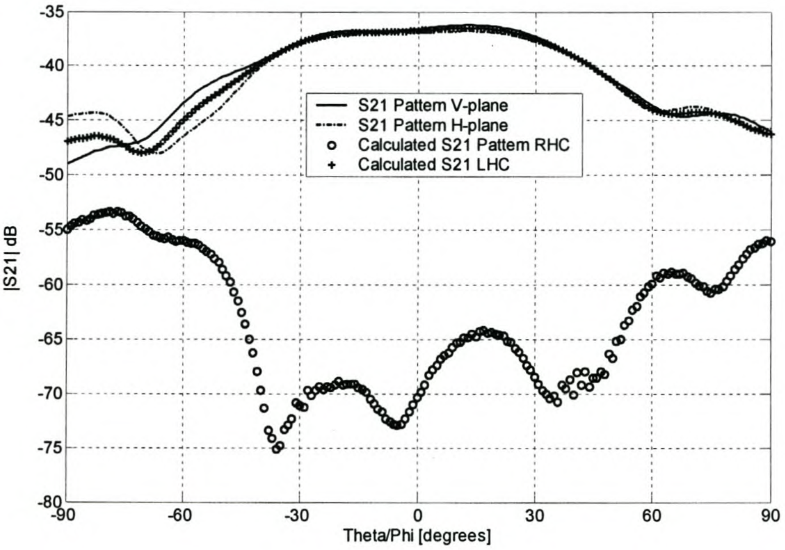

Figure 5-13: Measured vertical and horizontal plane $|S_{21}|$ patterns and calculated LHC and RHC $|S_{21}|$ patterns for the patch antenna.

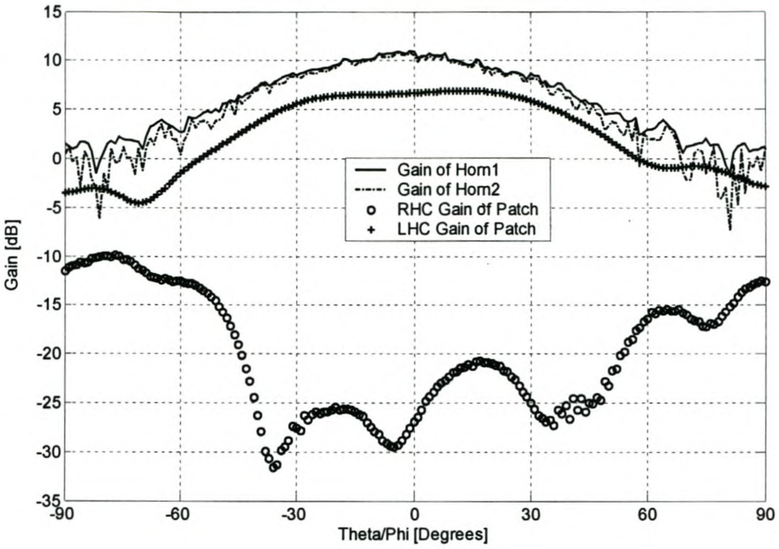

Figure 5-14: Measured radiation patterns of both horn antennas and LHC and RHC radiation patterns of the patch antenna.

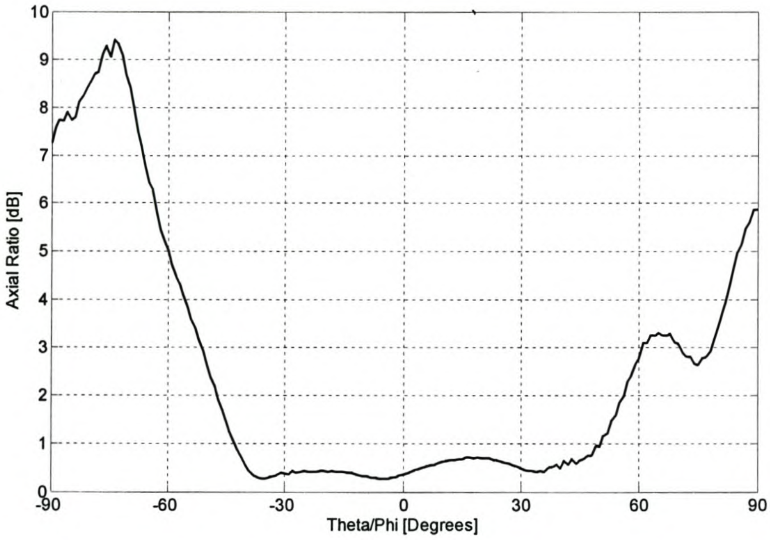

Figure 5-15: Measured axial ratio pattern of the patch antenna.

5.2 Helix antenna

5.2.1 Helix antenna theory

The first helix antenna was built and tested by JD Kraus in 1946. It immediately found wide application and after being used on Sputnik, the helical antenna became the workhorse of space communications for telephone, television and data transmitting, being employed both on satellites and at ground stations. The design and construction of a monofilar (one-wire) helix is relatively simple and it is known for wide bandwidth and good gain, and was therefore considered to be used in the FM-CW radar system [20 p265].

A monofilar helix with flat circular ground plane is shown in Figure 5-16 and the dimensions of the helix as described are [27] [29] [30]

- D = helix diameter (center to center)
- R = ground plane radius
- C = circumference of helix
- S = spacing between turns (center to center)
- α = pitch angle
- L = length of 1 turn
- N = number of turns
- A = axial length
- d = diameter of helix conductor

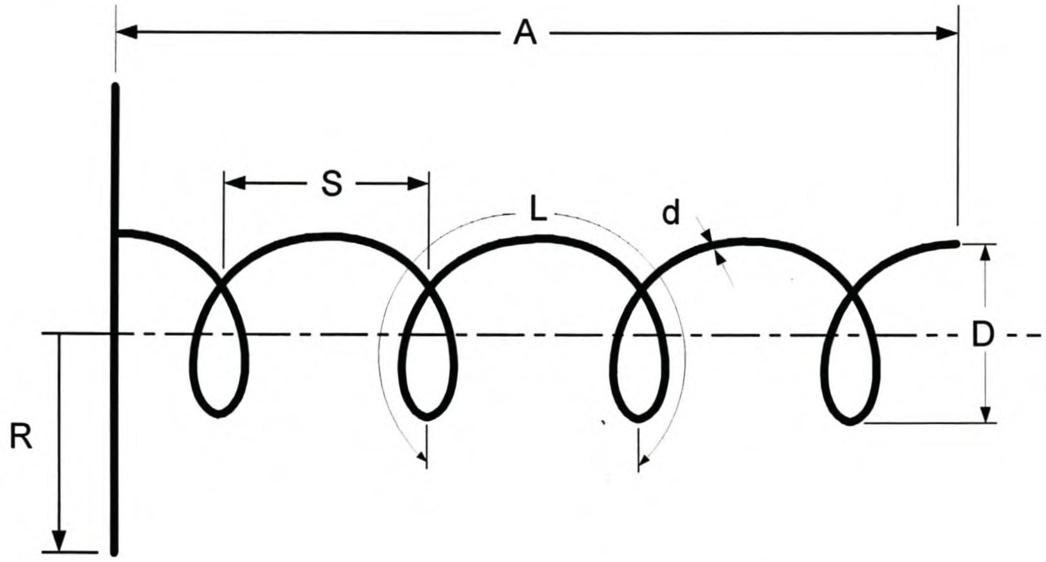

Figure 5-16: Typical monofilar helix with flat ground plane.

The helix is right- or left hand circularly polarized, depending on its rotation (Figure 5-16 has left-hand polarization). The optimum length of each turn L is equal to a single wavelength in free-space. The pitch angle α should be approximately 13° and is dependant on the turn-spacing S and helix diameter D given by

$$\alpha = \arctan\left(\frac{S}{\pi D}\right). \tag{5.11}$$

Important antenna parameters include gain, beam width, impedance and axial ratio. The gain and beam width are interdependent and their design parameters are functions of the number of turns, pitch angle and frequency. The ground plane radius R should be at least 3λ/8 and the conductor diameter d is not critical although it had an influence in the double helix design as explained later in this chapter. The effect of the number of turns and circumference of the helix on the field patterns are shown in Figure 5-17 and Figure 5-18.

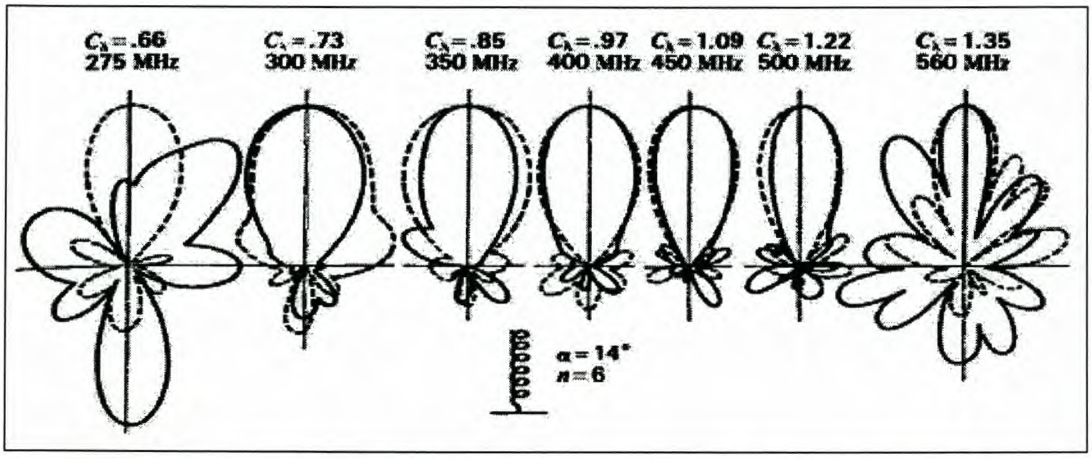

Figure 5-17: Measured field patters for different circumferences between 0.66λ and 0.135λ with N = 6 and α = 12.2°. The solid patterns are for the horizontally polarized field component (E_Φ) and the dashed for the vertically polarized filed component (E_Θ) [20 p283] [27] [28].

The impedance at the feed point of the helix, when fed axially, is given within 20% by R = 140C/λ. It is restricted to 0.8 λ ≤ C ≤ 1.2 λ, 12° ≤ α ≤ 14° and N ≥ 4. The terminal resistance can be matched to 50 Ω by gradually bending the last ¼ - turn of the helix closer to the ground plane. A tapered transition can be used between the 150 Ω helix impedance and the 50 Ω coaxial line and can be predicted mathematically. This, however, can be done empirically without using the tapering method, making it much simpler [20 p276-281].

A single monofilar helix antenna is not suitable for use in the required radar system since the transmitted and received signals have different polarizations. Therefore, two helices wound together using left- and right-hand polarization were used to transmit and receive respectively.

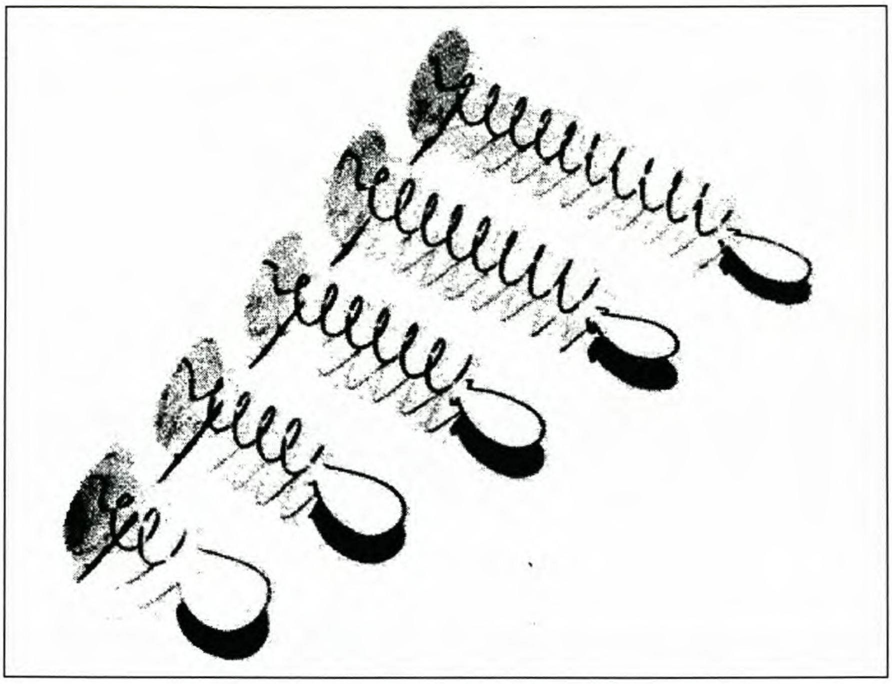

Figure 5-18: Effect of number of turns on measured field patterns. Helices have α = 12.2° and 2, 4, 6, 8, 10 turns [20 p 283] [27].

This setup can be defined as either one antenna with a dual-fed or as two separate helix antennas wound inside each other. Some of the same principles used for the single monofilar helix antenna were used to design the double helix antenna.

Before any design simulations were done, a very simple design was implemented: A 4-turn double helix at 2.5 GHz. A carton cylinder with length of 10 cm was used to support the two copper wire helices (d = 1 mm) with four turns each separated with S = 2.5 cm having a pitch angle α = 11.25° and wound for right- and left-hand circular polarization respectively. A small circular ground plane was cut out of a thin copper strip supported by a piece of cardboard paper and the helices on the carton cylinder were connected to the ground plane with two SMA connectors. The first step was to match one wire to 50 Ω by using the Smith chart of the Network Analyser. This was easily done by simply bringing the last ¼ - turn of the copper wire closer to the ground plane until the center frequency moved towards the middle of the Smith chart. The second wire was matched similarly but after matching the second helix, the impedance of the other helix had to be slightly adjusted to 50 Ω. The two helices seemed to effect each others characteristic impedance.

The measured gain was found to be approximately 8dB. From the measured reflection coefficients, $|S_{11}|$ and $|S_{22}|$, shown in Figure 5-19, the frequency bandwidth is much wider than that of the circular patch antenna.

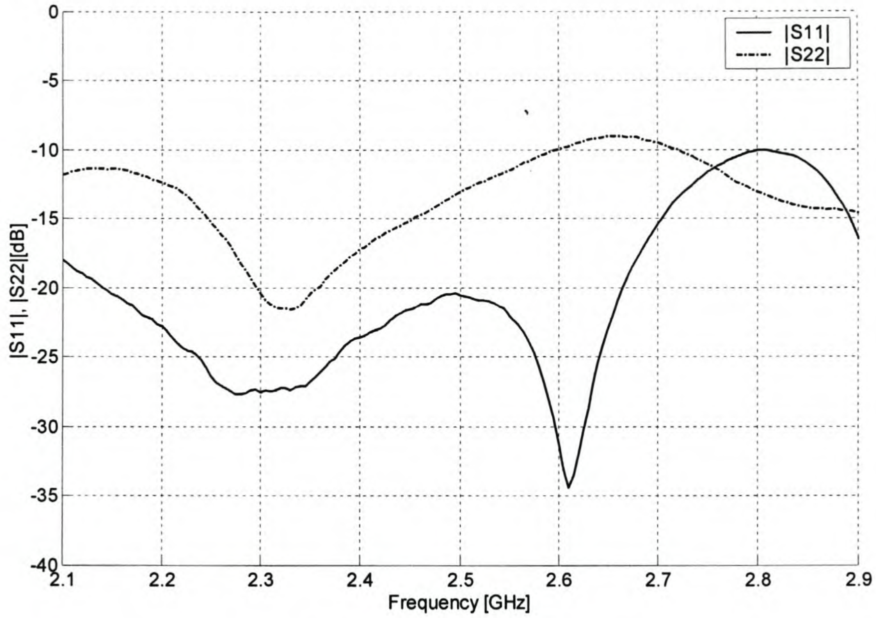

Figure 5-19: Measured reflection of the first test double helix antenna.

The importance of minimizing the coupling between the transmitted and received radar signals were discussed in sections 4.3 and 4.4. The aim was to use a Lange coupler instead of the circulator to isolate the transmitted and received signals. The isolation can also be improved by obtaining less coupling between the two helical wires seeing that two separate helices are used to transmit and receive. The minimum coupling $|S_{21}|$ between the helices has to be found without sacrificing a large amount of antenna gain. The measured coupling of the first simple test antenna was $|S_{21}|$ = -10 dB. The next section explains how *Feko* was used to find an optimum design with improved isolation and optimum gain.

5.2.2 *Feko* optimizations and design

In contrast to the circular patch antenna discussed in section 5.1, the double helix antenna has a large amount of design parameters that all need to be taken into account. This is where *Feko*'s [10] built in optimizer, *Optfeko* [21] becomes very useful. It was used in combination with *Matlab* [31] to optimize the helix antenna design for the best isolation and maximum gain. During the optimization process a general design method was sought that would simplify the design of future double helix antennas.

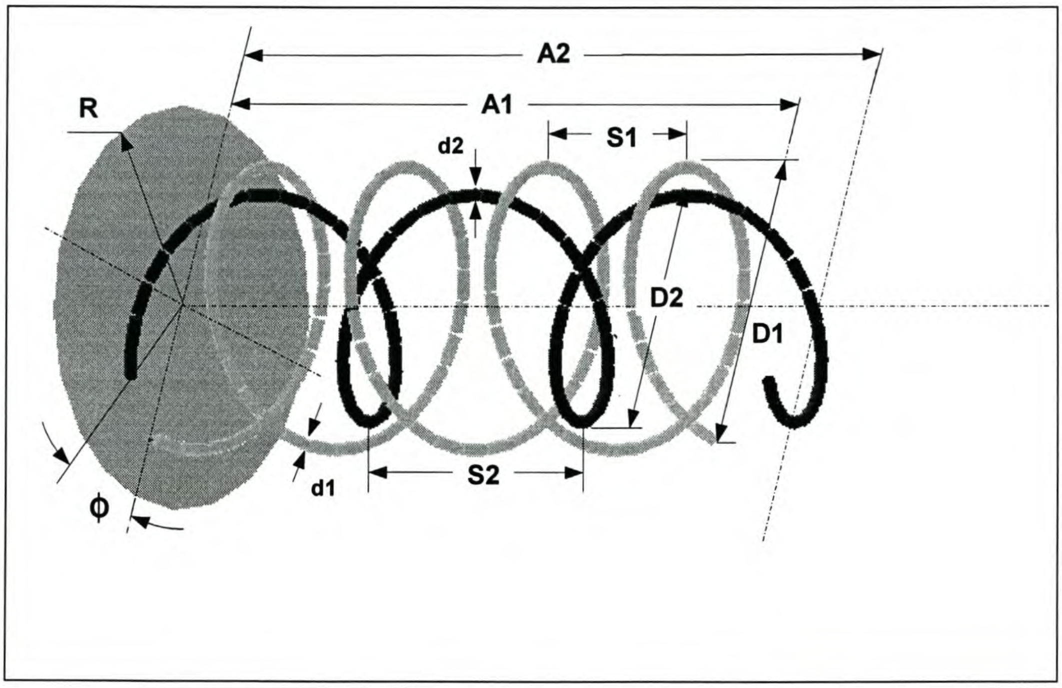

Figure 5-20: Double helix antenna structure as simulated in *Feko* with labels added.

A screen print of a typical double helix antenna, as simulated in *Feko* [18] is shown in Figure 5-20. The dimensions of the added design parameter labels in the figure are:

- D1 = Helix-1 diameter (center to center)
- D2 = Helix-2 diameter (center to center)
- R = ground plane radius
- S1 = Spacing between turns of Helix-1 (center to center)
- S2 = Spacing between turns of Helix-2 (center to center)
- Φ = Angle between the two feed points
- A1 and A2 = Helix-1 and Helix-2 axial length
- d1 and d2 = Helix-1 and Helix-2 conductor diameter

For clarity in the discussion that follows, the outer helix will be referred to as “Helix-1” and the inner helix will be referred to as “Helix-2”.

Optfeko [21] has a number of aim functions that can be used for general antenna optimizations of which only the *Gain aim* function will be useful for this design. Unfortunately there is no built-in *Scattering parameter aim* function, and a *Matlab* [31] program had to be written to obtain the required information. A normal *.pre* file first needed to be generated in *Feko's* editor where the double helix antenna was constructed using fixed values for each design parameter except for the two selected parameters. These parameters are changed stepwise between a specified minimum and maximum value during each *Optfeko* run (or optimization). A typical *Optfeko* file (*.opt) is shown in Figure 5-21. The ground radius R was varied between 30 and 60 mm in 16 steps (step size = 2 mm) and the feed angle Φ will be varied between 10 and 350° in 35 steps (step size = 10°). The optimization was run 16 x 35 = 560 times, generating 560 output (*.out) files. The S parameter information is contained in each output file (*.out) and the general antenna gain for each run is contained in a log file (*.log).

A *Matlab* [31] program was written to extract the required information by opening each output file and extracting all S parameters of each run into a matrix. The reflection parameters $|S_{11}|$ and $|S_{22}|$ at each port and the coupling parameter $|S_{21}|$ between the helices are displayed in a three dimensional graph. This clearly shows the optimum point with minimum coupling and reflection for specific values of each varied parameter. The same applies for the gain, which is displayed on a separate graph.

```
** Input file for the optimizer OPTFEKO
** for a double helix antenna

**Define optimisation parameters
**Name          Begin value     Minimum       Maximum

#Gnd_radius     30              30             60
#Feed_angle      10.0           10             350


**Optimisation method: discrete search

GRID_SEARCH
  16  35

**Aim function

**Gain - both polariztions
GAIN
   0   1

**End
```

Figure 5-21 A typical .opt file used in *Feko* to optimize for maximum gain.

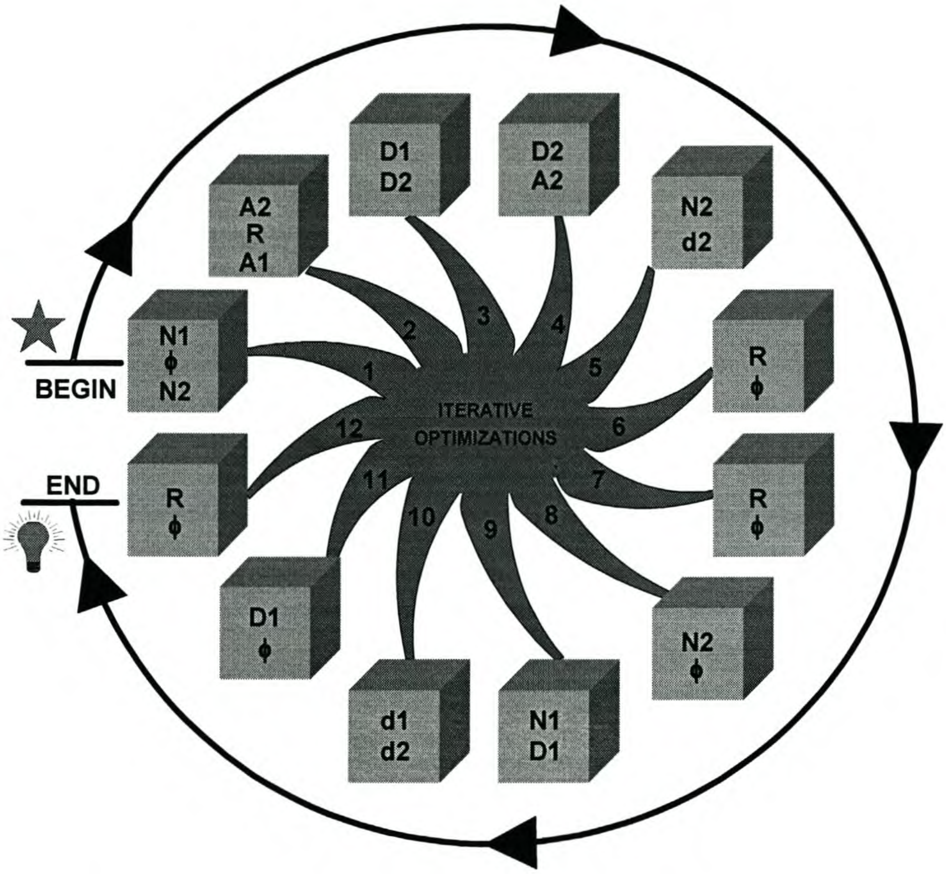

Figure 5-22: Flow diagram of the final optimization design model of the double helix antenna.

After each *Optfeko* optimization the two optimum parameters giving the best gain, reflection and isolation were chosen as fixed values and the process was repeated with two different parameters until a satisfactory design was achieved.

Various combinations of different antenna parameters were optimized and the method shown in the flow diagram of Figure 5-22 was found to give the best optimum results. This diagram shows the twelve *Optfeko* optimizations that were done before the final result was obtained. The remaining part of this section will be devoted to the discussion of each optimization and the explanation of the line of thought.

The design parameters of the first double helix antenna model discussed in section 5.2.1 were used to begin the first optimization.

Optimization 1: $3 \leq N1=N2 \leq 5$ and $90° \leq \Phi \leq 270°$

N1	**N2**	D1 [mm]	D2 [mm]	A1 [m]	A2 [m]	**Φ [°]**	R [mm]	d1 [mm]	d2 [mm]
3-5 (11 steps)	**N1**	40	40	11	11	**90-270 (19 steps)**	42	1	1

Table 5-1 Design parameters for Optimization 1.

The first optimization was done by changing the number of turns, N = N1 = N2 between 3 and 5 and by changing the feed angle Φ from 90° to 270°. Each design parameter value is shown in Table 5-1. This served as the starting point of the optimization as minimal information could be gathered from the gain or S parameter plots as shown in Figure 5-23 and Figure 5-24.

The mean value of the gain and S parameters relative to Φ and N, were added to the graphs on the X and Y planes respectively. This gave a better idea of each parameter's influence. The gain relative to the feed angle seems to have no definite pattern whereas relative to the number of turns there is a definite decline for lesser turns. This coincides with the basic helix antenna theory discussed in section 5.2.1.

The reflection and coupling seems to be inversely proportional. This can be expected since if more power is reflected back to the source less power will be radiated by the antenna and thus less power will couple between the two helices. What seems to improve the isolation, in this case, worsens the overall antenna performance. This also explains why the gain decreases when $|S_{11}|$ and $|S_{22}|$ increases. These results show that there will have to be trade-off between the antenna gain, reflection and coupling. Some gain will have to be sacrificed to improve the isolation. A good antenna typically has a reflection $|S_{11}|$ of at least -10 dB. The minimum satisfactory reflection was chosen as -10 dB. If necessary, an impedance matching section may be added before each antenna port to improve this parameter. This does not influence $|S_{21}|$, since it is only dependant on the physical antenna structure.

From the radar equation (3.1), it can be shown that the relationship between the maximum range R_{max} and antenna gain G is proportional ($R_{max} \propto \sqrt{G}$). Thus, every 6 dB improvement (linear multiplication of 4) of the antenna gain doubles the maximum range. A 3 dB improvement will increase R_{max} with a factor $\sqrt{2}$. The measured antenna gain of the circularly polarized patch is 6 dB. Therefore the aim for the helix antenna gain was chosen to be at least 9 dB. RadarOpt (discussed in chapter 3), indicated that more isolation will be needed between the transmit and receive signals to prevent mixer saturation. Therefore the minimum satisfactory coupling was chosen 10 dB lower than achieved with the first model antenna as – 20 dB.

Optimization 2: 0.10 ≤ A1 = A2 ≤ 0.13 m and 30 ≤ R ≤ 60 mm

N1	N2	D1 [mm]	D2 [mm]	**A1 [m]**	**A2** [m]	Φ [°]	**R [mm]**	d1 [mm]	d2 [mm]
4	4	40	40	**10-13 (16 steps)**	**A1**	180	**30-60 (16 steps)**	1	1

Table 5-2 Design parameters for Optimization 2.

For the second optimization N1 = N2 = 4 and Φ = 180° were chosen because more turns should give a higher gain and seeing that Φ = 180° is the furthest distance between the two feeds, the least coupling is expected. The ground plane radius R is changed over a span of 30 mm to 60 mm and the axial lengths A1 and A2 are similarly changed between 0.1 m and 0.13 m. The antenna gain is plotted in Figure 5-25 and is greater than 10 dB for each run. The gain seems to improve slightly with increasing axial length. Figure 5-26 clearly shows the inversely proportional behaviour of the reflection and coupling that was also seen in optimization 1. The optimum point indicated in Figure 5-26 is the minimum intersection between the two planes and does not meet requirements but will be used as the starting point for the next optimization. Generally, the coupling seems to decrease as axial length increases without really effecting the reflection. Reflection improves by decreasing the ground plane radius although the coupling slightly increases.

Optimization 3: 40 ≤ D1 ≤ 44 mm and 33 ≤ D2 ≤ 39 mm

N1	N2	**D1 [mm]**	**D2 [mm]**	A1 [m]	A2 [m]	Φ [°]	R [mm]	d1 [mm]	d2 [mm]
4	4	**40-44 (11 steps)**	**33-39 (16 steps)**	11	11	180	46	1	1

Table 5-3 Design parameters for Optimization 3.

From the first two optimizations it seemed that the only way to achieve a coupling in the -20dB range would be to physically separate the two helices. Thus, in the third optimization the diameters D1 and D2 of the two helices were changed rendering Helix-1 on the outside and Helix-2 on the inside. The gain and S parameter plots in Figure 5-27 and Figure 5-28 changed accordingly. The overall gain decreased with approximately 2 dB but the coupling improved significantly, decreasing from -4 dB to -22 dB.

By increasing D1 and decreasing D2, Helix-1 and Helix-2 will have a slightly lower f_0 and higher f_0 respectively. Hence f_0 is determined by the helix circumference. Due to the frequency difference there is an increase in the overall reflection $|S_{11}|$ and $|S_{22}|$ at 2.5 GHz and a slight decrease in the antenna gain. Unfortunately, there is still no optimum point that satisfies all the requirements. Interestingly, it was noted that the inner helix diameter D2 has a much greater influence on the gain as well as the reflection and coupling than the outer helix diameter D1.

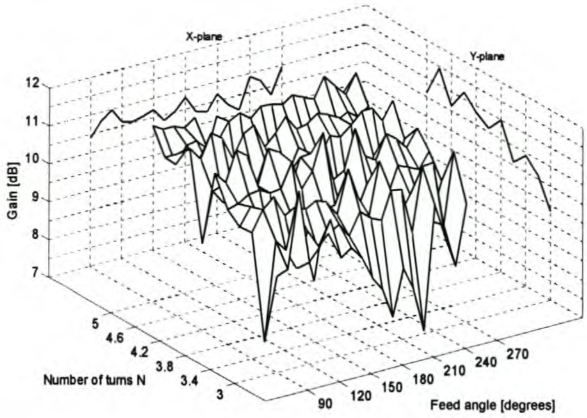

Figure 5-23: Optimization 1 – Antenna gain with mean values against Φ and N.

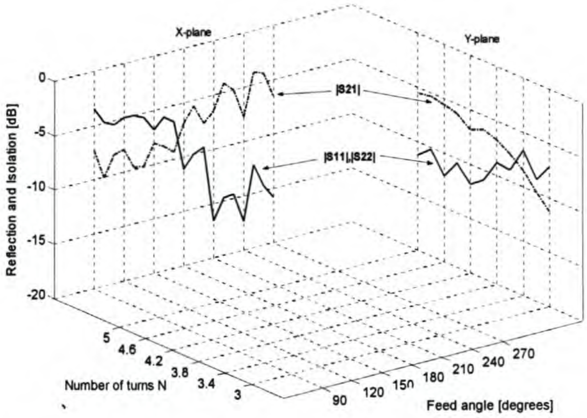

Figure 5-24: Optimization 1 - Mean values of reflection $|S_{11}|$, $|S_{22}|$ and coupling $|S_{21}|$ against Φ and N.

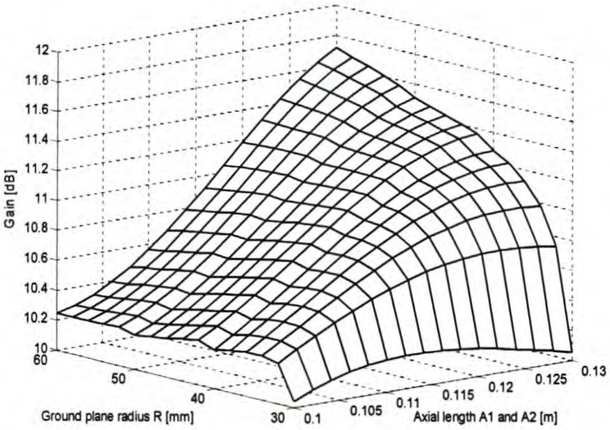

Figure 5-25: Optimization 2 – Antenna gain against R and A1 = A2.

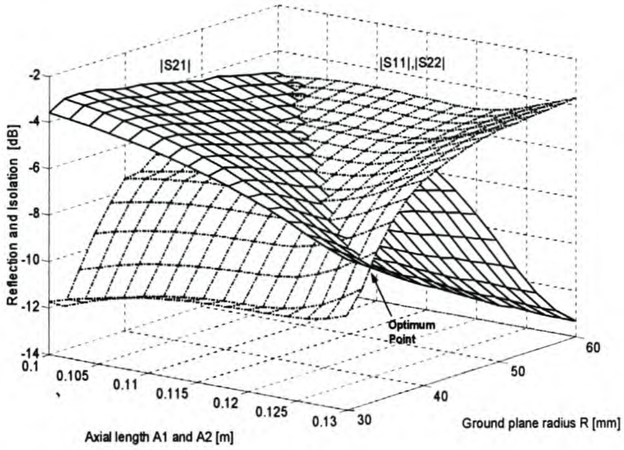

Figure 5-26: Optimization 2 - Antenna reflection $|S_{11}|$, $|S_{22}|$ and coupling $|S_{21}|$ against R and A1 = A2.

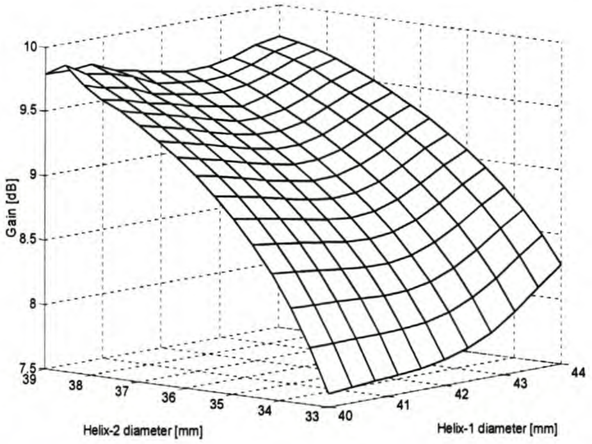

Figure 5-27: Optimization 3 – Antenna gain against D1 and D2.

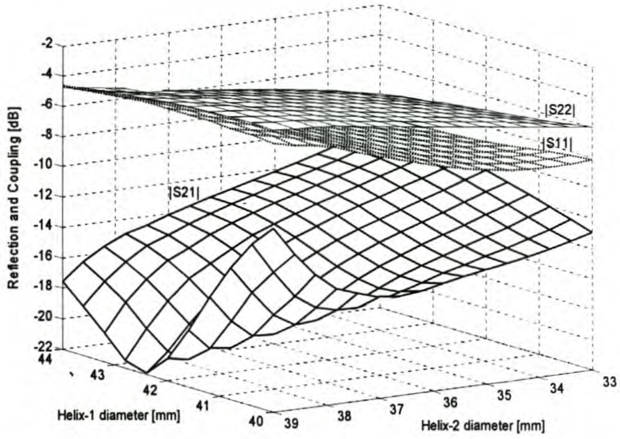

Figure 5-28: Optimization 3 - Antenna reflection $|S_{11}|$, $|S_{22}|$ and coupling $|S_{21}|$ against D1 and D2.

Optimization 4: **$0.1 \leq A2 \leq 0.13$ m and $33 \leq D2 \leq 39$ mm**

N1	N2	D1 [mm]	**D2 [mm]**	A1 [m]	**A2 [m]**	Φ [°]	R [mm]	d1 [mm]	d2 [mm]
4	4	40	**33-39 (11 steps)**	11	**10-13 (16 steps)**	180	46	1	1

Table 5-4 Design parameters for Optimization 4

Optimization 4 focused on the two main parameters of the inner Helix-2, namely D2 and A2. As previously stated, the optimum pitch angle for a monofilar helix should be limited to 12° ≤ α ≤ 14° to achieve optimum gain. With the distance between each turn S = A/N the pitch angle given by (5.11) becomes

$$\alpha = \arctan\left(\frac{A}{\pi DN}\right) \tag{5.12}$$

Both A2 and D2 are variables during this optimization, therefore the pitch angle changes with each parameter. The influence of the pitch angle is clearly shown in the gain plot of Figure 5-29. At the lowest gain the calculated pitch angle from (5.12) has a maximum of α =17.9° with A2 = 0.13 m and D2 = 32 mm. This is nearly 4° above the preferred limit. The minimum pitch angle α =11.25° with A2 = 0.1 m and D2 = 40 mm is just below the preferred limit. The peak gain overlaps with the optimum pitch angle at α =12.88° with A2 = 0.115 m and D2 = 40 mm. Unfortunately, the coupling and reflection in Figure 5-30 has to be taken into account and some of the gain will have to be sacrificed for better reflection and isolation. The point of optimum reflection has minimum gain and worst coupling, therefore the optimum point for all three parameters namely gain, coupling and reflection is where D2 = 35 mm and A2 = 0.125 m giving $|S_{11}|$ = - 9 dB, $|S_{22}|$ = -7 dB, $|S_{21}|$ = -17.5 dB and gain = 7.3 dB.

Optimization 5: **$2 \leq N2 \leq 6$ and $0.5 \leq d2 \leq 2$ mm**

N1	**N2**	D1 [mm]	D2 [mm]	A1 [m]	A2 [m]	Φ [°]	R [mm]	d1 [mm]	**d2 [mm]**
4	**2 - 6 (5 steps)**	40	35	0.11	12.5	180	46	1	**0.4 -2 (16 steps)**

Table 5-5 Design parameters for Optimization 5.

It should have been expected that by changing the number of turns the pitch angle would also change and the gain would decrease for N ≠ 4 as seen on the gain plot of Figure 5-31. The wire diameter does not make a big difference but there is a slight improvement on the reflection and the gain when using the thicker wire diameter of 2 mm.

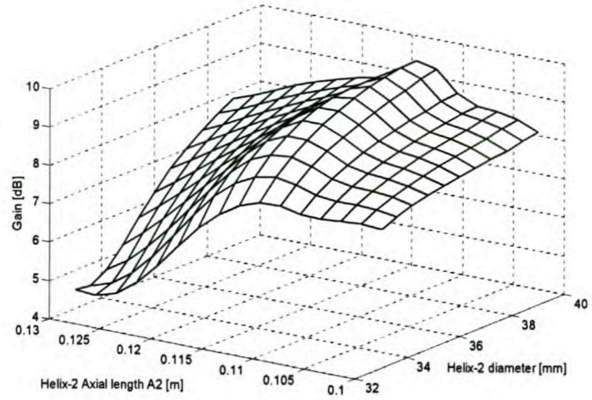

Figure 5-29: Optimization 4 – Antenna gain with mean values against A2 and D2.

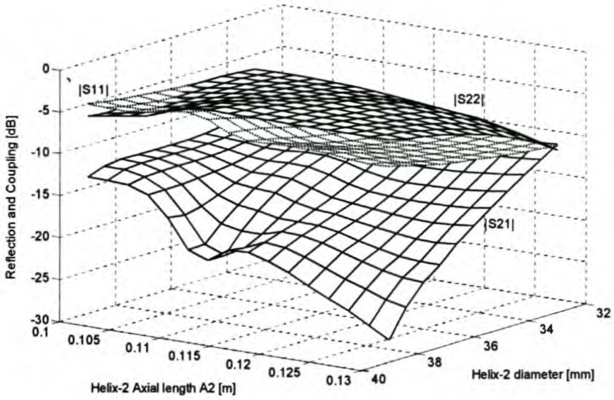

Figure 5-30: Optimization 4 - Antenna reflection $|S_{11}|$, $|S_{22}|$ and coupling $|S_{21}|$ against A2 and D2

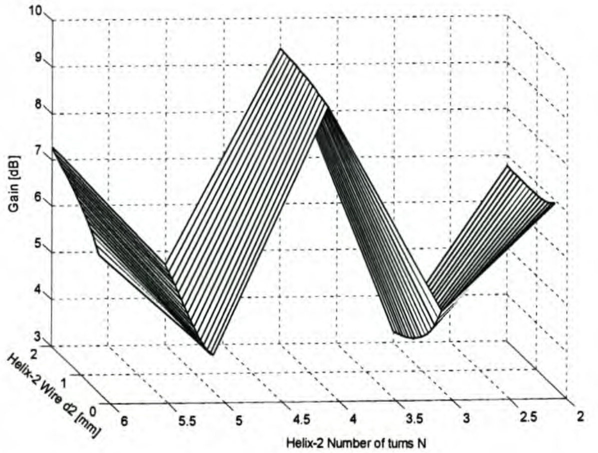

Figure 5-31: Optimization 5 – Antenna gain with mean values against A2 and D2.

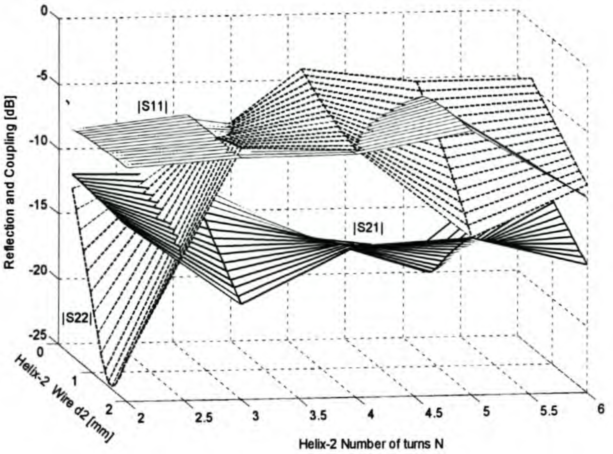

Figure 5-32: Optimization 5 - Antenna reflection $|S_{11}|$, $|S_{22}|$ and coupling $|S_{21}|$ against A2 and D2

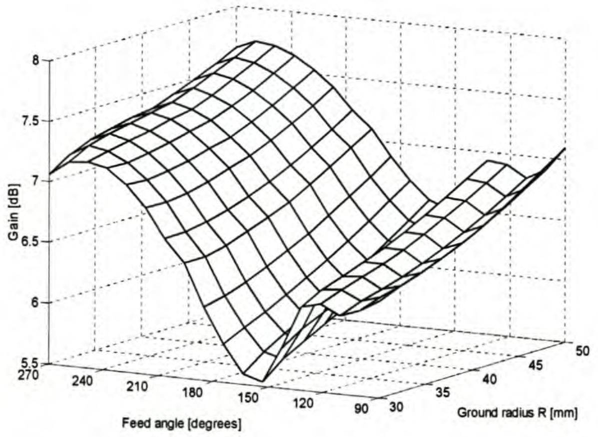

Figure 5-33: Optimization 6 – Antenna gain against R and feed angle.

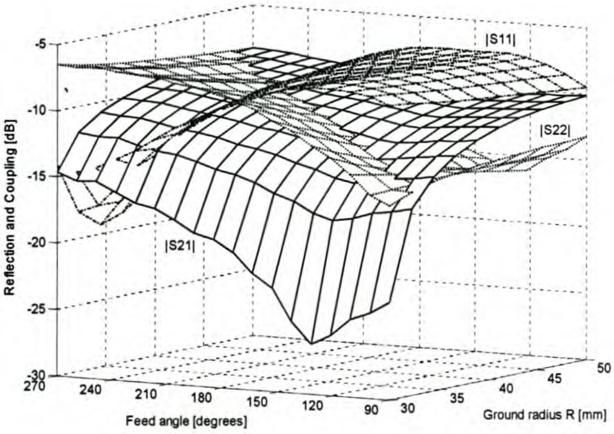

Figure 5-34: Optimization 6 - Antenna reflection $|S_{11}|$, $|S_{22}|$ and coupling $|S_{21}|$ against R and feed angle.

Optimization 6 and 7: **Opt 6: 90° ≤ Φ ≤ 270° and 30 ≤ R ≤ 50 mm** **Opt 7: 10° ≤ Φ ≤ 350° and 25 ≤ R ≤ 30 mm**

Opt	N1	N2	D1 [mm]	D2 [mm]	A1 [m]	A2 [m]	**Φ [°]**	**R [mm]**	d1 [mm]	d2 [mm]
6	4	3	40	35	11	12.5	**90-270 (19 steps)**	**30-50 (10 steps)**	1	2
7	4	3	40	35	11	12.5	**10-350 (35 steps)**	**25-30 (2 steps)**	1	2

Table 5-6 Design parameters for Optimization 6 and 7.

The number of turns for the inner helix was chosen equal to three (N2 = 3) to see if it would improve $|S_{21}|$ without sacrificing a large amount of gain. The resulting gain was 1 dB lower and the gain plot in Figure 5-33 made a large trench at Φ = 160° and increased toward Φ = 90° and 270°. The reflection planes $|S_{11}|$ and $|S_{22}|$ intersect in the middle of this trench which seems to be an optimum point (Figure 5-34). $|S_{21}|$ is mainly dependant on the ground plane radius R which does improve exponentially with decreasing R as can be seen in Figure 5-34.

Optimization 7 was run over a wider feed angle variation and focused only on the difference between R = 30 mm and R = 25 mm. There was a definite improvement in the reflection, gain and isolation for a smaller feed angle. The optimum point from Figure 5-35 and Figure 5-36 is where the reflection planes intersect at -10 dB with Φ = 30° and R = 30 mm. The coupling at this point satisfies the -20 dB aim and the antenna gain is a maximum of 8 dB.

Optimization 8: **3 ≤ N2 ≤ 5 and 30° ≤ Φ ≤ 60°**

N1	**N2**	D1 [mm]	D2 [mm]	A1 [m]	A2 [m]	**Φ [°]**	R [mm]	d1 [mm]	d2 [mm]
4	**3-5 (10 steps)**	40	35	11	12.5	**30-60 (10 steps)**	30	1	2

Table 5-7 Design parameters for Optimization 8.

Optimization 8 is a recap of the previous three optimizations, to determine if there might be an optimum point that was overseen. From the gain and S parameter plots in Figure 5-37 and Figure 5-38 the optimum point is still the same as in optimization 7 with Φ = 30° and N = 3.

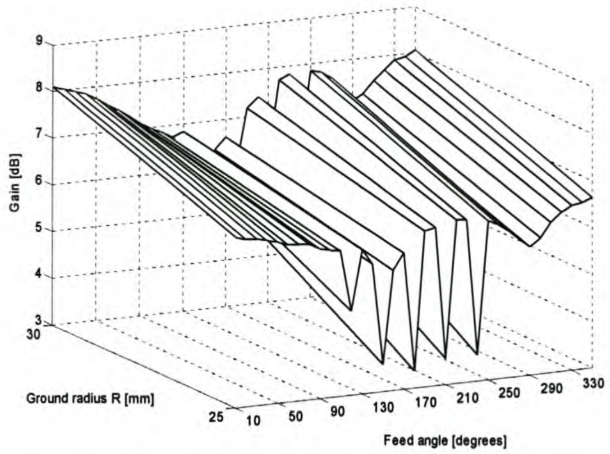

Figure 5-35: Optimization 7 – Antenna gain against feed angle and R.

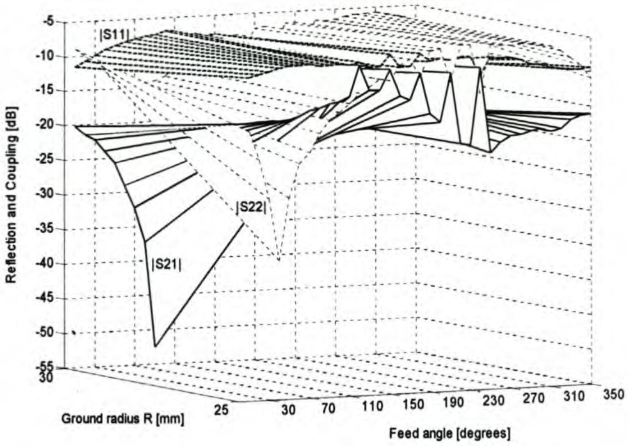

Figure 5-36: Optimization 7 - Antenna reflection $|S_{11}|$, $|S_{22}|$ and coupling $|S_{21}|$ against feed angle and R.

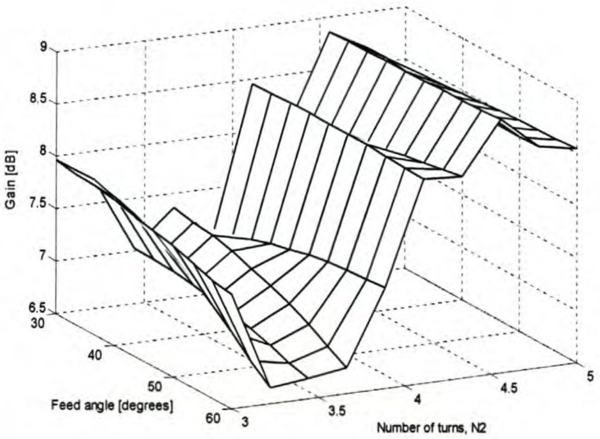

Figure 5-37: Optimization 8 – Antenna gain against Φ and N2.

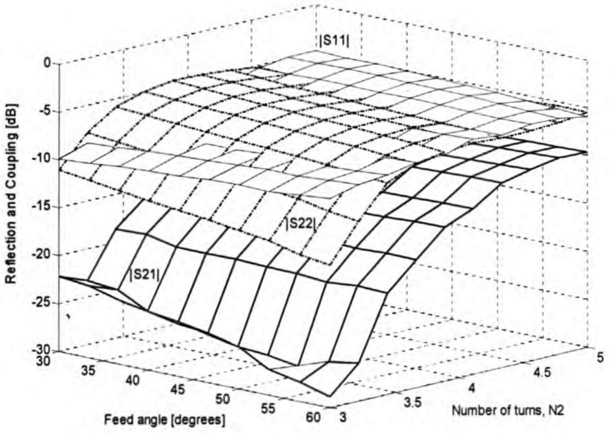

Figure 5-38: Optimization 8 - Antenna reflection $|S_{11}|$, $|S_{22}|$ and coupling $|S_{21}|$ against Φ and N2.

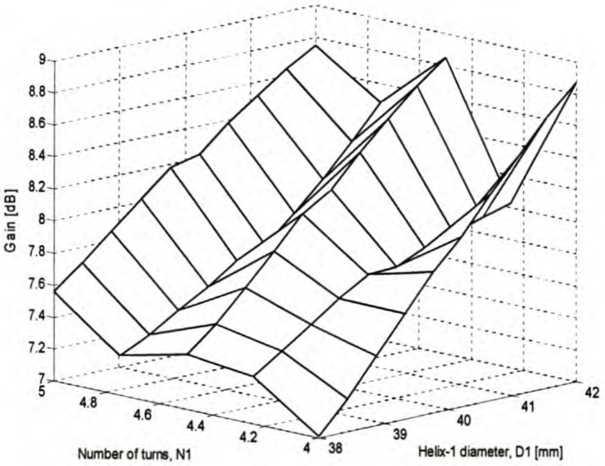

Figure 5-39: Optimization 9 – Antenna gain against D1 and N1.

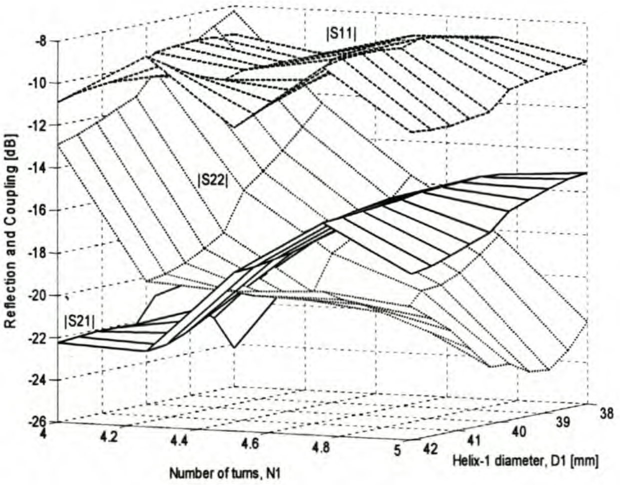

Figure 5-40: Optimization 9 - Antenna reflection $|S_{11}|$, $|S_{22}|$ and coupling $|S_{21}|$ against D1 and N1.

Optimization 9: 4 ≤ N1 ≤ 5 and 38 ≤ D1 ≤ 42 mm

N1	N2	**D1 [mm]**	D2 [mm]	A1 [m]	A2 [m]	Φ [°]	R [mm]	d1 [mm]	d2 [mm]
4-5 (5 steps)	3	**38-42 (10 steps)**	35	11	12.5	30	30	1	2

Table 5-8 Design parameters for Optimization 9.

For this optimization, the focus was shifted back to the outer Helix-1, with D1 and N1 as the chosen variable parameters. A slight increase in D1 improved the reflection and gain. (D1 = 42 mm). Although an increase in the number of turns improved the reflection, it worsened the isolation. A definite optimum point at N1 = 4 and D1 = 42 mm nearly meets the specified design requirements with $|S_{11}| = -11$ dB, $|S_{22}| = -13$ dB, $|S_{21}| = -22$ dB and antenna gain = 8.9 dB.

Optimization 10: 1 ≤ d1 ≤ 2 mm and 1 ≤ d2 ≤ 2 mm

N1	N2	D1 [mm]	D2 [mm]	A1 [m]	A2 [m]	Φ [°]	R [mm]	**d1 [mm]**	**d2 [mm]**
4	3	42	35	11	12.5	30	30	**1 - 2 (5 steps)**	**1 - 2 (5 steps)**

Table 5-9 Design parameters for Optimization 10.

With monofilar helices, the wire diameter does not have a very big influence but, according to the gain and S parameter plots in Figure 5-41 and Figure 5-42, it is a significant parameter, not to be ignored. The best gain is achieved for d1 = 2 mm and d2 = 1 mm but was chosen as d2 = d1 = 2 mm to compensate for the better isolation and reflection.

Optimization 11: 25° ≤ Φ ≤ 50° and 40 ≤ D1 ≤ 44 mm

N1	N2	**D1 [mm]**	D2 [mm]	A1 [m]	A2 [m]	**Φ [°]**	R [mm]	d1 [mm]	d2 [mm]
4	3	**40-44 (11 steps)**	35	11	12.5	**25-50 (6 steps)**	30	1	1

Table 5-10 Design parameters for Optimization 11.

Another optimization was run to recap and it was found that by increasing the feed angle, the coupling is minimized to an excellent -26 dB. Unfortunately, the opposite is true for the reflection which worsened to – 8.5 dB. The design thus stays unchanged with Φ = 30° and D1 = 42 mm.

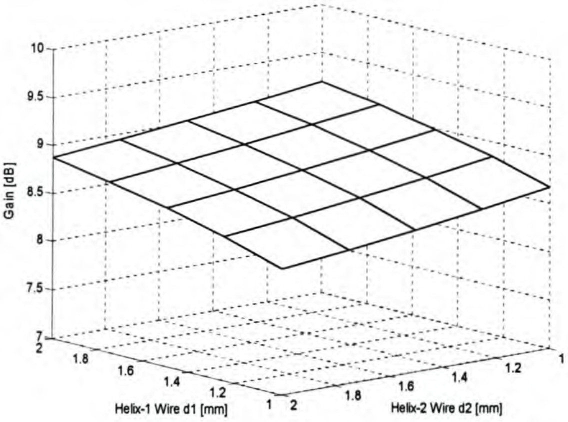

Figure 5-41: Optimization 10 – Antenna gain against d1 and d2.

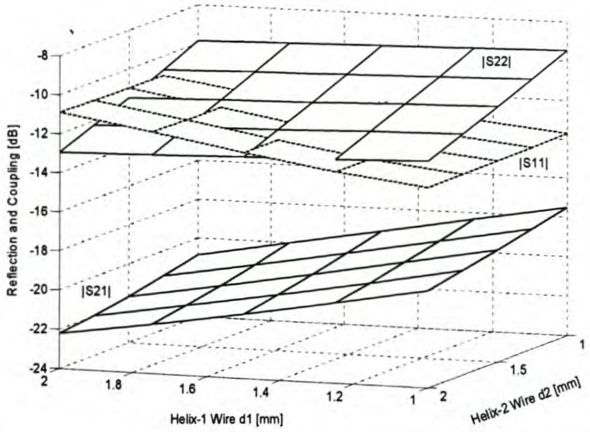

Figure 5-42: Optimization 10 - Antenna reflection $|S_{11}|$, $|S_{22}|$ and coupling $|S_{21}|$ against d1 and d2.

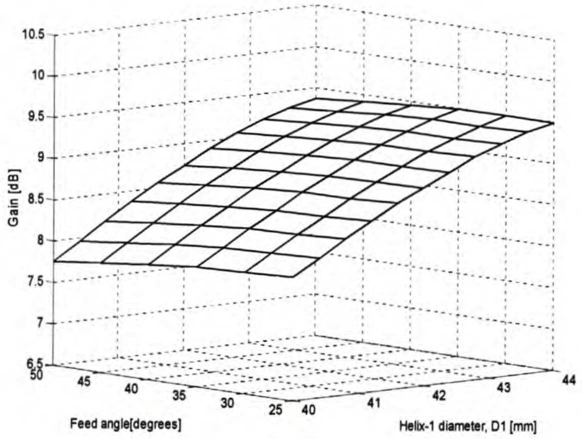

Figure 5-43: Optimization 11 – Antenna gain with against the feed angle Φ and D1.

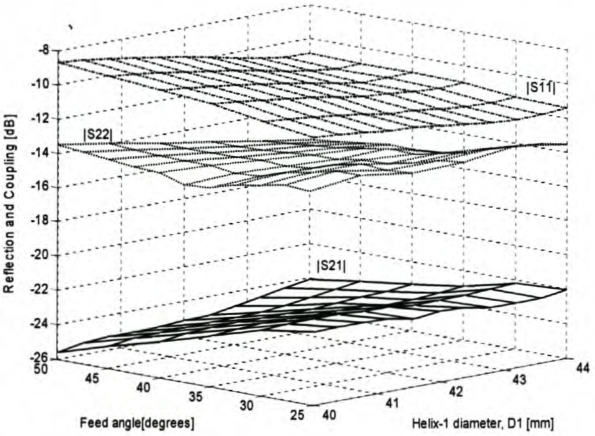

Figure 5-44: Optimization 11 - Antenna reflection $|S_{11}|$, $|S_{22}|$ and coupling $|S_{21}|$ against the feed angle Φ and D1.

Simulated results of the final optimized antenna design:

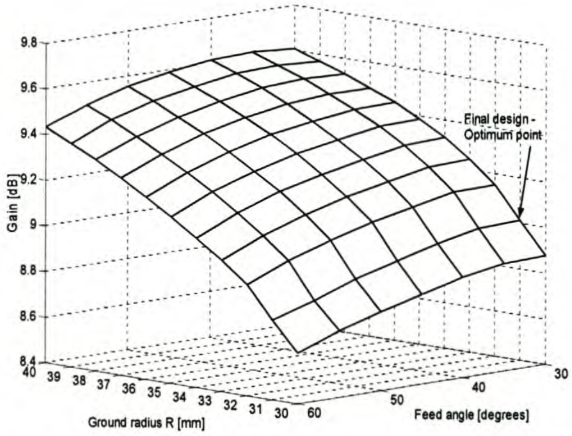

Figure 5-45: Optimization 12 – Antenna gain against the feed angle Φ and R.

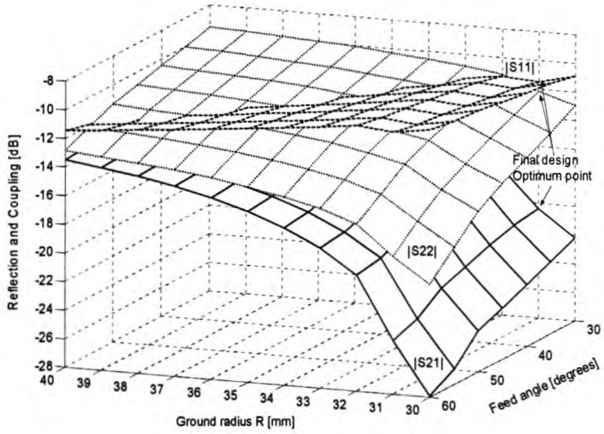

Figure 5-46: Optimization 12 - Antenna reflection $|S_{11}|$, $|S_{22}|$ and coupling $|S_{21}|$ against the feed angle Φ and R.

Optimization 12: $30° \leq \Phi \leq 60°$ and $30 \leq R \leq 40$ mm

N1	N2	D1 [mm]	D2 [mm]	A1 [m]	A2 [m]	**Φ [°]**	**R [mm]**	d1 [mm]	d2 [mm]
4	3	42	35	11	12.5	**30-60 (7 steps)**	**30-40 (11 steps)**	1	1

Table 5-11 Design parameters for Optimization 12.

The final optimization was done by closely inspecting the feed angle and ground plane radius. The idea was to find an optimum point that could meet all the requirements set in the beginning of the optimization process. Previous optimizations met the reflection and coupling requirements, but not the gain requirement, which was still below 9 dB. R was stepped in smaller steps (1 mm) in this optimization to improve the gain. From the gain and S parameter plots in Figure 5-45 and Figure 5-46 all the requirements are met at the point where R = 31 mm and $\Phi = 30°$. This finalizes the design with gain = 9 dB, $|S_{11}| = -11.8$ dB $|S_{22}| = -12$ dB and $|S_{21}| = -20.2$ dB.

A summary of the design process with each parameter for every optimization and the final design is given in Table 5-12.

Optimi-zation	**N1**	**N2**	**D1 [mm]**	**D2 [mm]**	**A1 [m]**	**A2 [m]**	**Φ [°]**	**R [mm]**	**d1 [mm]**	**d2 [mm]**
1	**3-5**	**N1**	40	40	11	11	**90-270**	42	1	1
2	4	4	40	40	**10-13**	**A1**	180	**30-60**	1	1
3	4	4	**40-44**	**33-39**	11	11	180	46	1	1
4	4	4	42	**33-39**	11	**10 -13**	180	46	1	1
5	4	**2-6**	42	35	11	12.5	180	46	1	**0.4-2**
6	4	4	42	35	11	12.5	**90-270**	**30-50**	1	2
7	4	4	42	35	11	12.5	**10-350**	**25-30**	1	2
8	4	**3-5**	42	35	11	12.5	**30-60**	30	1	2
9	**4-5**	3	**38-42**	35	11	12.5	30	30	1	2
10	4	3	42	35	11	12.5	30	30	**1-2**	**1-2**
11	4	3	**40-44**	35	11	12.5	**25-50**	30	2	2
12	4	3	42	35	11	12.5	**30-60**	**30-40**	2	2
final	**4**	**3**	**42**	**35**	**11**	**12.5**	**30**	**31**	**2**	**2**

Table 5-12 Summary of the optimization design procedure.

Table 5-13 gives a summary of each design parameter's influence on the antenna gain, isolation and reflection parameters. A final simulation of the optimized design was done in *Feko* over a wider frequency range. The gain, reflection and coupling are plotted in Figure 5-47 and Figure 5-48. The following section describes the building and measuring of the designed double helix antenna.

Design - Parameter	Gain	Isolation	Reflection
N1, N2	Improves with turn increase. An excessive number of turns will lower the pitch angle to < 12° thus decreasing the gain.	Improves if N1≠ N2. The optimum isolation point has to be determined empirically.	No pattern
D1 (Outer diameter)	Optimum for D1 = λ/π Not as sensitive to D1 as to D2	Improves for D1≠ D2 Extremely sensitive parameter	Optimum for D1 = λ/π
D2 (Inner diameter)	Optimum for D1 = λ/π More sensitive for D2 than for D1	Improves for D1≠ D2 Extremely sensitive parameter	Optimum for D1 = λ/π
A1 ,A2	No pattern. Gain is sensitive to pitch angle θ with $\theta \propto A$. Optimum gain when $12° \leq \theta \leq 14°$	Improves for A1≠ A2. The optimum isolation point has to be found empirically.	No pattern
Φ	Gain improves for smaller feed angle.	Improves for smaller feed angle. Optimum isolation at 30°	No pattern
R	Gain increase with increasing R.	Isolation improves for increasing R. Optimum isolation at R = 25 mm.	Reflection not sensitive to R.
d1 , d2	Gain Improves for smaller d2 and for greater d1	Improves for ,greater d1 and d2. Optimum isolation for d1 = d2 = 2 mm.	$\lvert S_{11}\rvert$ improves for smaller d1 (not sensitive to d2) $\lvert S_{22}\rvert$ improves for greater d2 (not sensitive to d1)

Table 5-13 Summary of each design parameter's influence on the gain, reflection and isolation.

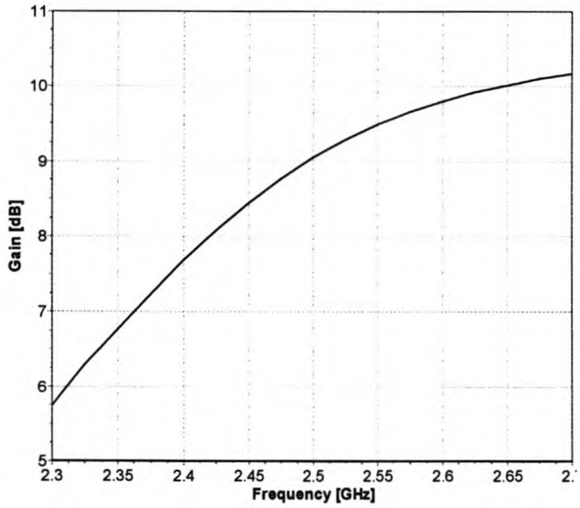

Figure 5-47 Final gain of the double helix antenna, simulated in *Feko*.

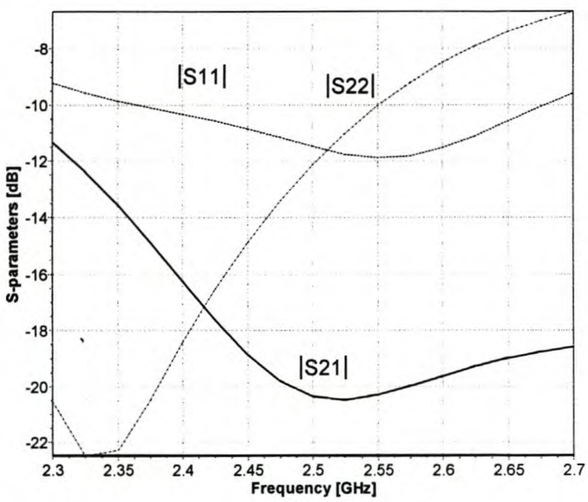

Figure 5-48 Final reflection and coupling of the double helix antenna, simulated in *Feko*.

5.2.3 Building and measuring the double helix antenna

Figure 5-49. Photograph of the double helix antenna that was built from the final design in section 5.2.2.

A photograph of the manufactured double helix antenna is shown in Figure 5-49. The antenna's S parameters, $|S_{11}|$, $|S_{22}|$ and $|S_{21}|$ were measured on the Network Analyzer as shown in Figure 5-50.

The measurement and simulation correlate except for the reflection at port 2 that is worse than the expected -10 dB. This can be improved by gradually tapering the first quarter wavelength of the wire at port 2 closer to the ground plane as explained in section 5.2.1. Seeing that it might increase the coupling between the helices, an impedance matching section can be added just before port-2 which should not affect $|S_{21}|$ as it is only dependant on the physical structure of the antenna. The measured isolation appears to be much better than what was expected.

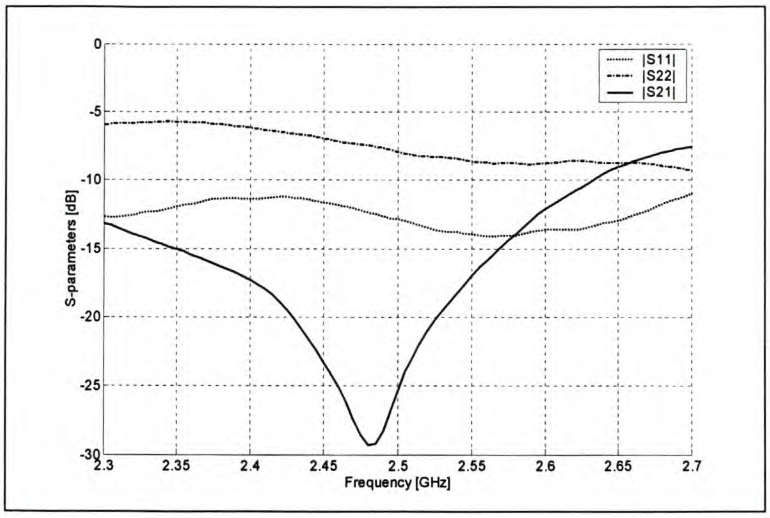

Figure 5-50. Antenna S parameter measurement on the 8753-Network Analyzer.

The gain and axial ratio of the double helix were calculated from the final S_{21} parameters that were measured in an anechoic chamber. Note that this measurement differs from the S_{21} measurement in Figure 5-50 because it refers to the ratio between the transmitted and received power between the two antennas under test. This measurement method is similar to the method that was used for the circularly polarized patch antenna in section 5.1.3. The two helices in the double helix antenna were measured separately to calculate the transmit and receive antenna gain. The inside antenna is RHC and the outside antenna is LHC, therefore it is expected that the polarization of the separate gain measurements will correspond to the antenna gain simulation of Figure 5-47.

Helix-1 measurements

The $|S_{21}|$ measurement results for the three antenna measurement setups are shown in Figure 5-51 to Figure 5-53 respectively. The calculated RHC and LHC S_{21}-parameter components of Helix-1 are also added on the graphs. The horn antenna gains as well as the the RHC and LHC gains of Helix-1 are displayed in Figure 5-54. The measured LHC gain is very close to the final simulation in Figure 5-47 and is 3 dB better than the measured gain of the circularly polarized patch antenna as expected. The axial ratio in Figure 5-55 shows that Helix-1 is not as perfectly circularly polarized as the patch antenna. The measured 2 dB axial ratio at the center frequency is still reasonable if compared to a 20 dB axial ratio of a perfectly linear polarized antenna. The $|S_{21}|$, radiation and axial ratio patterns in both the vertical and horizontal planes for -90° to 90° rotation are shown in Figure 5-56 to Figure 5-58 respectively. Helix-1 has a narrower beam width than the patch antenna which implies a better directivity and, as a result, less unwanted signals will reflect off interfering objects.

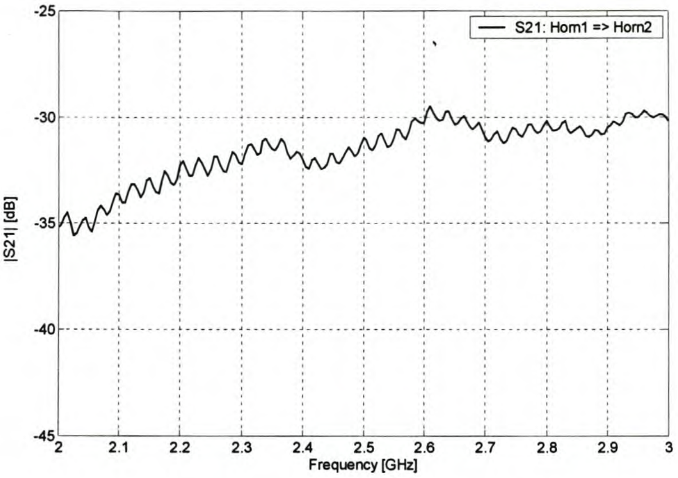

Figure 5-51: Measured $|S_{21}|$ between the two horn antennas.

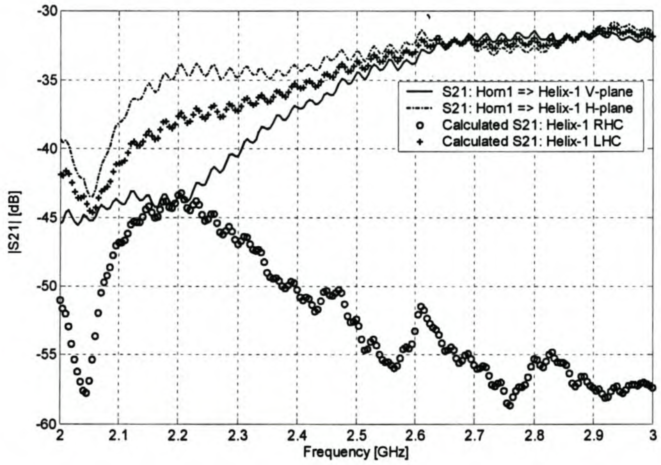

Figure 5-52: Measured $|S_{21}|$ between Helix-1 and horn-1 in the vertical and horizontal planes and the calculated LHC and RHC $|S_{21}|$.

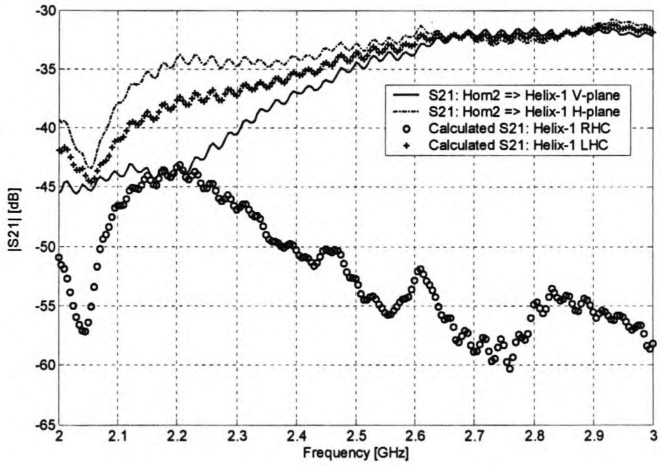

Figure 5-53: Measured $|S_{21}|$ between Helix-1 and horn-2 in the vertical and horizontal planes and the calculated LHC and RHC $|S_{21}|$.

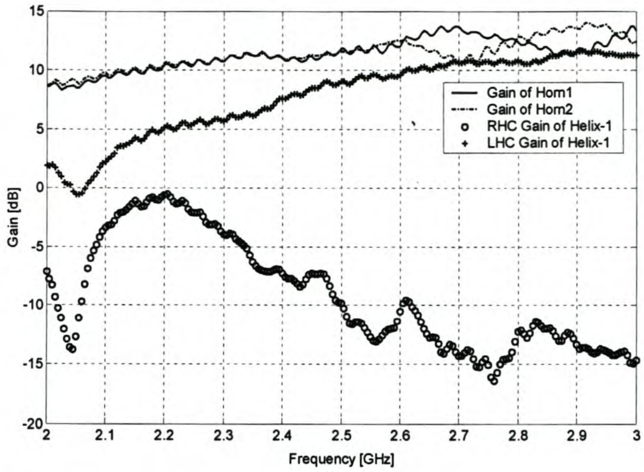

Figure 5-54: Gain of both horn antennas and LHC and RHC gain of Helix-1.

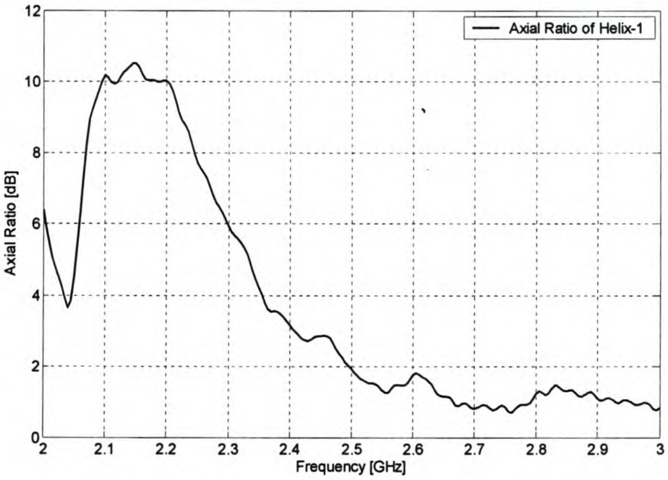

Figure 5-55: Axial Ratio of Helix-1.

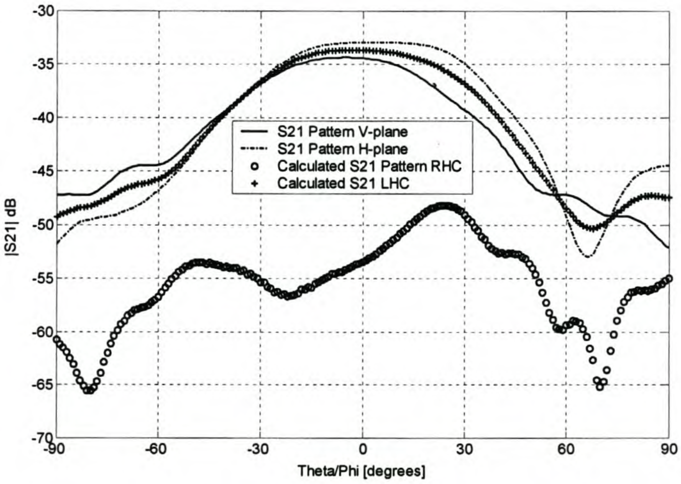

Figure 5-56: Measured vertical and horizontal plane $|S_{21}|$ patterns and calculated LHC and RHC $|S_{21}|$ patterns Helix-1.

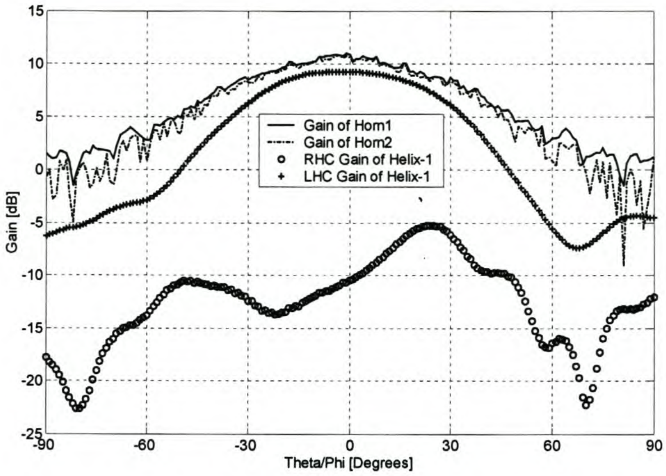

Figure 5-57: Radiation patterns of both horn antennas and LHC and RHC patterns of Helix-1.

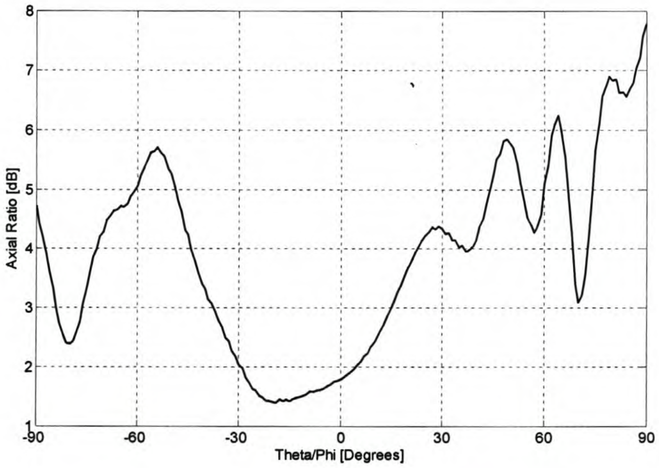

Figure 5-58: Axial Ratio pattern of Helix-1.

Helix-2 measurements

The same measurement routine for Helix-1 was followed for Helix-2. The $|S_{21}|$ measurements and calculated RHC and LHC S_{21}-parameter components are shown in Figure 5-59 and Figure 5-60. The gain of Helix-2 shown in Figure 5-61 is RHC but is 3.5 dB lower than 9 dB, which was expected from the antenna gain simulation shown in Figure 5-47. This difference lowers the maximum range with 25 % as explained in section 5.2.2 and is the price that was paid to achieve the best isolation between the two helices. The trade-off between the gain and isolation is valid because the isolation prerequisite is of paramount importance to the final radar system. This could not have been predicted from the simulations because the *Gain aim* function in *Optfeko* that was used for the simulations gives the average gain for the antenna and does not distinguish between the two helices. An alternative method that would still have separate helices with right- and left hand circular polarization and good isolation, as well as a higher gain is possible. In this method the helices are separated further apart on a single ground plane, each having an equal number of turns and diameter. It is uncertain if this change would present an improvement on the current double helix antenna as this method was not further inspected due to its large physical constraints. It is also not as unique as the designed double helix antenna, but it remains an alternative for a future helix antenna radar system.

The axial ratio of Helix-2 in Figure 5-62 indicates that it is not as circularly polarized as for Helix-1. This might influence the operation of the Lange coupler as its operation is greatly dependant on the correct phase between the different ports. The $|S_{21}|$, radiation and axial ratio patterns for Helix-2 are shown in Figure 5-63 to Figure 5-65 respectively.

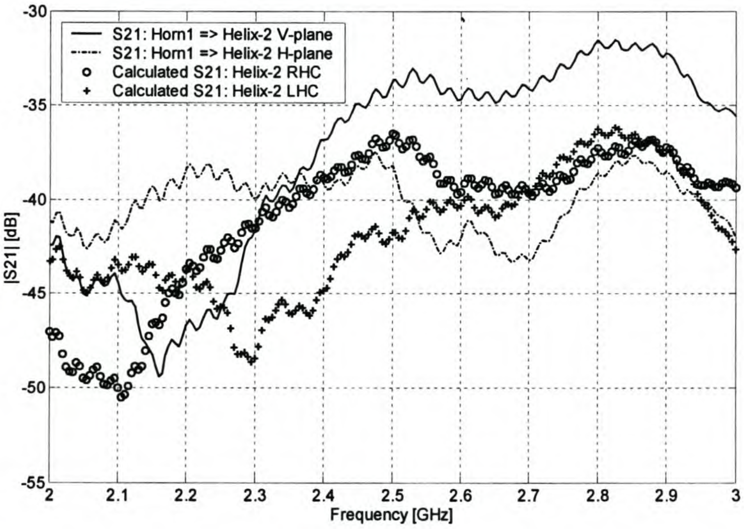

Figure 5-59: Measured $|S_{21}|$ between Helix-2 and horn-1 in the vertical and horizontal planes and the calculated LHC and RHC $|S_{21}|$.

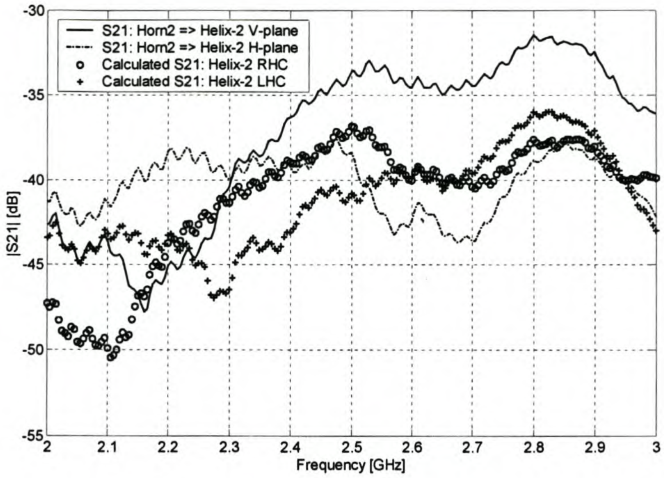

Figure 5-60: Measured $|S_{21}|$ between Helix-2 and horn-2 in the vertical and horizontal planes and the calculated LHC and RHC $|S_{21}|$.

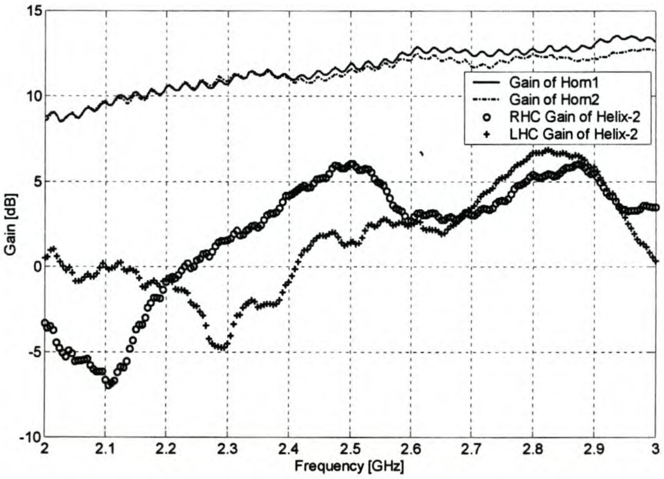

Figure 5-61: Gain of both horn antennas and LHC and RHC gain of Helix-2.

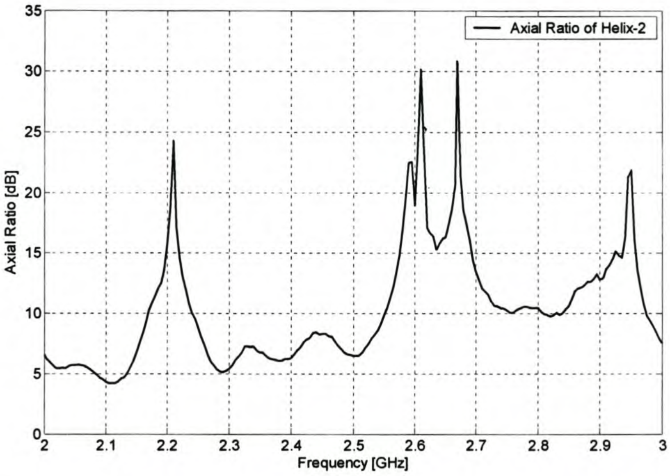

Figure 5-62: Axial Ratio of Helix-2.

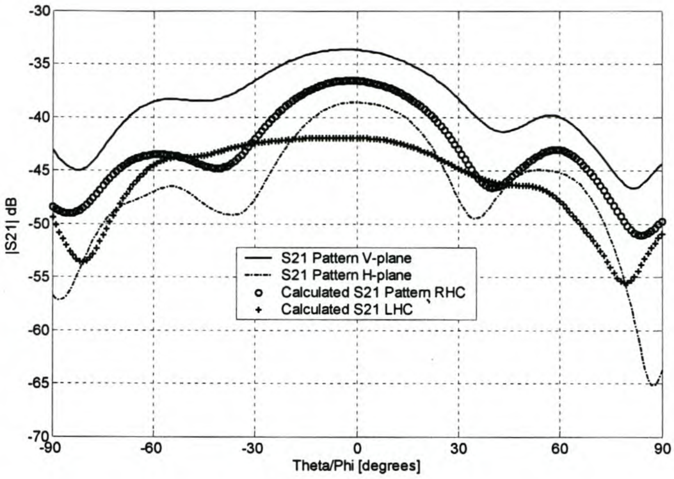

Figure 5-63: Measured vertical and horizontal plane $|S_{21}|$ patterns and calculated LHC and RHC $|S_{21}|$ patterns Helix-2.

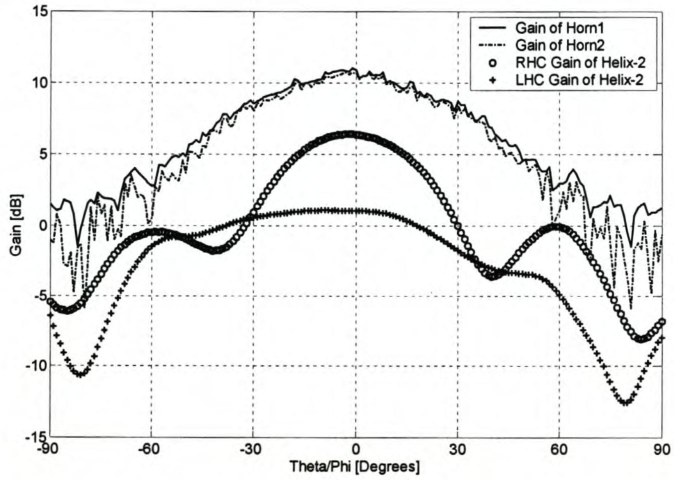

Figure 5-64: Radiation patterns of both horn antennas and LHC and RHC patterns of Helix-2.

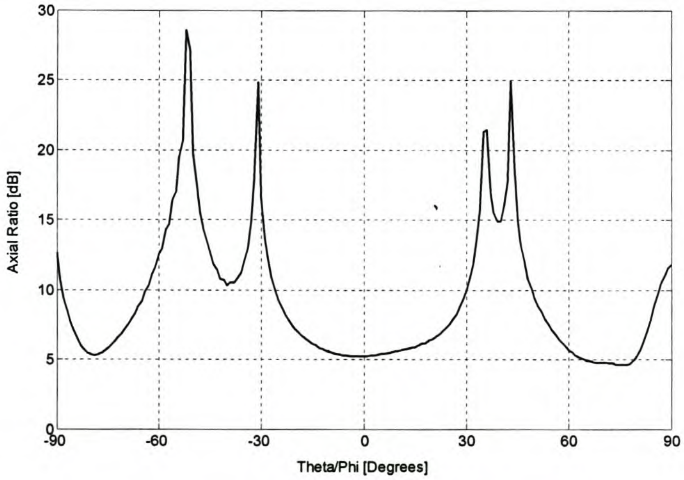

Figure 5-65: Axial Ratio pattern of Helix-2.

5.3 Conclusion

Circularly polarized Patch Antenna

- The patch antenna design is relatively simple and easy to manufacture.
- The input impedance of the antenna is well matched at the desired center frequency, but has a narrow bandwidth of 2% where the reflection coefficient is below -10 dB. This bandwidth is less than required.
- The antenna has a reasonable gain of 6.5 dB,
- it is nearly perfectly circularly polarized
- and is cost efficient.

Double Helix Antenna

- The double helix design and construction is somewhat more complicated than that of circularly polarized patch antenna.
- It has very good isolation between the transmitted and received helices that improves the radar's dynamic range.
- Helix-1 has a higher gain than the patch antenna of 9.5 dB. This will increase the radar's maximum detectible range, R_{max}. On the contrary Helix-2 has a lower gain of 5.5 dB, which will decrease R_{max}.
- The double-helix is well matched and has sufficient gain over a much wider bandwidth than the patch antenna.
- The antenna is cost efficient.
- It is foreseen to be more effective than the patch antenna in the radar system.

6. Preliminary measurements

Up to this point in the FM-CW radar system design, all the modules of the system have been designed and measured separately as discussed in chapter 4 and 5. The aim of this chapter is to discuss the preliminary radar system as shown in block diagram form in Figure 6-1.

The different components were connected with SMA connectors and low loss cables, to form an elementary radar system. The time delay between the transmitted and received signals, as discussed in chapter 2, was produced by using a long cable between the output of the coupled line and mixer RF-port. Therefore the antenna and Lange coupler were not necessary in this elementary system. The first reason for using a cable in the preliminary system is to determine if the basic system, consisting of the VCO, line coupler and mixer will operate as expected. Secondly, a much higher return signal power with bigger time delay can be realized with a cable than with the antenna and Lange coupler, which gives more accurate results. An advantage of this setup is that the components are not permanent and can easily be replaced until a satisfactory design is realized. The cable also makes it possible to know the exact distance that the transmitted signal will travel and no interfering signals or return signals that could reflect from unwanted objects will cause interference.

Section 6.1 and 6.2 discuss two measurement setups using a 30- and 12 meter cable respectively. The measured difference-frequency signal at the mixer IF-port will be compared with the simulations in section 2.3 and section 4.1 in both time and frequency domains. The last section 6.3 gives a summarizing conclusion of all the measurements.

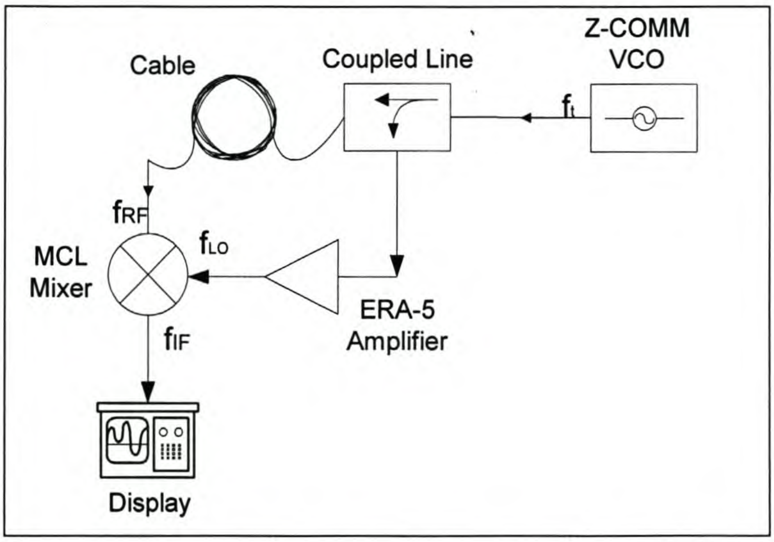

Figure 6-1: Preliminary radar system.

6.1 Preliminary measurements: 30 m cable

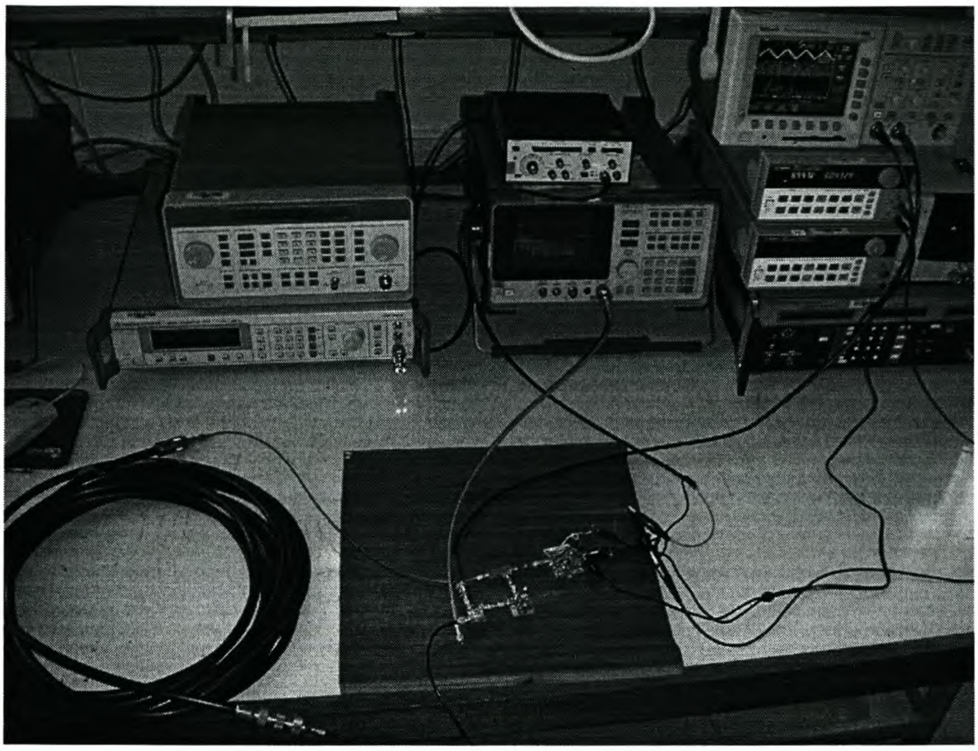

Figure 6-2: Preliminary measurement setup

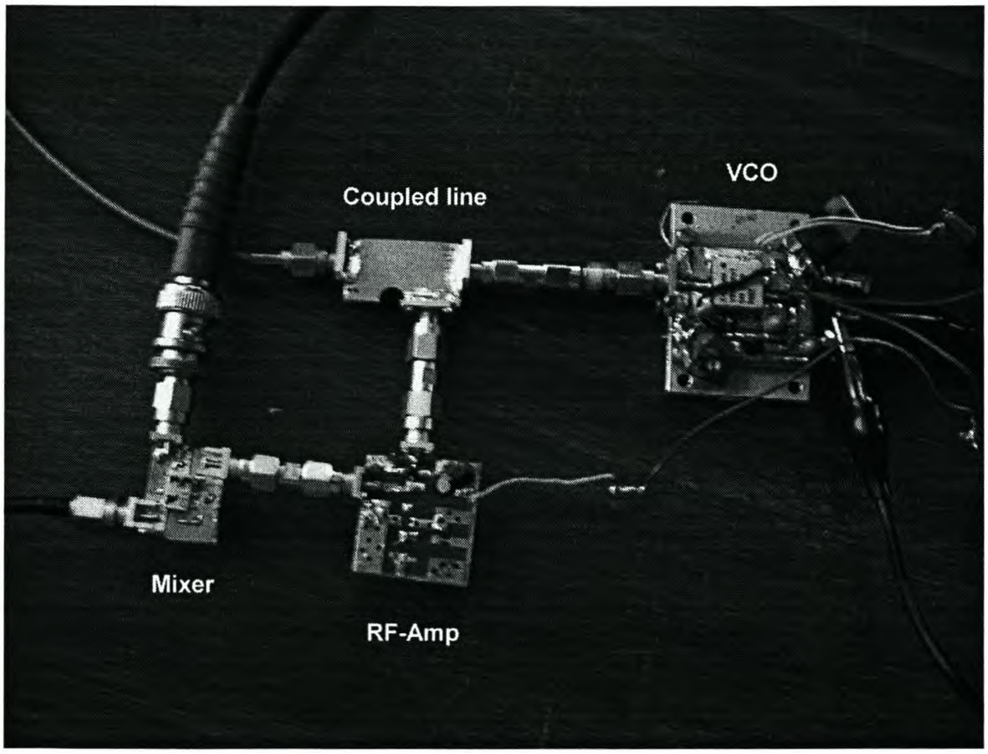

Figure 6-3: Top view of the preliminary system.

A picture of the preliminary system setup is shown in Figure 6-2. This setup was used for all the measurements by simply exchanging the 30- and 12 meter cables. Before any measurements were done, the maximum power at the output of the cable had to be measured. This was done to ensure that the maximum input power specified at the mixer RF-port is not exceeded. The power loss of each cable was high enough to ensure that the power level limits were not exceeded. The difference-frequency signal at the mixer IF- port was measured on the spectrum analyser and *Tectronix* oscilloscope to give the results in the frequency and time domains respectively. Comparisons between these domains and between the simulations that were done in the previous sections follow in this section.

Measurement 1: 30 meter cable, Δf = 200 MHz

The first measurement was done with a 30 m cable connected between the coupled line output and the mixer RF- input. The VCO was modulated with a 1 kHz triangular signal and 200 MHz deviation. When using a cable to realize the time delay, the range R in equation (2.2) is equal to half the cable length, L, because the cable replicates the distance to the target and back. In this case the eqivilant range R is 15 m. Thus the beat frequency becomes:

$$f_b = \frac{2Lf_m\Delta f}{c} \tag{6.1}$$

The expected beat frequency for this measurement is calculated from the above values as f_b = 40 kHz. The measured frequency and time domain of the difference-frequency signal were done on the spectrum analyzer and *Tectronix* oscilloscope respectively. The effect of the non-linearity of the VCO on the frequency spectrum, as simulated in section 4.1, is confirmed by the spectrum analyser measurement shown in Figure 6-4(a). Note that the highest peak is situated at the calculated beat frequency. The spectrum analyzer measurement was repeated over a narrow frequency span between 20 – 60 kHz to focus on the frequency spectrum adjacent to the beat frequency. The result is shown in Figure 6-4 (b) and can be compared with the difference-frequency signal simulations of section 2.3 (Figure 2-16 and Figure 2-17). All the peak frequencies adjacent to the beat frequency are spaced 1 kHz apart which is exactly the modulation frequency.

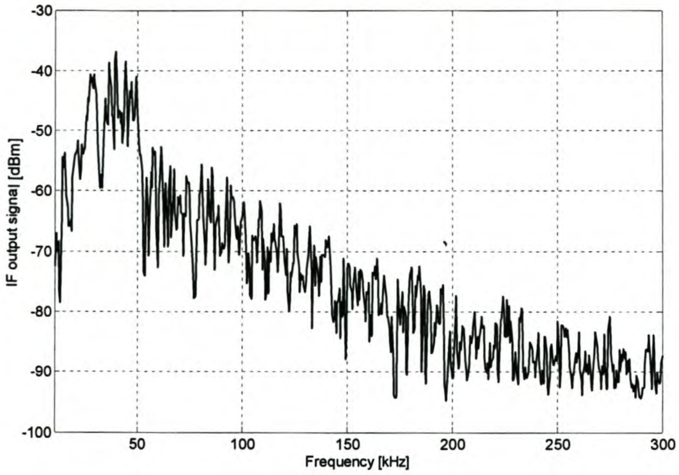

(a)

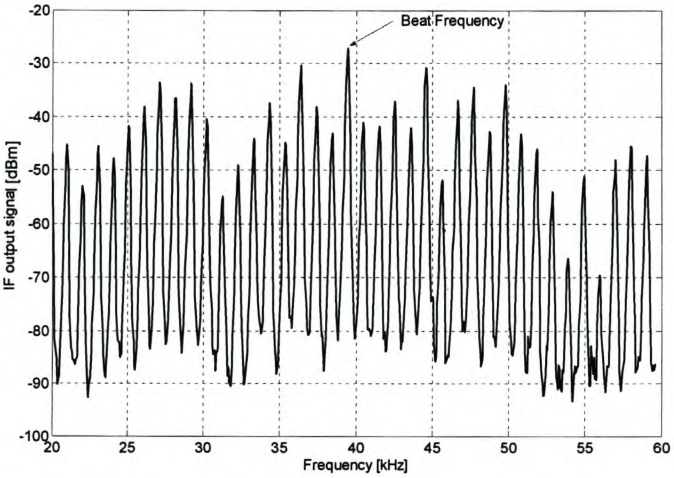

(b)

Figure 6-4: Measurement of the difference-frequency signal on spectrum analyzer. F_m = 1 kHz, Δf = 200 MHz, L = 30 m, f_b = 40 kHz. (a) Measured between 10 – 300 kHz (b) Measured between 20 – 60 kHz.

The time domain measurement shown in Figure 6-5 illustrates the difference-frequency signal v_d and triangular modulation VCO input signal. The measured triangular wave was scaled to fit on the same graph to see the effect of the beat note on v_d. This effect is not very clear in Figure 6-5 and is discussed with the results of the measurement that followed. The *Math-FFT* function of the oscilloscope was used to convert the time domain measurement to the frequency domain as shown in Figure 6-6. This result correlates with the spectrum analyzer measurement of Figure 6-4(a).

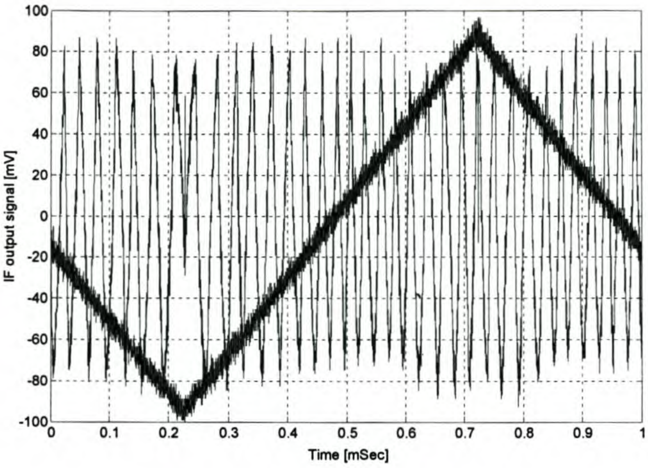

Figure 6-5: Time domain measurement of the difference-frequency signal on the oscilloscope. F_m = 1 kHz, Δf = 200 MHz, L = 30 m, f_b = 40 kHz.

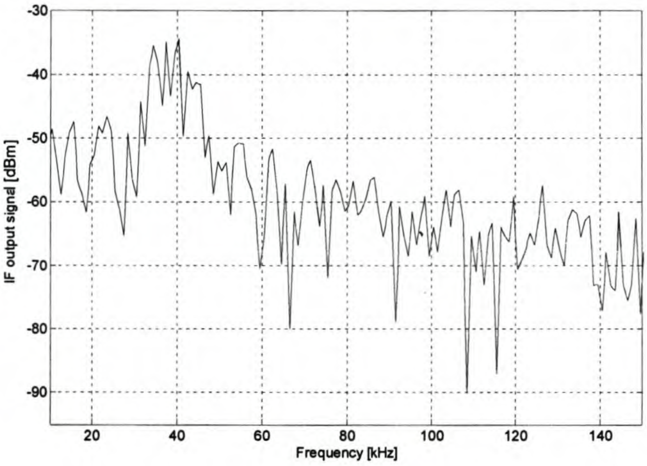

Figure 6-6: The FFT function on the oscilloscope was used to convert the time domain measurement in Figure 6-5 to the frequency domain.

Measurement 2: 30 meter cable, Δf = 100 MHz

The second measurement was done for a 100 MHz deviation of the VCO output signal. The measurement setup is similar to measurement 1. The new beat frequency was calculated with equation (6.1) as f_b = 20 kHz. The measurement of the frequency spectrum with the spectrum analyzer is shown in Figure 6-7. The beat frequency in Figure 6-7 (a) is more precise and has less adjacent frequency peaks than the measured results in Figure 6-4 (a). This can only be caused by the difference in the deviation of the VCO signal between the two measurements. Thus the improvement in the clarity of the beat frequency in measurement 2 is due to the VCO signal being more linear over a narrower frequency between 2.45 – 2.55 GHz. The result in Figure 6-7 (b) can be compared with the result of Figure 6-4 (b).

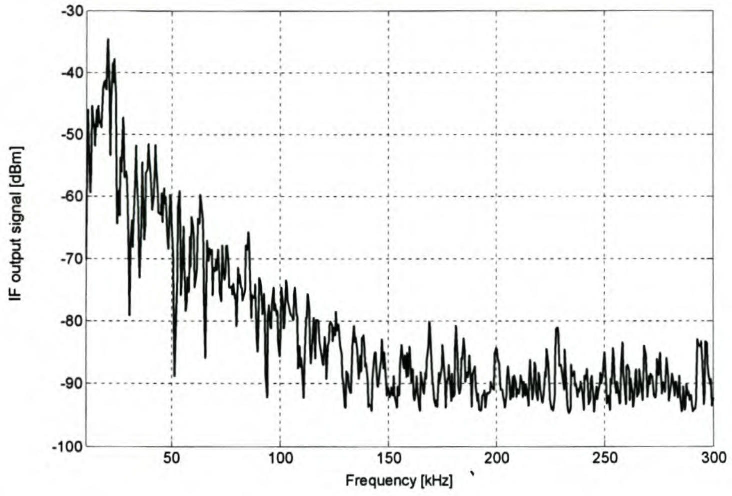

(a)

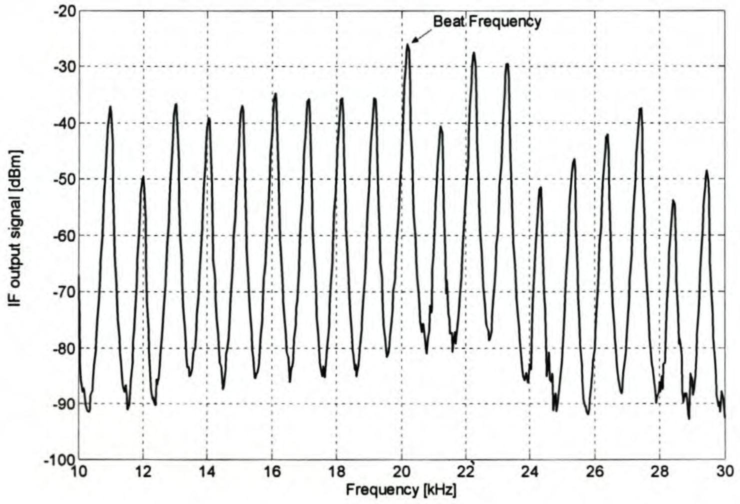

(b)

Figure 6-7: Measurement of the difference-frequency signal on the spectrum analyzer. F_m = 1 kHz, Δf = 100 MHz, L = 30 m, f_b = 20 kHz. (a) Measured between 10 – 300 kHz (b) Measured between 10 – 30 kHz.

The time domain measurements of the difference-frequency signal and triangular modulation frequency signals are shown in Figure 6-8. The effect of the beat note, as explained in section 2.2, on v_d can be seen at every peak of the triangular wave. v_d undergoes a 180° phase after each beat note. This is due to the rate of change in the frequency of the VCO that changes from positive to negative for each up or down cycle of the triangular wave.

It was expected that the 180° phase shift after each beat note will add to give a zero result on the spectrum analyzer, seeing that $V_d\angle 0° + V_d\angle 180° = 0$. This was shown differently as the spectrum analyzer measurements in Figure 6-7 almost correlates with the FFT of v_d shown in Figure 6-9. Figure 6-10 shows the FFT over a longer period of T = 10 ms (10 periods of f_m) and there are more frequency peaks adjacent to the beat frequency that have nearly the same amplitude. All the frequencies surrounding the beat frequency are multiples of the modulation frequency f_m and correlates with the measurement of Figure 6-4 (b) and Figure 6-7 (b). It would thus be more accurate to measure or sample over a half-period of the modulation frequency signal seeing that this will reduce the effect of the beat note on the difference-frequency signal.

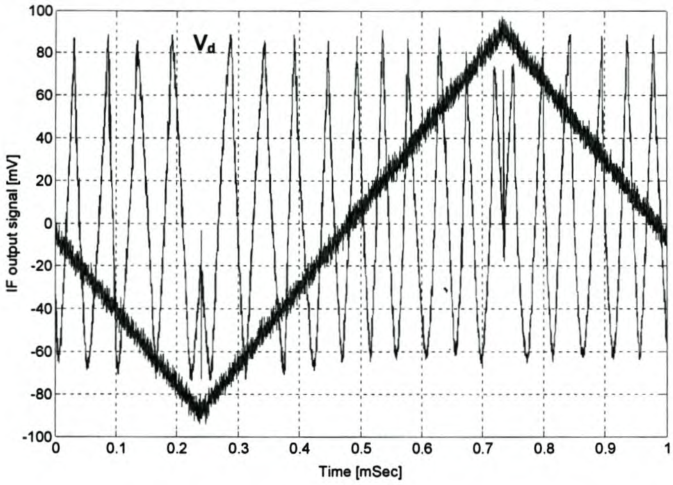

Figure 6-8: Time domain measurement of the difference-frequency signal on the oscilloscope. F_m = 1 kHz, Δf = 100 MHz, L = 30 m, f_b = 20 kHz.

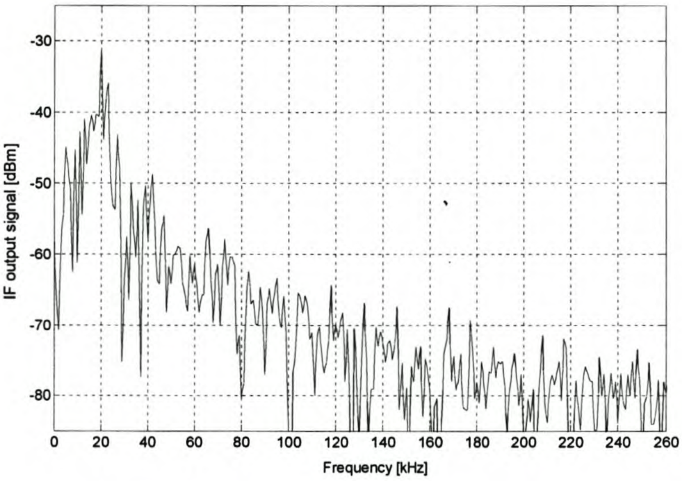

Figure 6-9: FFT of the time domain signal shown in Figure 6-8.

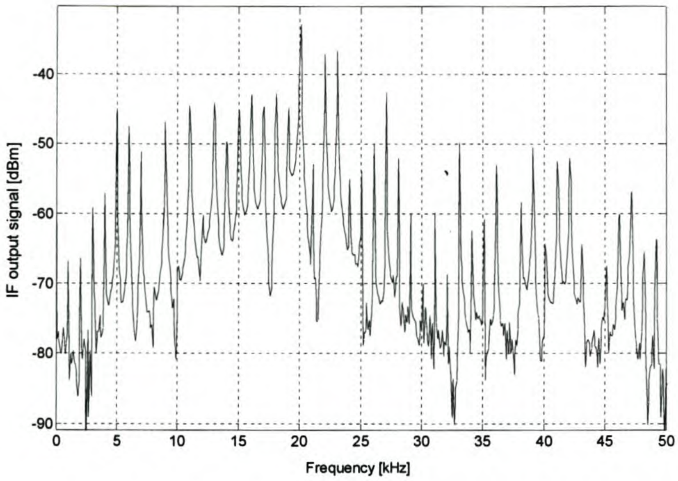

Figure 6-10: FFT of the above time domain signal over T = 10 ms (10 f_m cycles).

6.2 Preliminary measurements: 12 m cable

The measurements in section 6.1 were repeated by exchanging the 30 meter cable with a 12 meter cable. This will result in a smaller beat frequency that is closer to the modulation frequency, as explained in section 2.2.

Measurement 3: 12 meter cable, Δf = 200 MHz

The third measurement was done with a 12 m cable connected between the coupled line output and the mixer RF-port. The VCO was modulated with a 1 kHz triangular signal and 200 MHz deviation. The calculated beat frequency for this measurement is f_b = 16 kHz.

The frequency domain of the difference-frequency signal, v_d that was measured on the spectrum analyzer is shown in Figure 6-11. As the beat frequency becomes smaller, less periods fit into one half-period of f_m. For a further decrease, the beat frequency will become indefinable. Thus the degrading effect of the beat note that was seen in section 6.1 increased in the time domain measurement of Figure 6-12.

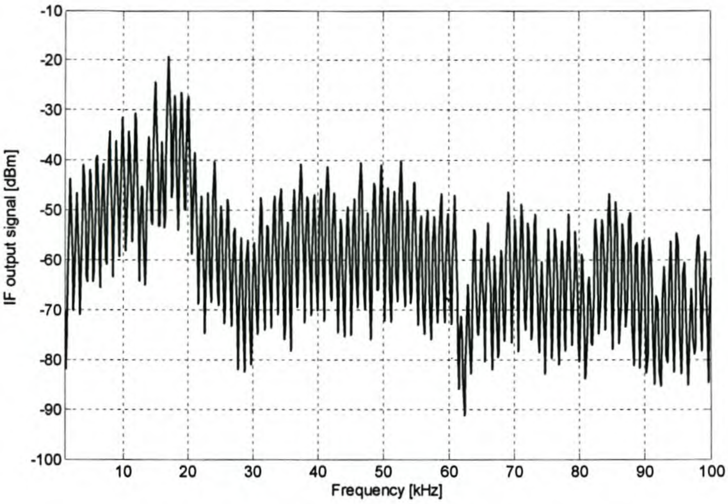

Figure 6-11: Measurement of the difference-frequency signal on Spectrum analyzer. F_m = 1 kHz, Δf = 200 MHz, L = 10 m, f_b= 16 kHz.

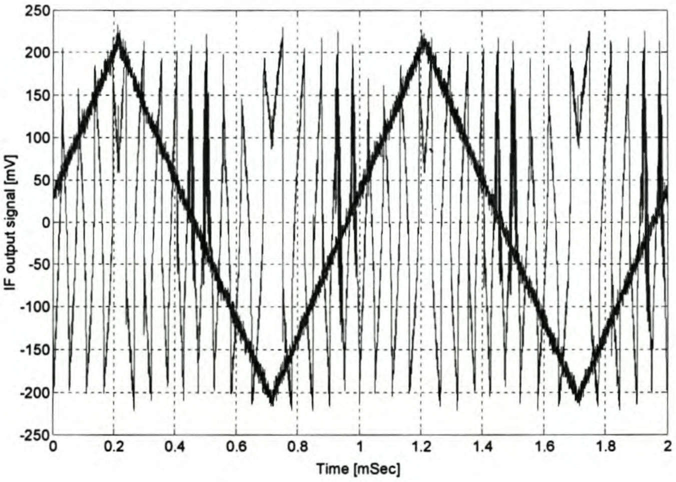

Figure 6-12: Time domain measurement of the difference-frequency signal on the ocilloscope. F_m = 1 kHz, Δf = 200 MHz, L = 12 m, f_b = 16 kHz.

Measurement 4: 12 meter cable, Δf = 100 MHz

The fourth measurement was done for 100 MHz deviation of the VCO output signal. The rest of this measurement setup is similar to the previous one. The calculated beat frequency for this measurement is f_b = 8 kHz. The measurement of V_d on the spectrum analyzer is shown in Figure 6-13. The time domain measurement of V_d is shown in Figure 6-14. There are only three beat frequency periods between each beat note. Every fourth period is distorted by the effect of the beat note. Thus, the closer the beat frequency is to the modulation frequency, the greater this effect. The FFT was done over two periods and over a single period of f_m. The results are shown in Figure 6-15 and Figure 6-16 respectively. There is a single peak frequency at f_b in Figure 6-16 which clearly shows the improvement when measuring or sampling the difference-frequency over a half-period of f_m. This measurement technique is only possible when using signal processing to set the sampling period to half the modulation frequency period, $T_s = 2/f_m$.

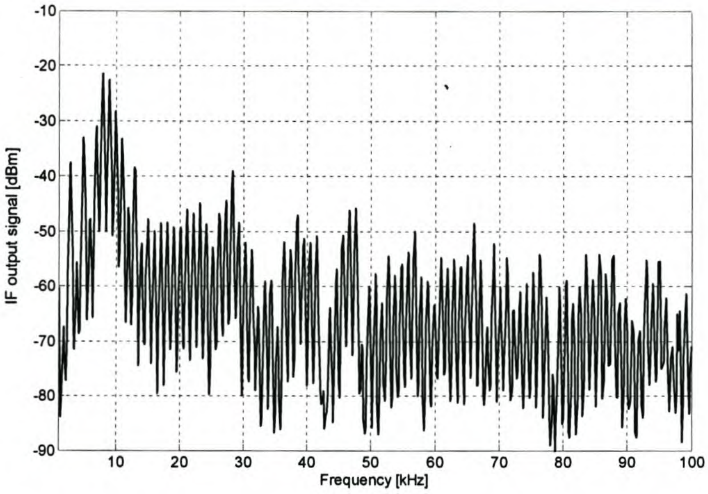

Figure 6-13: Measurement of the difference-frequency signal on the spectrum analyzer. F_m = 1 kHz, Δf = 100 MHz, L = 12 m, f_b = 8 kHz.

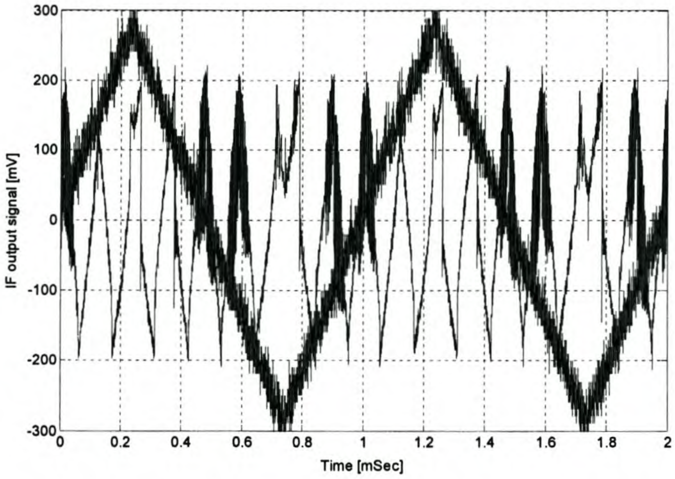

Figure 6-14: Time domain measurement of the difference-frequency signal on the oscilloscope. F_m = 1 kHz, Δf = 100 MHz, L = 12 m, f_b= 8 kHz.

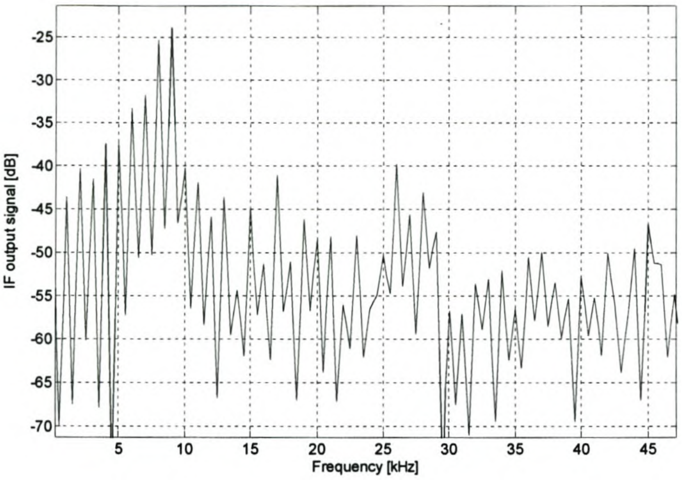

Figure 6-15: FFT of the time domain signal shown in Figure 6-14.

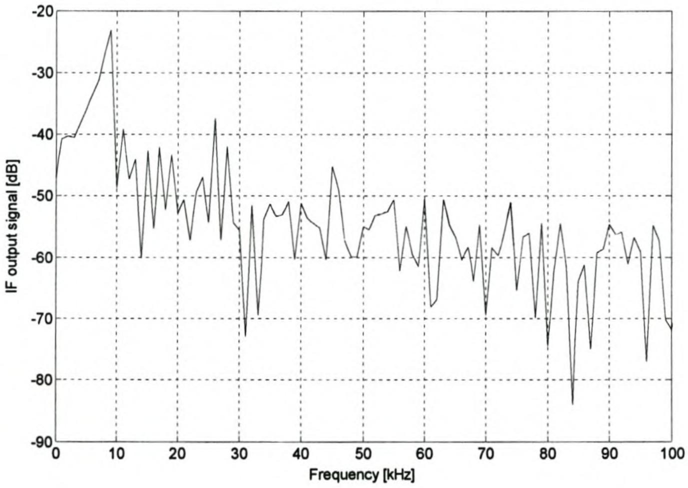

Figure 6-16: FFT of the above time domain signal over T = 1 ms (1 f_m cycles).

6.3 Conclusion

- All the measurements nearly correlated with the simulations that were done in sections 2.3 and 4.1.
- There are different measurement techniques available to measure the beat frequency. The best results were attained when measuring or sampling over a half-period of the modulation frequency because this minimized the degrading effect of the beat note on frequency spectrum.
- The time domain results showed that there is a 180° phase shift in v_d after each beat note. This did not influence the measurements on the spectrum analyzer.
- The effect of the beat note on the beat frequency increased when f_b moved closer to f_m.
- The preliminary radar system operated as expected. The whole radar system could now be safely assembled and measured. The next chapter deals with the final radar system measurements.

7. Radar measurements

The preliminary system that was discussed in chapter 6 proved to be satisfactory. This chapter continues with the last radar measurements and clearly explains the progression towards a final radar system. The final radar was laid out on a 60 mm diameter PCB with the double helix antenna mounted on top. Several concluding measurements were done to reveal that the final radar system works remarkably well.

The first radar system was constructed by replacing the cable in the preliminary system with two identical horn antennas and with a single horn antenna and circulator respectively, as explained in section 7.1 of this chapter. In section 7.2 the horn antenna and circulator is replaced with the circularly polarized patch antenna and Lange coupler that were designed, built and measured as explained in chapters 4 and 5. Measurements and results of the final radar system are discussed in section 7.3. This system used a double helix antenna instead of the patch antenna because it has a higher gain and bandwidth and can detect a greater maximum range. The final radar system was used to measure the distance to the wall of a building with a metal object on top of the roof. The radar detected the range of both the wall and metal object simultaneously in one measurement. The height of the metal object from the ground level could be determined by using the results of two measurements as explained in section 7.4. The measured results of the final radar system are summarized in section 7.5.

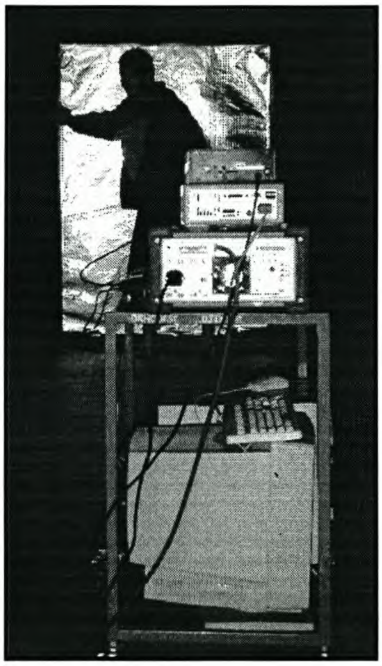

Figure 7-1: Outside measurement setup with a 1.7 x 1.3 m^2 reflector.

A picture of the radar measurement setup outside on top of the 5th floor of the engineering building at the University of Stellenbosch is shown in Figure 7-1. Two different reflectors were used to simulate a target and to reflect the transmitted signal. The reflector in Figure 7-1 is an upright grid covered with reflective foil and is more mobile than the metal plate that was used as the reflector in the first measurements. This reflector, with physical dimensions of 1.3 x 1.7 m^2, was used for the measurements discussed in sections 7.2 and 7.3.

7.1 Horn antenna – radar measurements

This section looks at the radar system using two horns and a single horn with a circulator respectively. A smaller reflector with size of 0.6 x 1.5 m^2 was used for the horn antenna radar measurements. The maximum range that could be measured with relatively small interfering reflective objects was 40 meter. The term "relatively" is used because it seemed as if the radar picked up small interfering signals that reflected off the side railings and thermal reflective layer on top of the roof, which interfered with the beat frequency measurement in the lower frequency range (1-10 kHz). These unwanted reflections, however, did not significantly distort the desired return signal.

7.1.1 Two horn antennas - radar system

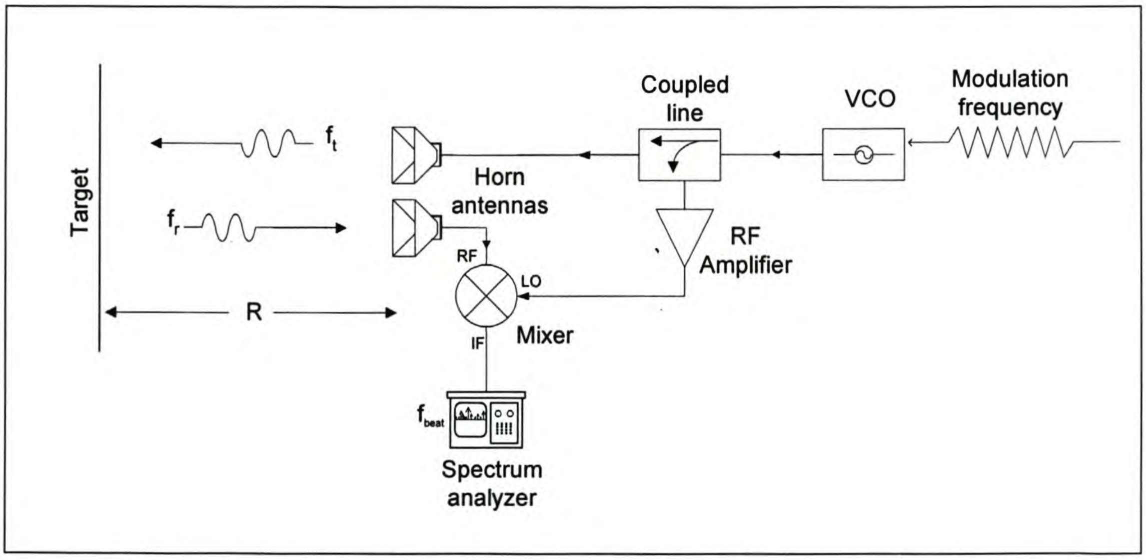

Figure 7-2: Block diagram of the two-horn antenna radar system and measurement setup.

A block diagram that demonstrates the first radar system is shown in Figure 7-2. This radar system is similar to the preliminary system that was discussed in chapter 6 with the exception of the cable that was replaced by two separate horn antennas. This radar system could be used as a reference point to start and to compare the results attained from the following radar system measurements. The two horn antennas are well isolated thus no circulator is necessary in this system.

Before any radar measurements were done, the power level of the RF-port signal was measured to verify that it would not saturate or damage the mixer. The maximum allowed mixer RF- input power is +1 dBm and the measured coupled power at the output port of the receiver horn antenna was -10 dBm. The power at the mixer LO-port was measured as 10 dBm which is above the required input power of 7 dBm.

The center frequency of the VCO was set to f_0 = 2.5 GHz with 200 MHz deviation, using a linear triangular wave with modulation frequency of f_m = 1 kHz. The reflector was placed at various distances from the radar ranging from 5 to 30 meters. Some results of the measured difference-frequency signal on the spectrum analyzer are shown in Figure 7-3 to Figure 7-6. The beat frequency corresponding to each distance can clearly be seen in all the measurements. Equation (2.2) was used to calculate the beat frequency at the specific range of each measurement. These values are given in the title of each figure, which can be compared with each beat frequency measurement to determine the accuracy of the radar.

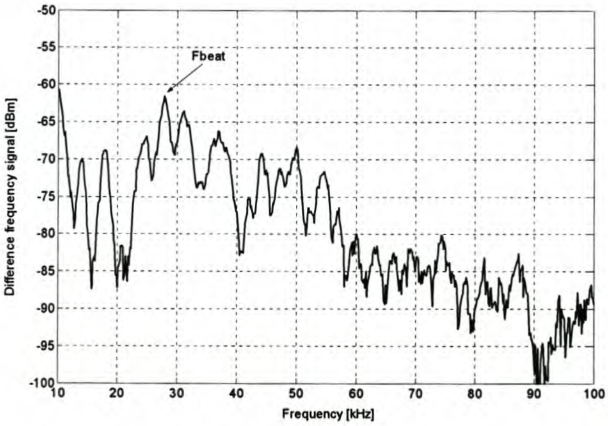

Figure 7-3: Two horns - radar measurement. Distance, R = 10 m, f_b = 26.7 kHz.

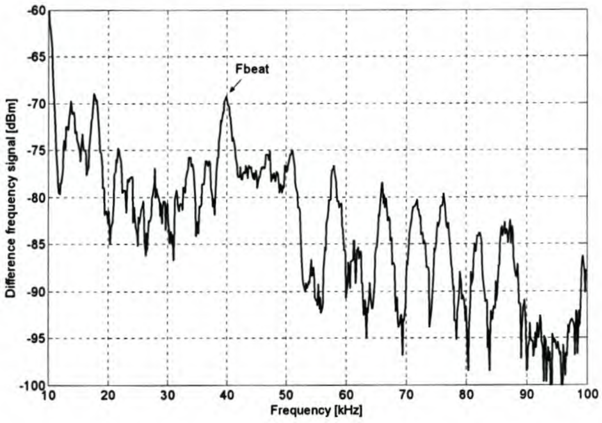

Figure 7-4: Two horns - radar measurement. Distance, R = 15 m, f_b = 40 kHz.

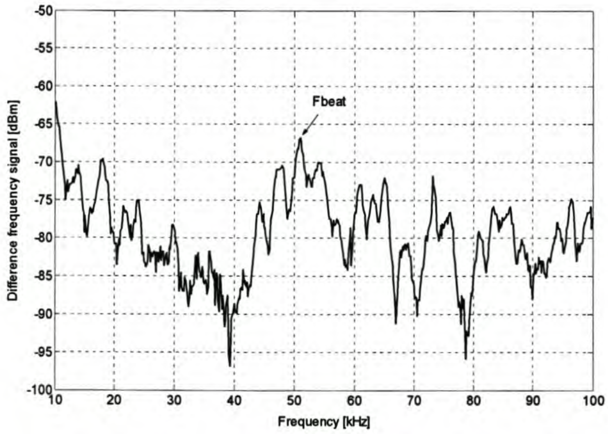

Figure 7-5: Two horns - radar measurement. Distance, R = 20 m, f_b = 53.3 kHz.

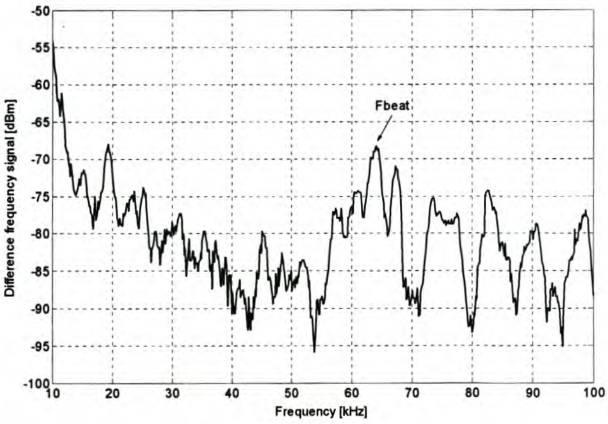

Figure 7-6: Two horns - radar measurement. Distance, R = 25 m, f_b = 66.7 kHz.

7.1.2 Single horn antenna – radar system

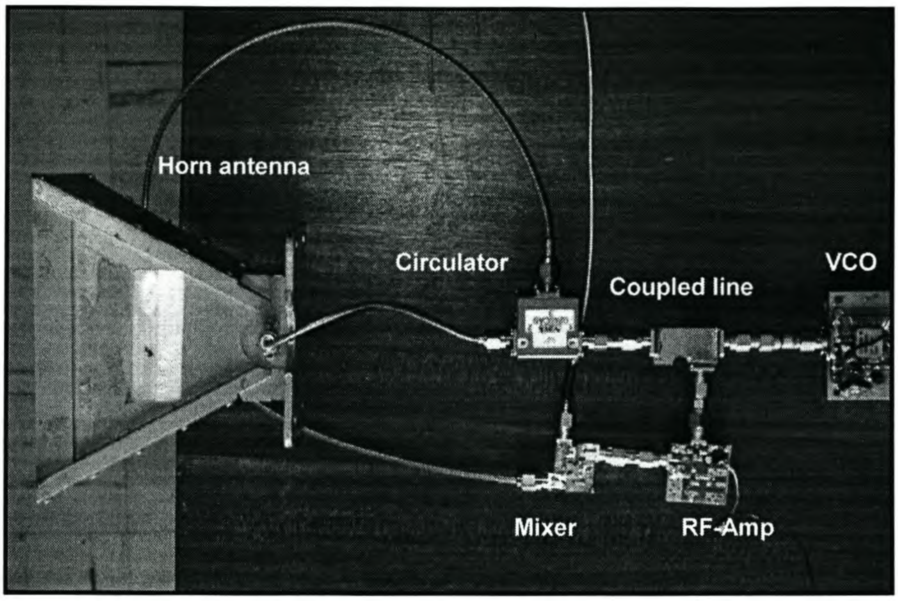

Figure 7-7: Top view of the single horn radar system.

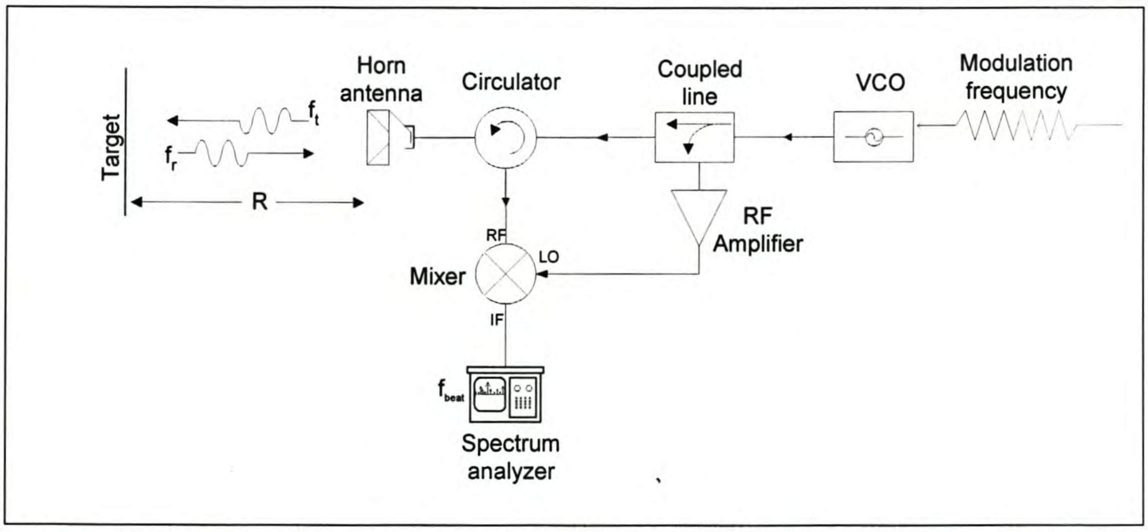

Figure 7-8: Block diagram of the single horn antenna radar system and measurement setup.

This radar system uses a single horn antenna with a circulator that was discussed in section 4.3. Before measuring the system, the power at the isolated port of the circulator was measured to be -14dBm. This was determined to confirm that the input RF power is lower than the maximum mixer RF-input power of +1dBm. The center frequency of the VCO was set to 2.5 GHz with a wider deviation of 325 MHz using a linear triangular wave with modulation frequency of f_m = 1 kHz. The deviation was increased to see what the effect would be on the beat frequency measurement. The results are shown in Figure 7-10 to Figure 7-14.

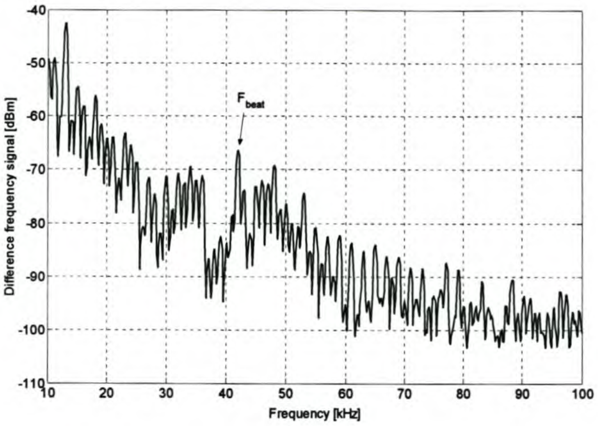

Figure 7-9: Single horn - radar measurement. R = 10 m, f_b = 43.3 kHz.

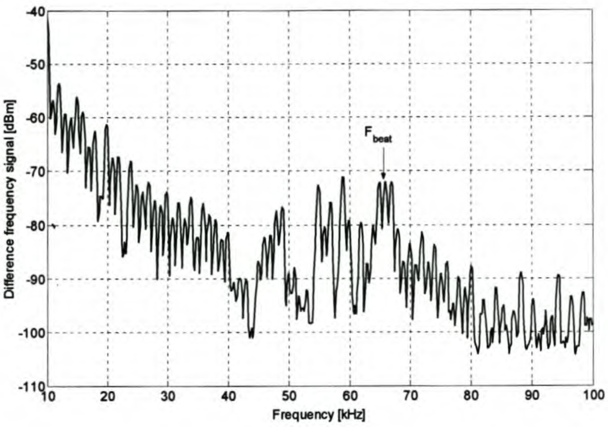

Figure 7-10: Single horn - radar measurement. R = 15 m, f_b = 65 kHz.

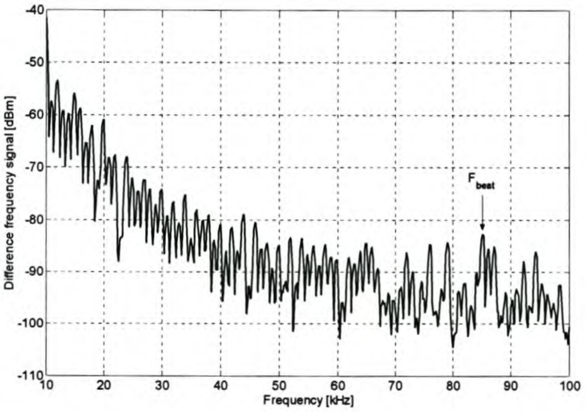

Figure 7-11: Single horn - radar measurement. R = 20 m, f_b = 86.7 kHz.

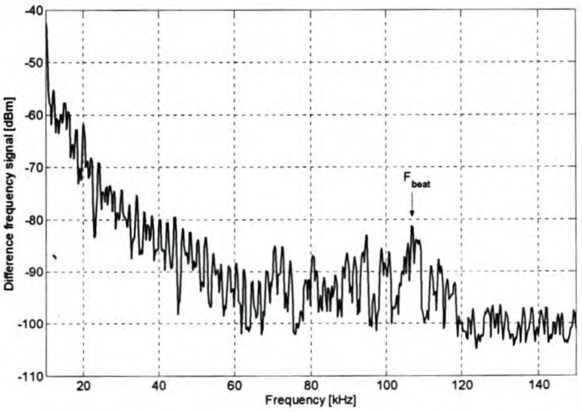

Figure 7-12: Single horn - radar measurement. R = 25 m, f_b = 108.3 kHz.

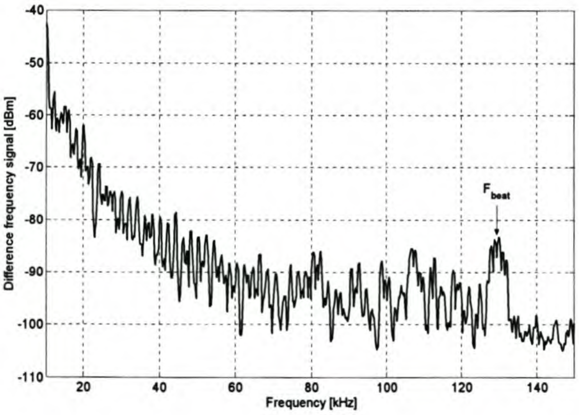

Figure 7-13: Single horn - radar measurement. R = 30 m, f_b = 130 kHz.

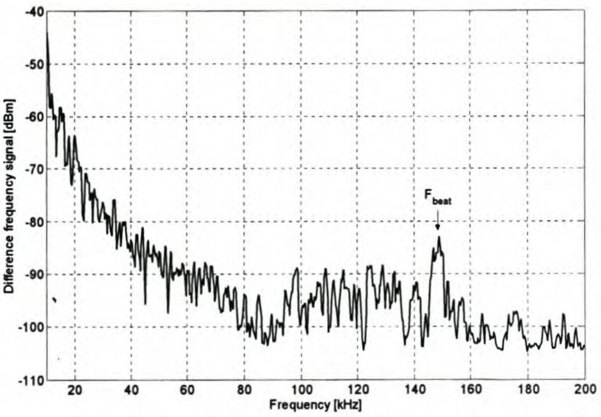

Figure 7-14: Single horn - radar measurement. R = 35 m, f_b = 151.7 kHz.

The beat frequencies in the above measurements are much higher than the modulation frequency when compared to the results of the two-horn antenna radar system. The non-linearity of the VCO has a greater influence because it sweeps over a wider frequency bandwidth. This non-linearity effect was already seen in chapters 4 and 6. The beat frequency measurements for the single horn antenna radar system are influenced by the non-linearity of the VCO, thus forming a bundle of peaks around the beat frequency, which makes the measurement less accurate.

7.2 Patch antenna – radar system

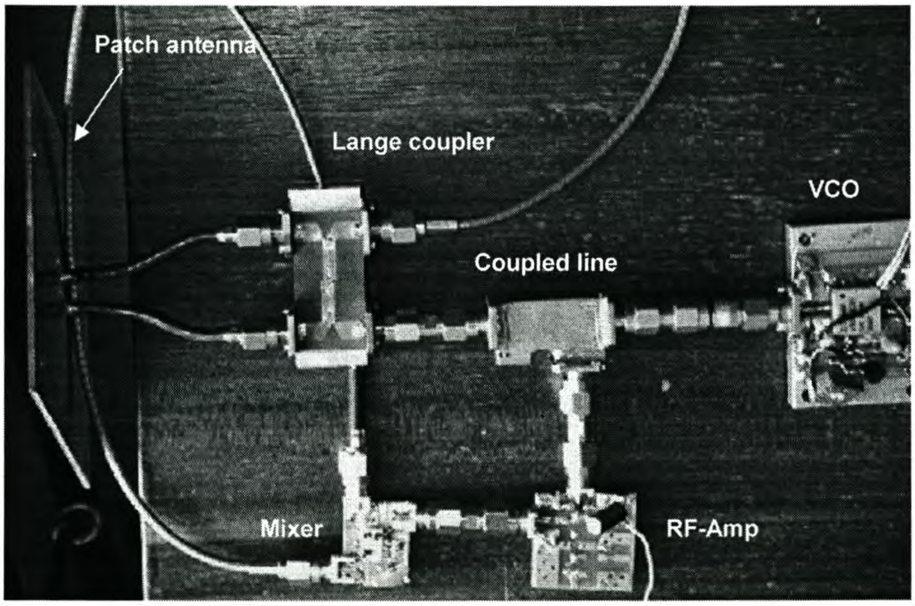

Figure 7-15: Top view of the radar system measurement setup where the single horn antenna and circulator is replaced by a patch antenna and Lange coupler.

In this system the single horn antenna and circulator in the previous radar system was replaced with a patch antenna and a Lange coupler. As explained in sections 4.3 and 5.1, the Lange coupler fulfils two functions: It firstly serves as a 90° hybrid which divides the power of transmitted signal equally between the input ports of the dual-fed patch antenna. The 90° phase difference between the two feed ports causes circular polarization. The second function of the Lange coupler is to isolate the transmitted and received signals. A photograph and block diagram of the circularly polarized patch antenna and Lange coupler radar system is shown in Figure 7-15 and Figure 7-16.

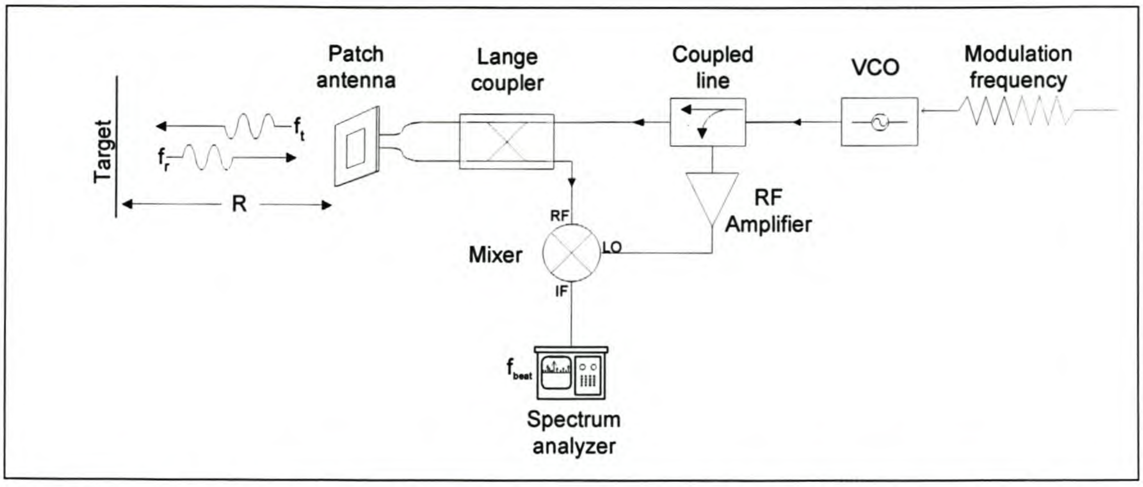

Figure 7-16: Block diagram of the radar system, using a dual-fed circularly polarized patch antenna and Lange coupler.

The 1.3 x 1.7 m^2 reflector that is shown in Figure 7-1 was used to measure the difference-frequency signal of this radar on the spectrum analyzer. The patch antenna has a much narrower frequency bandwidth than the horn or helix antennas as seen from the measurements in section 5.1. Therefore, the VCO output signal was swept over a smaller deviation of 80 MHz. This caused the beat frequency to be much lower than the measured beat frequencies in section 7.1. The measurement of the difference-frequency signal that is shown in Figure 7-17 was for R = 15 m, f_m = 1 kHz, Δf = 80 MHz. The calculated and measured beat frequency at this range is 16 kHz, which is much lower than the previous beat frequency measurements due to the smaller deviation. This, in turn, causes more interference of the modulation frequency signal harmonics with the lower beat frequency. A steep high pass filter can be used to extract the beat frequency while eliminating the interfering harmonics at lower frequencies. This radar system was measured and worked well up to 25 m, after which the beat frequency signal became too small and was masked by the noise floor.

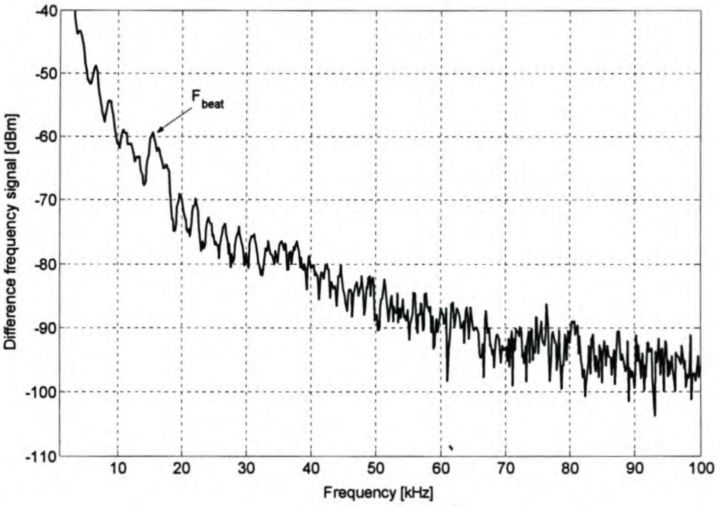

Figure 7-17: Beat frequency measurement of the patch antenna and Lange coupler radar system. R = 15 m, f_m = 1 kHz, Δf = 80 MHz and f_b = 16 kHz.

7.3 Final radar system measurements

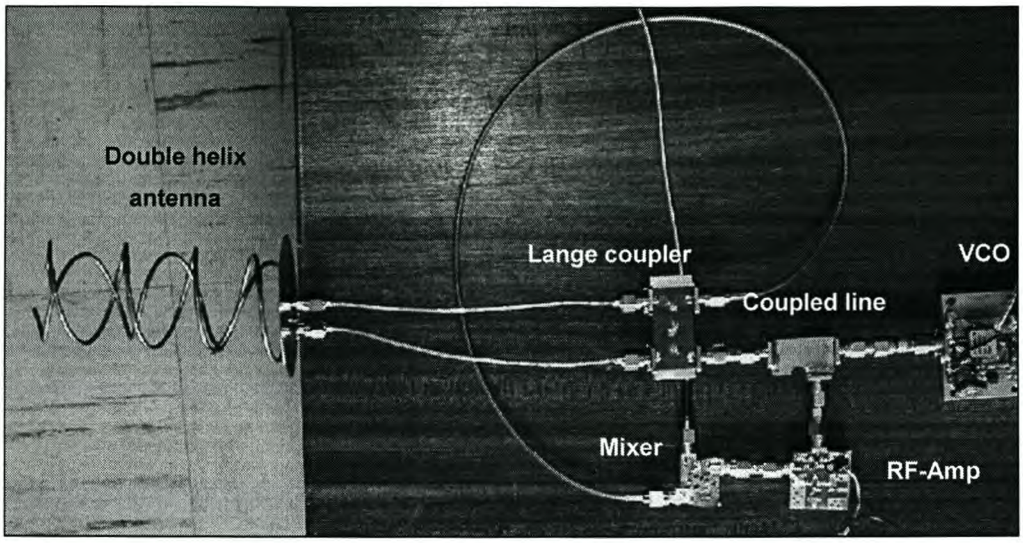

Figure 7-18: Top view of the radar system measurement setup using the double helix antenna that was designed and measured in section 5.2.

The double helix antenna that was designed and built as explained in section 5.2 was lastly substituted in the place of the patch antenna in the radar system as shown in Figure 7-18. This helix was originally designed for better isolation between the transmitted and received signals. By measuring the coupling between the *Input* and *Isolated* ports of the Lange coupler it was determined that isolation was improved. Some of the antenna gain had to be sacrificed and in spite of the improvement in the isolation between the transmitted and received signals, the measured maximum range was the same as for the patch antenna.

A second double helix antenna, similar to the antenna of section 5.2, was designed and built for optimum gain. The isolation was not considered as for the previous antenna, which made the design process and construction of the antenna much simpler, because both helices had the same diameter, number of turns and pitch angle. After the impedance at the two input ports were matched to 50 Ω the gain of each helix was measured in the anechoic room, shown in Figure 5-7. The measured gains of both helices were above 9 dB with RHC and LHC respectively. The measured isolation between the two helices is -10 dB. Range measurements that were done on the radar system containing the new double helix antenna demonstrated a maximum range of 40m.

The final radar system was laid out on a 60 mm diameter PCB (Figure 7-19). The *Design Explorer 99* [35] document of the final PCB and electronic circuit schematics are included in the appendix CD for future use. An onboard 14-pin *ICL8038* DIP- package was used to create the triangular wave. This signal is the modulation input signal of the VCO. The DC-offset and peak-to-peak voltage of this triangular wave can be adjusted by using two variable resistors. This makes it possible to change the VCO's center frequency and deviation, which makes the radar more versatile and enables the use of different antennas for various applications.

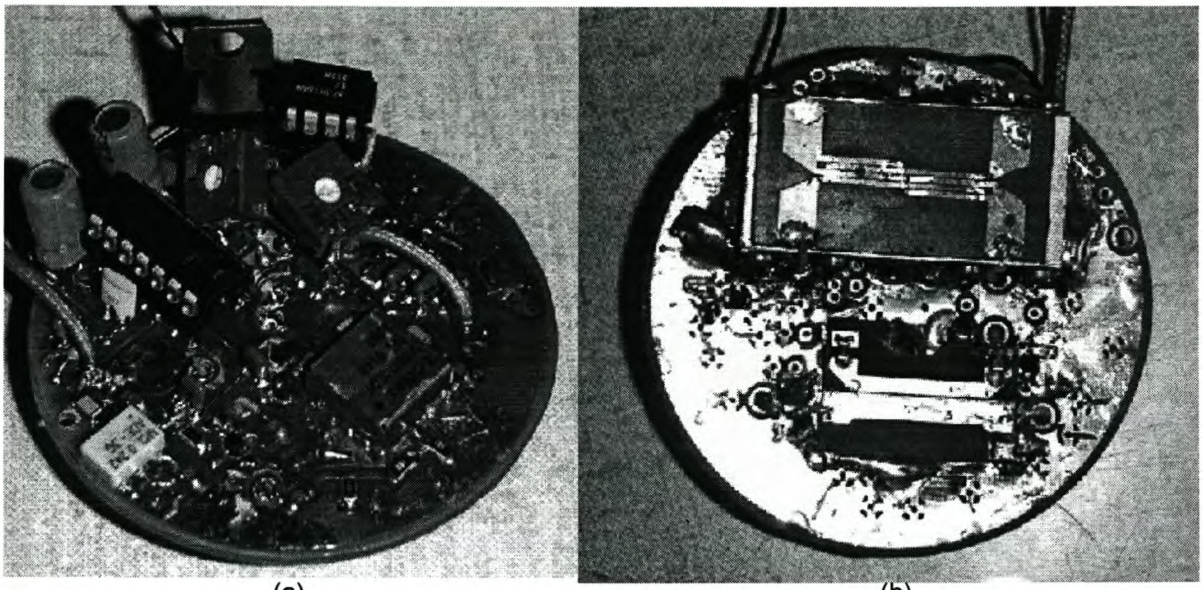

(a) (b)

Figure 7-19: Final radar system. (a) Top view (b) Bottom view.

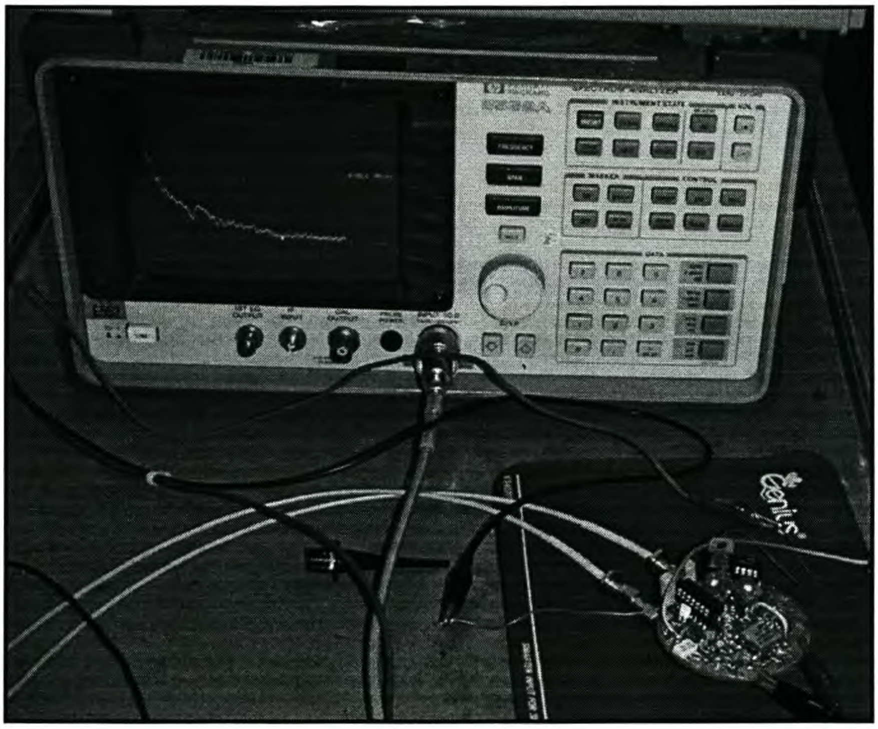

Figure 7-20: Measurement setup of the final radar system. The spectrum analyzer displays the beat frequency at range, <u>R = 11 m</u>.

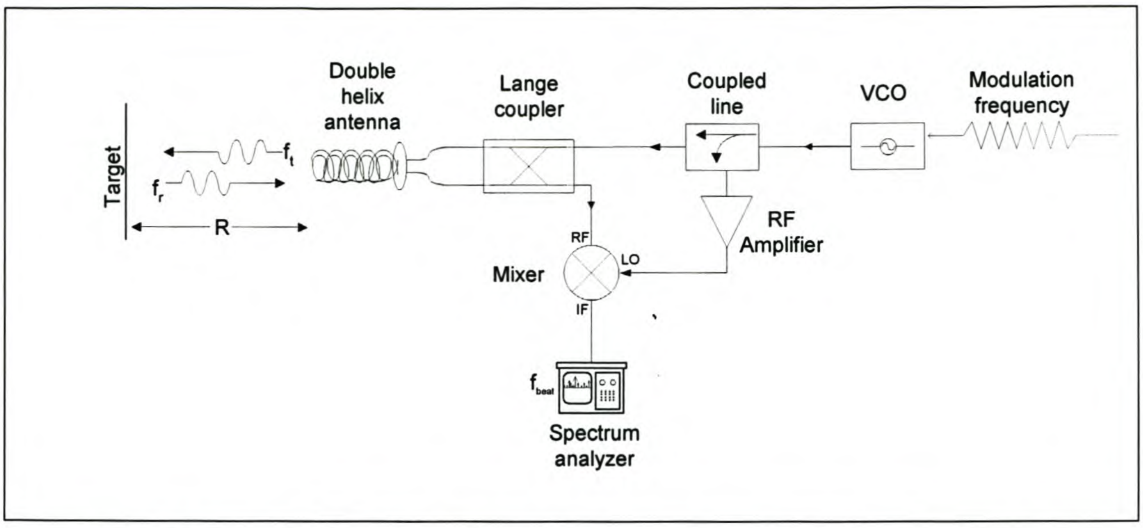

Figure 7-21: Block diagram of the final radar system and measurement setup.

A block diagram of the final radar system and measurement setup is shown in Figure 7-21. The beat frequency of the final radar system was measured on the spectrum analyzer at different absolute distances from the 1.3 x 1.7 m^2 reflector. The center frequency of the final radar system was chosen as 2.5 GHz with a deviation of 100 MHz and 1 kHz modulation frequency. The final radar system's beat frequency was measured on the spectrum analyzer for range R = 5 m to 40 m. The internal bandwidth filter of the spectrum analyzer was set to 1 kHz and the video bandwidth was set to 300 Hz with 20 dB attenuation. These settings were chosen to clearly display the peak beat frequency as shown in Figure 7-22 to Figure 7-27.

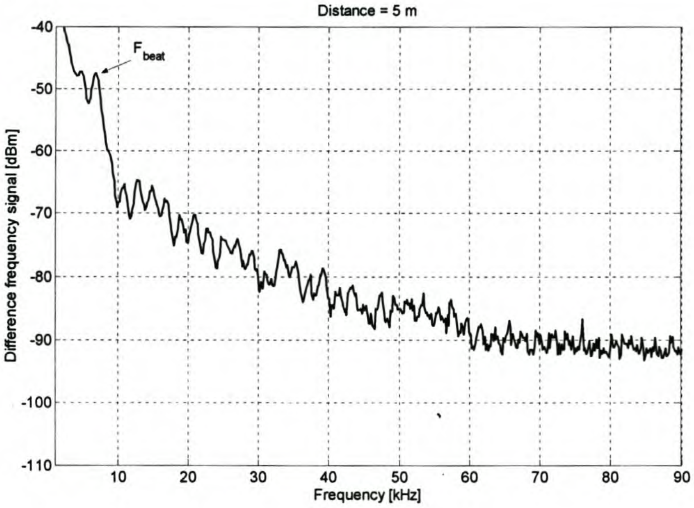

Figure 7-22: Beat frequency measurement of the final radar system. R = 5 m, f_b = 6.7 kHz.

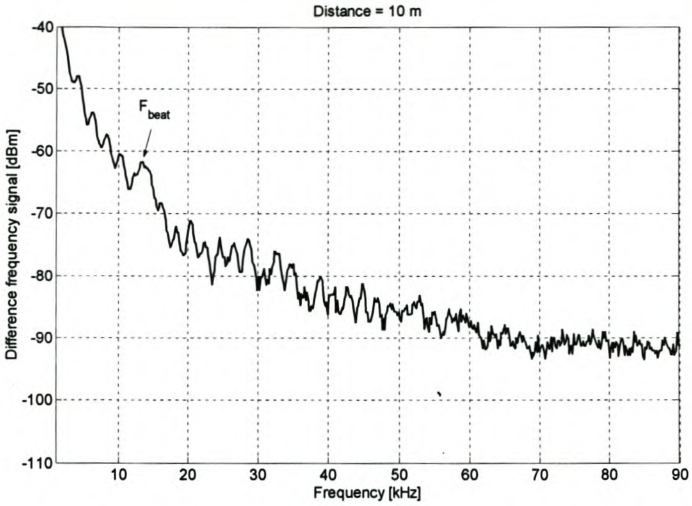

Figure 7-23: Beat frequency measurement of the final radar system. R = 10 m, f_b = 13.3 kHz.

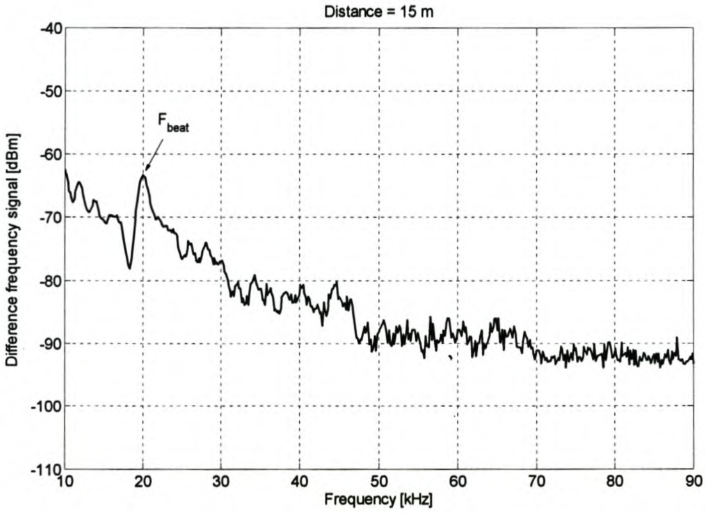

Figure 7-24: Beat frequency measurement of the final radar system. R = 15 m, f_b = 20 kHz.

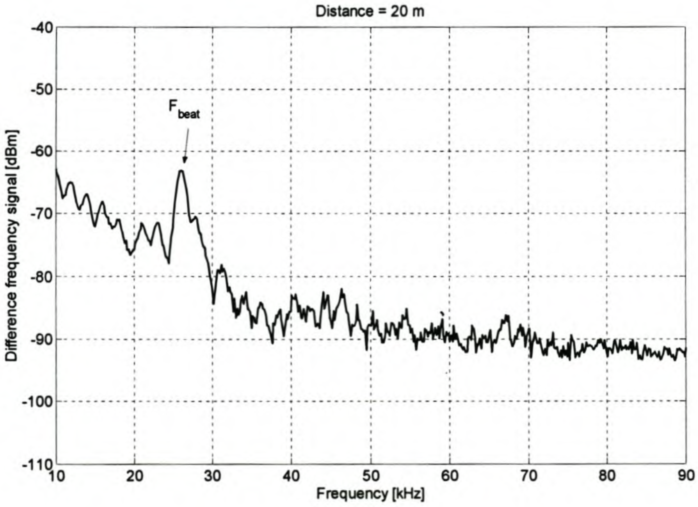

Figure 7-25: Beat frequency measurement of the final radar system. R = 20 m, f_b = 26.7 kHz.

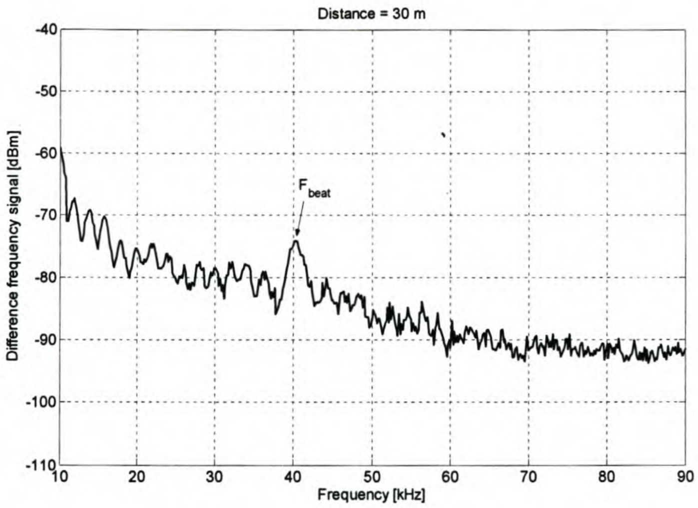

Figure 7-26: Beat frequency measurement of the final radar system. R = 30 m, f_b = 40 kHz.

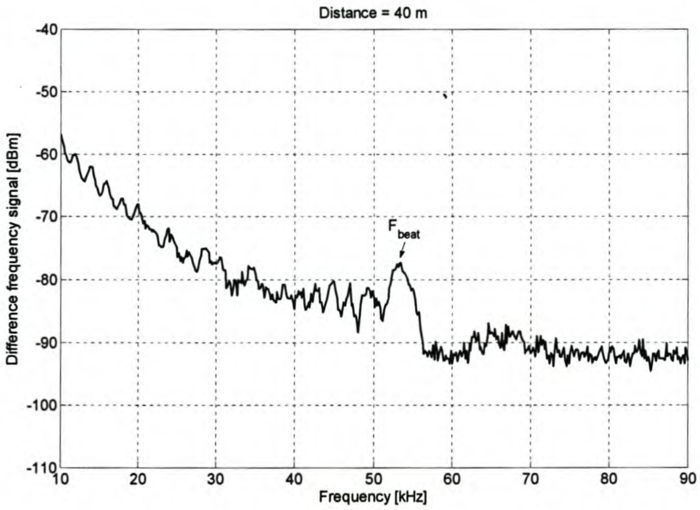

Figure 7-27: Beat frequency measurement of the final radar system. R = 40 m, f_b = 53.3 kHz.

The measured results of Figure 7-22 to Figure 7-27 revealed distinct beat frequencies. The value of each measured beat frequency correlates with the calculations according to equation (2.2). The 5 m and 10 m beat frequency measurements of Figure 7-22 and Figure 7-23 are very close to the modulation frequency and are not as easily distinguished. However, the further the range, the higher the frequency of the measured beat frequency signal therefore resulting in a smaller interference of the unwanted harmonics of the 1 kHz modulation frequency signal. The signal strength of the return signal decreased with increasing range, but the beat frequency measurements in Figure 7-26 and Figure 7-27 at R = 30m and R = 40 meter, showed that the amplitude of each of these signals was at least 5 dB above the noise floor.

The following measurements were done to determine the accuracy and resolution of the final radar. Smaller distance variations of one meter increments between ten and twenty meters were used to see if the beat frequency measurements were accurate. The *resolution* of a radar is the ability to distinguish between two closely separated echoes while the *accuracy* determines the radar's ability to determine the exact range. Figure 7-28 shows three beat frequency measurements at R = 13m, 14m and 15`m respectively that are plotted on the same graph. The calculated beat frequencies at these distances are 17.3, 18.7 and 20 kHz respectively. The measurements are accurate and distinguishable to a certain extent. It will however become more difficult to discern between beat frequencies that are separated closer than 1 meter apart. This is largely due to non-linearity of the VCO and will improve if a better VCO, PLL or synthesizer is used. However, this would also imply that the final system will be more expensive [24].

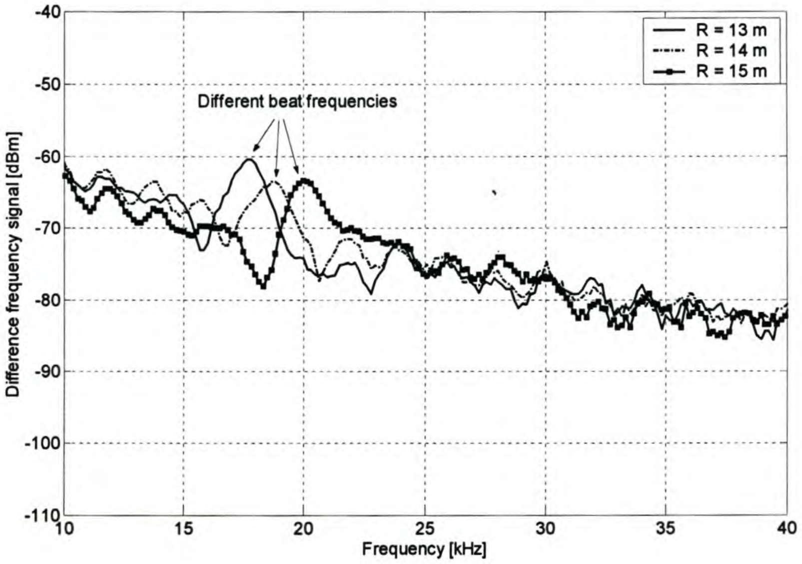

Figure 7-28: Measurement of the accuracy and resolution of the final radar.

7.4 Detecting two targets simultaneously.

All the previous measurements were done with a flat, vertical, conductive reflector. However, in reality these characteristics will not describe a typical target. The radar will be used to detect the distance from an imperfect reflector such as a wall or the ground. Thus measurements had to be done to determine if the final radar system can determine the distance from an irregular reflector, the most obvious target being the side of a building. The height of the building wall was measured as 5.4 m and three measurements were taken at R = 20 m, 30 m and 40 m respectively.

Two definite peaks on the frequency display were noted for each measurement. Especially for the beat frequency measurement at 30 m and 40 m. The second peak was realized to be an extra reflection from a big metal dish antenna, mounted on the top of the building. A diagram of each measurement setup with the measured results are shown in Figure 7-31 to Figure 7-34.

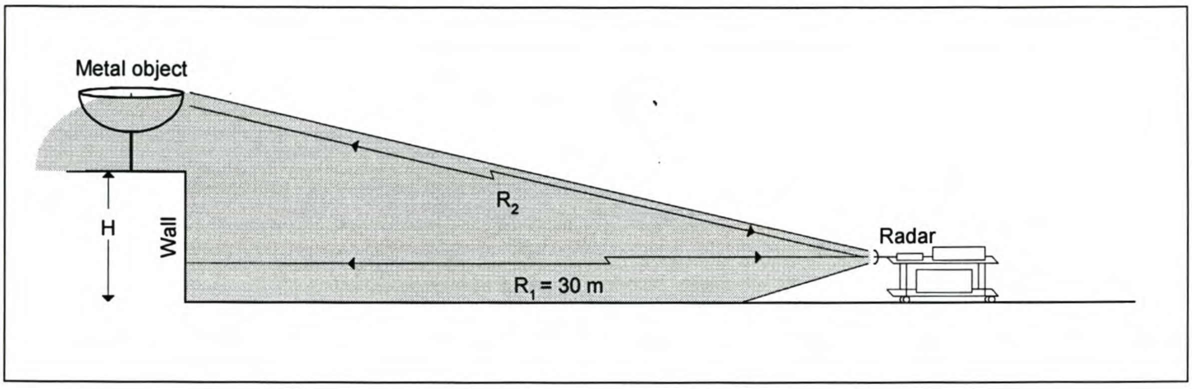

Figure 7-29: Measurement of two irregular reflectors at $\underline{R_1 = 30\text{ m}}$.

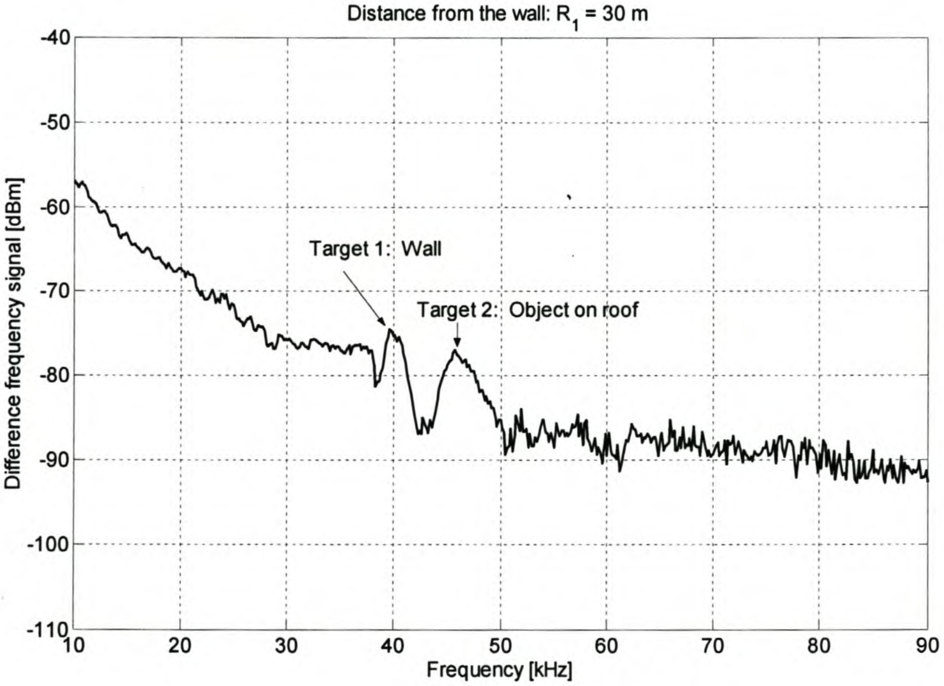

Figure 7-30: Beat frequency measurement of two irregular reflectors at $\underline{R_1 = 30\text{ m}}$.

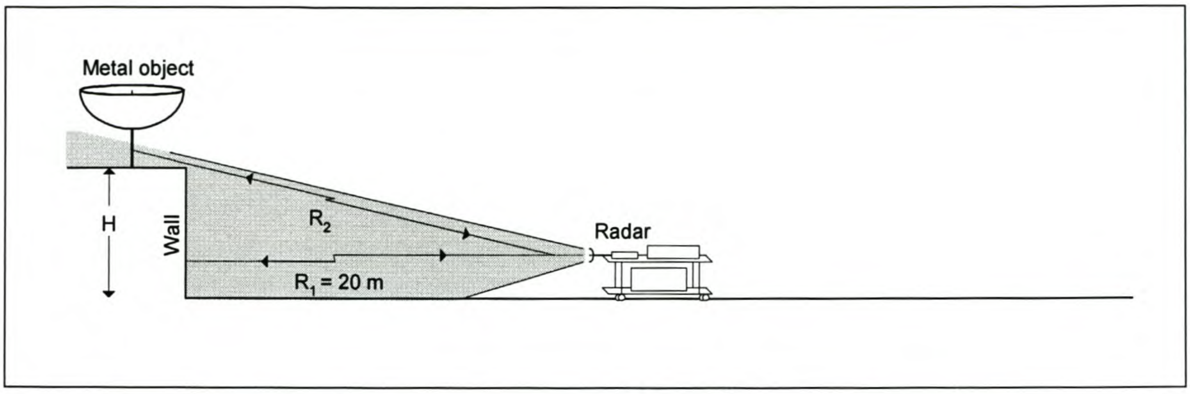

Figure 7-31: Measurement of two irregular reflectors at R_1 = 20 m.

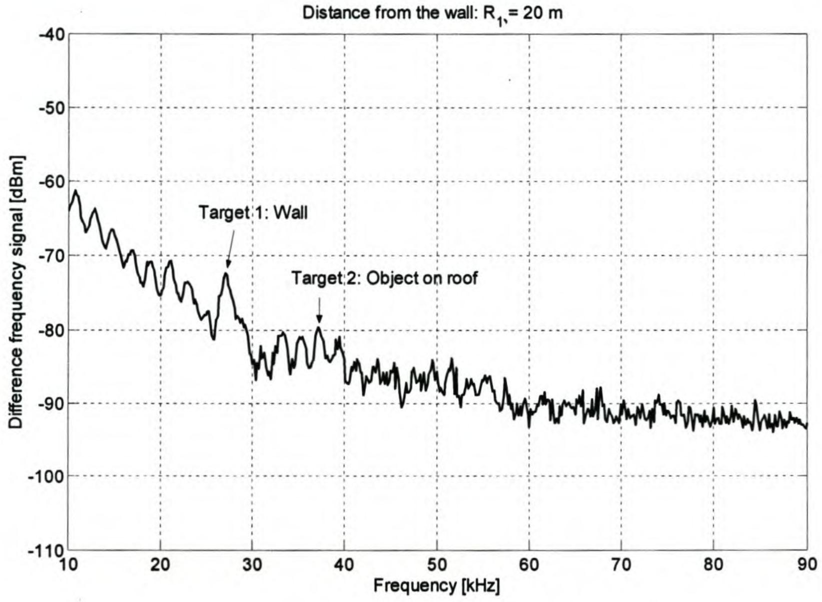

Figure 7-32: Beat frequency measurement of two irregular reflectors at R_1 = 20 m.

After comparing the results of the three different measurements, it was interesting to note that the result of the measurement closest to the wall with R_1 = 20 gave a very small beat frequency amplitude for the object on the roof as shown in Figure 7-32. This can be explained by when moving closer to the wall, the object on the roof becomes overshadowed by the wall, making it less detectable.

When moving further away from the wall, the object on the roof becomes more exposed to the radar beam and can easily be detected as shown in Figure 7-29 and Figure 7-33.

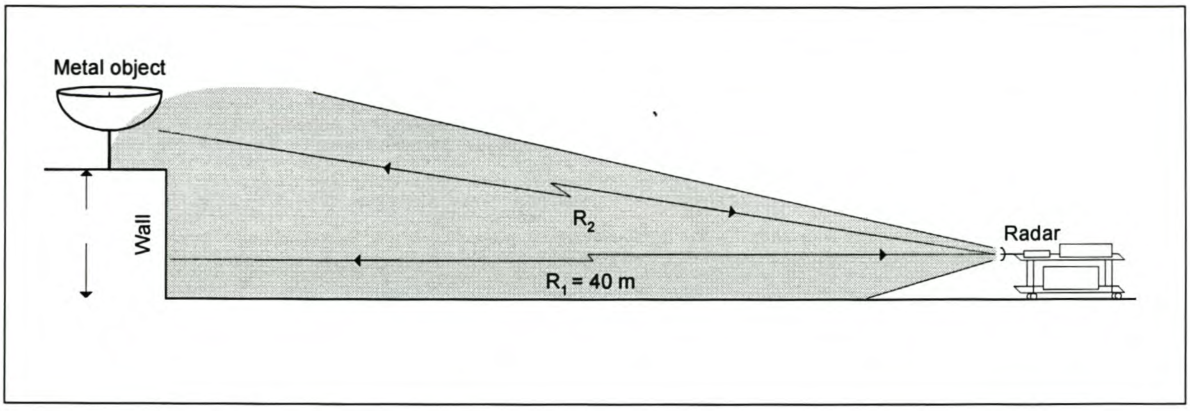

Figure 7-33: Measurement of two irregular reflectors at $R_1 = 40$ m.

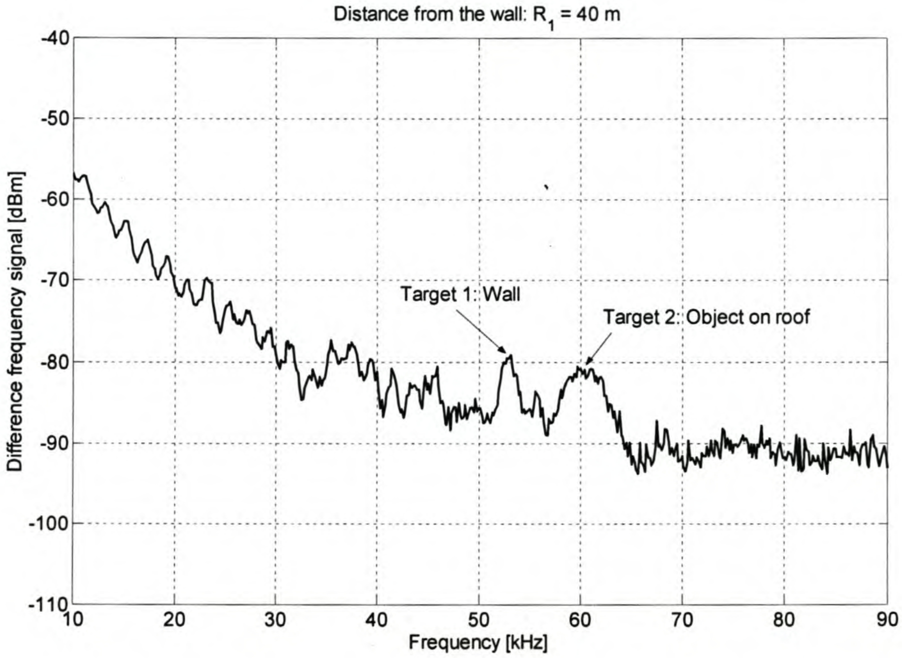

Figure 7-34: Beat frequency measurement of two irregular reflectors at $R_1 = 40$ m.

The object on the roof's height and distance from the ground level could be determined by using the results from the three measurements. The measured distance from the object on the roof (R_2 in Figure 7-29, Figure 7-31 and Figure 7-33), was calculated by using the beat frequency equation (2.2) to give:

- $R_2 = 27.0$ m for $R_1 = 20$ m
- $R_2 = 36.5$ m for $R_1 = 30$ m
- $R_2 = 46.0$ m for $R_1 = 40$ m

The height of the metal object was determined from the above measurements to be approximately 10 m from the ground level.

7.5 Measurements conclusion

From the measured results of the final radar system, the system proved to meet the original design specifications. The measured results of the final radar system can be summarized as:

- Measured maximum range: R_{max} = 40 m
- Measured minimum range: R_{min} = 5 m
- Can detect more than one target simultaneously.
- Measured resolution is 1 m.

8. Final Conclusion

8.1 Overview

The complete design process of an FM-CW radar that can be used in short range measurement applications is discussed in this document.

The basic theory and principles of an FM-CW radar were considered. The relationships between the center frequency, beat frequency, modulation frequency and frequency deviation were discussed at the hand of the theory and simulations. Time domain and frequency domain simulations of the difference-frequency signal were compared for different values of the before mentioned parameters. This was done to find the optimum beat frequency measurement and to determine an accurate range. Different ways of modulation were discussed and considered. Linear triangular modulation was chosen for the final design because it is more accurate than sinusoidal modulation, and less signal processing is then necessary to calculate the correct range.

A software analysis program called *RadarOpt* was written to simulate the radar's maximum range and minimum return signal. *RadarOpt* included extra functions such as calculating the beat frequency or computing the antenna gain from the measured S_{21} parameters.

Different possible radar components were evaluated for optimum system performance with the best cost efficiency. The effect of the non-linearly of the VCO on the beat frequency measurements were discussed. The measured values were used to simulate the effect of the non-linearity on the radar system and it was found that the beat frequency signal was not as accurately determined as when using a perfectly linear VCO.

The circulator that is used in most single antenna radar systems was replaced with a Lange coupler, which made the final system more cost efficient. Different types of mixers were compared and measured in the system to find an optimum mixer for the final design.

Two basic antenna designs such as the circularly polarized dual-fed patch antenna and double helix antenna were discussed and designed. The manufactured antennas were measured in an anechoic chamber and were compared in the final radar system. The double helix antenna was designed to have less coupling between the transmitted and received helices without compromising too much antenna gain. The design was simulated and optimized with *Feko*'s optimizer called *Optfeko*. The final measured gain of the double helix antenna was less than expected but the measured isolation exceeded the design requirements.

A preliminary radar system was used for the first beat frequency measurements. A long 30 m and 12 m cable were used instead of an antenna or circulator to achieve a time delay between the transmitted and received signals, without any interfering signals. These measurements correlated with the simulations in chapters 2 and 4.

Different radar systems with various antennas, circulators and Lange coupler combinations were built and measured, until a final radar system was found that met and exceeded the design specifications. This radar system was laid out on a 60 mm diameter PCB with a double helix antenna mounted on top. The radar was designed and built to be versatile. For instance, the double helix antenna can be replaced with a small circularly polarized patch antenna which can be rebuilt into a much smaller package. The patch antenna has a lower gain and the radar can detect a closer maximum range while remaining within design specification limits.

The final radar system can determine the distance from and between two separate objects up to 40 m range under the condition that both objects are positioned in the radar's field of view. The resolution of the radar is accurate for separations greater than 1m.

Table 8-1 presents a summary of the performance of the final radar system.

Frequency Range :	2450 – 2550 MHz
Maximum detectible range	40 m
Minimum detectible range	5 m
Power output	5 dBm
Minimum beat frequency amplitude	-81dBm (at R = 40 m, 5 dB above the noise floor)
Modulation	Triangular, 1 kHz
VCO sweep (Deviation)	100 MHz
Total current	120 mA
Total weight	95.1 g
Total size	Cylinder: 60 mm diameter, 195 mm length

Table 8-1: Final system performance.

A breakdown of the cost of the components of the final FM-CW radar at the time of printing (2003) is given in Table 8-2.

Description	Price [R]
Z-COMM V807ME01 - VCO module	R 100.00
ICL8038 - Triangular waveform generator	R 66.00
LF353 - Op-Amp	R 0.20
ERA5 - RF amplifier	R 75.00
Mini-Circuits ADE-3G - Mixer	R 70.00
LM7809 and LM7909 - +9V and –9V voltage regulators	R 7.50
Lange coupler manufacturing	R 30.00
Coupled line manufacturing	R 30.00
RT-Duroid 5870 substrate [R 72/ cm^2]	R 7.20
RF capacitors and resistors	R 5.00
Total	**R 390.90**

Table 8-2: Final radar system - cost break down.

8.2 Recommendations

The final FM-CW radar system was designed to function in co-operation with a signal processing unit. This unit can typically be designed on a separate PCB that will link with the radar circuit that was designed in this project. The function of the signal processing unit is to process the beat frequency at the mixer IF- output port until the range can be displayed on an LCD. The minimum and maximum measured beat frequencies of the final radar system for R_{min} = 5 m and R_{max} = 40 are 6.67 kHz and 53.3 kHz respectively. A band pass filter can be used to capture the desired beat frequencies in this frequency range. A low noise amplifier can then be used to amplify the filtered beat frequency signal and , a level detector or frequency counter can typically be used to determine the measured range. Another possibility is to use a digital processor such as a DSP or ALTERA processor to process the beat frequency until the measured range can be displayed on an LCD.

During the radar design, emphasis was placed on the double helix design to improve the isolation between the two helices that are used for transmitting and receiving respectively. The isolation was improved and the measured coupling, $|S_{21}|$ between the helices was -23 dB. After implementing this antenna in the radar system, the isolation between the transmitted signal and the RF-port improved exceptionally. This improvement however, was of little benefit for the final system since the measured coupled power at the RF-port was far less than the maximum specification. This double helix antenna design was still worth the effort as it can be very useful when the transmitted power is increased to measure a higher maximum range.

It is recommended that the VCO in this radar system be designed by using point elements and transistors for better cost efficiency. All the components on the present final radar system can be replaced with surface mount components to reduce size and cost.

Unlike various FM-CW radar systems that have been designed for military applications, this design does not need an external modulation frequency signal. The onboard *ICL8038* triangular waveform generator can be adjusted which, in turn, makes it possible to change the center frequency and deviation of the VCO. Thus, the final radar system is versatile and antennas with different bandwidth and center frequencies can be used. With a little effort, this FM-CW radar can be reproduced commercially as a general short range sensor that can be used in short range measurement applications.

Bibliography

---

[1] Radar Technology and Saab - A Brief History, © Emerson, 1996-2002, www.emersonprocess.com/australia/Pages/News/2002.10-02.html

[2] Merrill I Skolnik, Introduction to radar systems, McGraw-Hill book company, Inc, 1962

[3] Igor V Komarov, Fundamentals of Short-Range F_m Radar, Artech House, 2003

[4] P Hanks and J Pearsall, The new Oxford Dictionary of English, Clarendon press, 1998

[5] David M Pozar, Microwave Engineering, Second edition, John Wiley & Sons, Inc, 1998

[6] WL Stutzman and GA Thiele, Antenna theory and design, Second edition, John Wiley & Sons, Inc, 1998

[7] AS Green and J de Swardt, Report on Studies defined at design review meeting no1, EM-LAB Document no EML 90-81, Electromagnetic laboratory (PTY) LTD, 19 November 1990.

[8] RT / duroid 5870 / 5880 High Frequency Laminates, Datasheets, Rogers Corporation, 1991-2002

[9] Txline, Freeware, interactive transmission line calculator included in the *Microwave Office 2002* suite [22], software runs on Microsoft Windows 2000/XP, © Applied Wave Research, Inc, www.appwave.com/products/txline.html

[10] David M Pozar, Microwave and RF design of wireless systems, John Wiley & Sons, Inc, 2001

[11] Peter Vizmuller, RF design guide: Systems, circuits and equations, Artech House, Inc, 1995

[12] SA Maas, The RF and microwave circuit design cookbook, Artech House, 1998

[13] RF/IF designers guide, Mini-Circuits, 2001

[14] JR James & PS Hall, Handbook of Microstrip Antennas, Volume 1, Peter Perigrinus, IEE, 1989

[15] Sullivan and Schaubert, Aperture Coupled Microstrip Antenna, IEEE Transactions on antennas and propagation, Vol-34, No. 8, August, 1996

[16] RE Munson, Conformal Microstrip Antennas and Microstrip Phased Arrays, IEEE Trans. Antennas and Propagation, Vol. AP-22, Jan. 1974

[17] JH Cloete, D Davidson and K Palmer, Introduction to Microstrip Antennas, 12 lecture courses presented by K Palmer at *Institut für Höchstfrequenztechnik und Elektronik Karlsruhe* University Germany, University of Stellenbosch, November 1996

[18] Full wave, method of moments based, computer code for the analysis of electromagnetic problems, Feko Suite 3.2.1, © EM Software & Systems – SA (PTY) LTD, 1998-2002, www.feko.co.za/index.htm

[19] GE Evans, Antenna Measurement Techniques, Artech House, Inc, 1990

[20] John D Krauss, Antennas, Second edition, McGraw-Hill series in electrical engineering, McGraw-Hill Book Company,1988

[21] OptFEKO is a geometric optimization package included in Feko Suite 3.2.1 [18], © EM Software & Systems – SA (PTY) LTD, 1998-2002, www.feko.co.za/tec_mod.htm

[22] Software high frequency design suite, Microwave office Version 5.51, © Applied wave research, Inc, 2002, www.appwave.com/products/mwoffice/

[23] DP Meyer and HA Mayer, Radar target detection, Academic press, 1973

[24] JF Reintjes and GT Coate, Principles of radar, third edition, Massachusetts Institute of technology, 1952

[25] DK Barbon and HR Word, Handbook of radar measurement, Artech House, Inc, 1984

[26] FE Nathanson, Radar design principles, McGraw-Hill Book Company, 1969

[27] AW Rudge, K Milne, AD Olver and P Knight, The handbook of antenna design, Volume 1, Peter Peregrinus Ltd, 1982

[28] King, HE and Wong JL, Gain pattern characteristics of 1 to 8 wavelenght uniform helical antennas, Internal symposium on antennas and propagationm Washington DC, May 1978

[29] CA Balans, Antenna theory analysis and design, Harper and Row Publishers, 1982

[30] H Jasik, Antenna engineering handbook, McGraw-Hill Book Company, 1961

[31] Software language and technical computing environment, *Matlab*, Version 6.0.88, Release 12, ©The MathWorks, Inc., 1984-2000, www.mathworks.com

[32] A complete design-to-deploy, model driven architecture software package, Borland Delphi Professional Studio, Version 6.0, © Borland Software Corporation, 1983-2001, www.borland.com

[33] Jeremy Everard, Fundamentals of RF circuit design with low noise oscillators, John Wiley & Sons, Ltd, 2001

[34] The ARRL handbook for radio amateurs, seventy-seventh edition, ARRL, 2000

[35] J Lange, Interdigitated Stripline Quadrature Hybrid, IEEE Trans. Microwave theory and Techniques, Volume MMT-20, p777-779, November 1972

[36] Complete board-level design system for Windows, Design Explorer 99, Version 6.0.4, © Protel International Limited, 1995-1999

[37] Simon R. Saunders, Antennas and propagation for wireless communication systems, John Wiley & Sons, LTD, 1999

Appendix

Final FM-CW radar - Schematic diagram

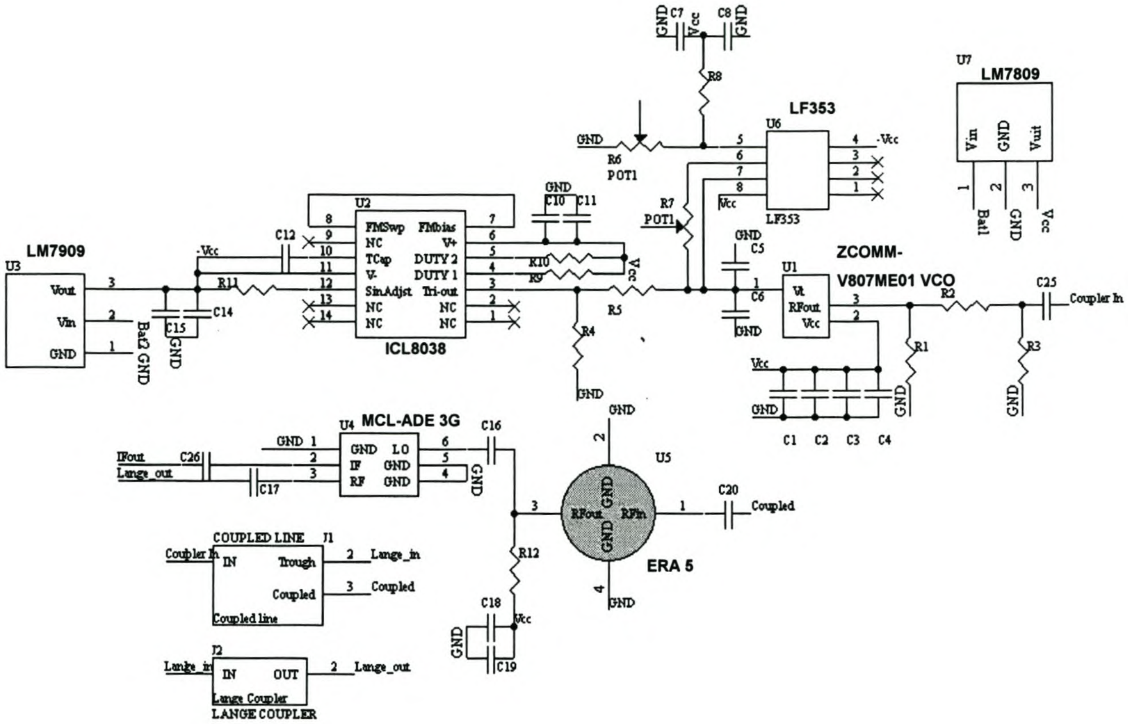

Capacitors:

C_1, C_2, C_7, C_8, C_{10}, C_{11}, C_{14}, C_{15}, C_{18}, C_{19}	100 nF
C_3, C_6, C_{16}, C_{17}, C_{20}, C_{25}, C_{26}	42 pF (surface mount)
C_4, C_5	1 nF (surface mount)
C_{12}	3.3 nF

Resistors:

R_1, R_3	30 Ω	(surface mount)
R_2	180 Ω	(surface mount)
R_4, R_8	10 kΩ	
R_6	22 kΩ Pot	
R_7	1 kΩ Pot	
R_5	1 kΩ	
R_9, R_{10}	100 kΩ	
R_{11}	82 kΩ	
R_{12}	110 Ω	(surface mount)

Components:

Z-COMM V807ME01
ICL8038
LF353
ERA5
MCL – ADE-3G
LM7809
LM709
Lange coupler
Coupled line